An Experimental Investigation
of the Flap-Lag-Torsion
Aeroelastic Stability
of a Small-Scale Hingeless
Helicopter Rotor in Hover

David L. Sharpe

NASA

An Experimental Investigation
of the Flap-Lag-Torsion
Aeroelastic Stability
of a Small-Scale Hingeless
Helicopter Rotor in Hover

David L. Sharpe

*Aeroflightdynamics Directorate*
*USAARTA-AVSCOM*
*Ames Research Center*
*Moffett Field, California*

## TABLE OF CONTENTS

PRECEDING PAGE BLANK NOT FILMED

PAGE _II_ INTENTIONALLY BLANK

## SYMBOLS

| | |
|---|---|
| $A$ | cross sectional area, $m^2$ |
| $a$ | airfoil section lift curve slope, $rad^{-1}$ |
| $b$ | number of blades |
| $c$ | blade chord, m |
| $c_{d_O}$ | airfoil section profile drag coefficient |
| $d$ | chordwise distance between blade section center of gravity and elastic axis, m |
| $E$ | Young's modulus, $N/m^2$ |
| $e$ | hub offset, dimensionless radius where uniform properties of flexible blade begin, $(R - L)/R$ |
| $e_1$ | hub offset ratio, $eR/L$ |
| $F$ | applied force, N |
| $f$ | ratio of control system torsional stiffness to blade torsional rigidity, $K_\theta L/GJ$ |
| $f_{rot}$ | rotating torsional stiffness ratio, equation (B1) |
| $G$ | shear modulus, $N/m^2$ |
| $g$ | acceleration due to gravity, $m/sec^2$ |
| $h$ | distance separating blade and hot wire element, cm |
| $I$ | polar mass moment of inertia, $kg\text{-}m^2$ |
| $I_\beta$ | blade flapwise cross sectional area moment of inertia, $m^4$ |
| $I_\zeta$ | blade chordwise cross sectional area moment of inertia, $m^4$ |
| $I_{CG}$ | polar mass moment of inertia of the entire blade about the chordwise center of gravity, $kg\text{-}m^2$ |
| $I_{EA}$ | polar mass moment of inertia of the blade about the chordwise elastic axis, $kg\text{-}m^2$ |
| $\bar{I}_{EA}$ | dimensionless polar mass moment of inertia of the blade about the chordwise elastic axis, $I_{EA}/\mu L^3$ |
| $I_P$ | polar mass moment of inertia of hub components about centerline of pitch flexure, $kg\text{-}m^2$ |
| $\bar{I}_P$ | dimensionless polar moment of inertia of hub components about centerline of pitch flexure, $I_P/\mu L^3$ |
| $I_{TE}$ | polar moment of inertia of the blade about the trailing edge, $kg\text{-}m^2$ |
| $J$ | torsional cross sectional inertia, $m^4$ |
| $K_\beta, K_\zeta, K_\theta$ | pitch flexure stiffness in flap, lead-lag, and torsion, N-m/deg |

| $L$ | blade length, length of flexible portion of blade, m |
|---|---|
| $L'$ | blade free length, uniform blade section between clamp and root cuff, equations (A2) and (A3), m |
| $M_\beta, M_\zeta, M_\theta$ | steady blade moments in flap, lead-lag and torsion, N-m |
| $M_{\theta F}$ | steady torsional moment measured at pitch flexure, N-m |
| $R$ | rotor blade radius, m |
| $r$ | blade station measured from center of rotation, m |
| $r_1$ | distance from trailing edge to chordwise center of gravity, m |
| $W$ | blade weight, N |
| $\beta_d$ | droop angle, positive measured downward from plane of rotation, figure 5, deg |
| $\beta_{pc}$ | precone angle, positive measured upward from plane of rotation, figure 5, deg |
| $\gamma$ | Lock number, $3\rho acL/\mu$ |
| $\zeta$ | blade sweep angle outboard of hub, equation (A12), rad, positive forward |
| $\zeta_{LL}$ | nonrotating lead-lag structural damping |
| $\theta$ | angular deflection, equations (A3) and (A7) |
| $\theta_O$ | blade pitch angle, deg |
| $\mu$ | blade mass per unit length, kg/m |
| $\kappa$ | dimensionless torsional rigidity, $GJ/\mu\Omega_O^2 L^4$ |
| $\rho$ | density of air, kg/m$^3$ |
| $\sigma$ | lead-lag damping exponent, sec$^{-1}$ |
| $\sigma_s$ | rotor solidity, $bc/\pi R$ |
| $\Omega$ | rotor speed, rad/sec except where noted |
| $\overline{\Omega}$ | normalized rotor speed, $\Omega/\Omega_O$ |
| $\Omega_O$ | nominal rotor speed, rad/sec except where noted |
| $\omega$ | system natural frequency, rad/sec |
| $\omega_{\beta NR}, \omega_{\zeta NR}, \omega_{\theta NR}$ | nonrotating blade natural frequencies in flap, lead-lag, and torsion, rad/sec except where noted |
| $\overline{\omega}_{\beta NR}, \overline{\omega}_{\zeta NR}, \overline{\omega}_{\theta NR}$ | normalized nonrotating blade natural frequencies in flap, lead-lag and torsion, $\omega_{\beta NR}/\Omega_O$, etc. |

# AN EXPERIMENTAL INVESTIGATION OF THE FLAP-LAG-TORSION AEROELASTIC STABILITY

## OF A SMALL-SCALE HINGELESS HELICOPTER ROTOR IN HOVER

David L. Sharpe

Ames Research Center
and
Aeroflightdynamics Directorate, U.S. Army Aviation Research and Technology Activity — AVSCOM

## SUMMARY

*A small scale, 1.92 m diam, torsionally soft, hingeless helicopter rotor was investigated in hover to determine isolated rotor stability characteristics. The two bladed, untwisted rotor was tested on a rigid test stand at tip speeds up to 101 m/sec. The rotor mode of interest in this investigation was the lightly damped lead-lag mode. The dimensionless lead-lag frequency of the mode is approximately 1.5 at the highest tip speed. The hub was designed to allow variation in precone, blade droop, pitch control stiffness, and blade pitch angle. Measurements of modal frequency and damping were obtained for several combinations of these hub parameters at several values of rotor speed. Steady blade bending moments were also measured. The lead-lag damping measurements were found to agree well with theoretical predictions for low values of blade pitch angle. The test data confirmed the predicted effects of precone, droop, and pitch control stiffness parameters on lead-lag damping. The correlation between theory and experiment was found to be poor for the mid-to-high range of pitch angles where the theory substantially overpredicted the experimental lead-lag damping. The poor correlation in the mid-to-high blade pitch angle range is attributed to low Reynolds number nonlinear aerodynamics effects not included in the theory. The experimental results also revealed an asymmetry in lead-lag damping between positive and negative thrust conditions. Investigations of the rotor induced velocity field suggest that the asymmetry in lead-lag damping is not caused by the aerodynamic inflow but more likely from the influence of blade weight on the equilibrium blade deflection. Comparison of measured steady state blade bending and torsion loads with theoretical predictions showed good agreement after correcting the lead-lag bending moments for a small chordwise offset of the blade tension axis.*

## INTRODUCTION

Past experience with hingeless rotor helicopters has shown that particular care must be exercised in each new design to preclude undesirable kinematic or aeroelastic coupling that could lead to catastrophic rotor blade instabilities. These instabilities may be avoided on future designs through the use of sophisticated aeroelastic math models which are now practical because of the increased computational power of today's digital computers. To establish confidence in these theoretical models, however, requires validation of the theory with experimental results. The present experiments were designed to provide a set of carefully documented experimental data to be used for the validation of the theoretical model discussed in references 1-4.

The validation of aeroelastic stability analyses for hingeless rotors has been an ongoing research effort for several years. Earlier experiments reported in reference 5 focused on a two degree-of-freedom flap and lead-lag model using rigid blades, and flap and lead-lag flexures. This work was further expanded in reference 6, by investigating the effect of flap-lag elastic coupling and low Reynold's number airfoil stall effects. In reference 7, the effects of hingeless rotor pitch lag and flap-lag coupling were introduced by skewing the flap and lag flexures axes. All these experiments were restricted to isolated blade stability, without including coupling with fuselage degrees-of-freedom. The influence of the torsional mode for all these experiments was virtually eliminated by keeping the torsional stiffness high. The theoretical analysis of references 1-4 was developed to extend the simplified rigid, hinged blade representation to model elastic blades including both bending and torsional motion, and the effect of pitch link or control system flexibility. Only blades with uniform mass and stiffness distributions were treated, and chordwise offsets between the aerodynamic center, mass center, elastic axis, and tension were not included. The results showed that configuration parameters such as precone

and droop play an important role in lead-lag damping. In reference 2, it was demonstrated that the effect of torsion could be represented as effective pitch-lag and pitch-flap couplings, and that the influence of precone and droop on the lead-lag damping was primarily due to their influence on the effective pitch-lag coupling.

In order to determine the validity of the elastic blade theory, the present experimental investigation was undertaken. The configuration of the experimental model used for validation of the theory was crucial to the success of this investigation. It was necessary that the blades be of uniform mass and stiffness to match those in the theory. The torsional stiffness of the experimental rotor blade was designed to be relatively low to emphasize the influence of torsion in flap-lag-torsion effects. The pitch control system flexibility effect on stability was studied using torsional pitch flexures to simulate the control system flexibility. The experimental model incorporated provisions for precone and droop to demonstrate the effects of these important configuration parameters. The experimental model design was made as simple as possible to minimize sources of error and unknowns (such as mechanical damping). To ensure that the design specifications were met and that all parameters required for the theoretical calculations were correctly determined, a thorough component test program was completed for each individual blade and the hub component.

This report describes the model rotor used for the experiments, the test procedures and data analysis methods used, and the results of the stability investigations. The experiment was conducted in two parts: the first with an initial set of rotor blades which had small variations in mass, stiffness and geometric properties, referred to as blade set 1; and a second part with a set of improved rotor blades, referred to as blade set 2. Two appendices are included in the report. The first appendix describes the measurement procedures used to determine the model properties and the results of the measurements. The second appendix includes a brief description of the theoretical model of references 1–4 and the values of the theoretical model configuration parameters used for the theoretical calculations.

## MODEL DESCRIPTION

### Blade Design

The rotor blade used in this investigation was designed to match as closely as possible the mathematical representation of a rotor blade used in references 1–4. A schematic of this rotor blade is shown in figure 1. In this theoretical model, blade properties outboard of the pitch-change bearing are uniform and control system flexibility is represented by a root spring. The theory assumes that the pitch-change bearing is located at the hub center-line. The experimental model

blade design is shown in figure 2. The blade properties for the model are uniform from 9.5% of the blade radius to the tip. The properties are not uniform inboard of 9.5% blade radius because of a necessary experimental compromise to allow space for blade attachment hardware and the hub itself. The blade structure was designed to minimize the blade torsional frequency while maintaining appropriate flap and lead-lag stiffness. The blade stiffness properties are primarily determined by the unidirectional Kevlar spar and 0.0762 mm fiberglass skin. The blade profile is maintained by a polyurethane foam core. The blade is bonded to an aluminum blade root cuff having a cavity matching the airfoil section profile of the blade. For the portion of the blade bonded within the cavity of the blade root cuff, the polyurethane core is replaced with a solid fiberglass plug. Therefore, the Kevlar spar and fiberglass skin of the blade are securely bonded between the aluminum blade root cuff and the fiberglass plug. The segmented tantalum leading edge weights contribute little to the lead-lag stiffness of the blade but significantly increase the blade cross-sectional polar moment of inertia, hence reducing the blade torsional frequency. The various structural components have been carefully positioned to ensure that the cross-section center of gravity and the elastic axis are located at the quarter chord.

The design parameters of the rotor blade were chosen to be representative of typical full-scale helicopter rotor blades. At the nominal rotor speed of 1000 rpm, the model corresponds to a stiff inplane hingeless rotor with a dimensionless first lead-lag frequency of approximately 1.5. The calculated dimensionless first flap frequency is 1.13, typical of a moderately stiff hingeless rotor. The large difference in flap and lead-lag bending stiffness provides significant flap-lag structural coupling for this configuration. The dimensionless first torsion frequencies are 2.87 and 2.56 with the stiff and soft pitch flexures, respectively. These values are less than typical full scale values and were chosen to emphasize the influence of bending-torsion coupling phenomena.

### Hub Design

The rotor hub components, figure 3, were designed to permit several important rotor configuration parameters to be varied. The control system or pitch link flexibility included in the theoretical model is represented in the experimental model by pitch flexures mounted inboard of the blade. Pitch flexures of two different values of torsional stiffness were used in the experiment and are shown in figure 4. The partial cruciform cross-section of these pitch flexures provides relatively high stiffness in the flap and lead-lag directions, while the torsional stiffness is controlled by the thickness of the cruciform flexure elements. The ratio of the torsional stiffness in the pitch flexure to the blade torsion stiffness has a significant influence on rotor stability. This ratio is defined in reference 4 by the parameter $f$

$$f = \frac{K_\theta L}{GJ} \quad (1)$$

The soft pitch flexure provides a value of $f = 7.062$ for the nonrotating condition while the stiff pitch flexure, essentially rigid in torsion, gives $f \cong 10,000$. In this case, nearly all of the torsional flexibility is in the blade.

Precone and droop are both important to the rotor designer as a means to reduce steady flap bending stresses for a hingeless rotor. Although this design approach will relieve the steady flap bending loads, it may have a detrimental effect on rotor blade stability. From the stability point of view, it is important whether the structural coning is placed inboard of the pitch change bearing (precone); or outboard of the pitch change bearing (droop). This distinction is shown in the schematic of figure 5. As can be seen, precone is the inclination of the pitch axis and is positive up; while droop is the inclination of the blade outboard of the pitch bearing (represented by the pitch flexure for this model) and is positive down.

From the point of view of steady blade bending loads, $5°$ of precone is the same as $5°$ of negative droop. For blade lead-lag stability, however, this similarity exists only if there is no control system flexibility. If there is flexibility in the pitch flexure, the equivalent precone and droop angles will have substantially different influence on blade stability. The way in which precone and droop are incorporated in the model is shown in figures 3 and 5. Precone was varied with interchangeable hubs having $0°$, $2.5°$, or $5°$. Droop was varied with interchangeable droop wedges having $0°$, $\pm 2.5°$, or $\pm 5°$. In all cases the blade pitch angle was changed by rotating the blade outboard of the pitch flexure, at the interface between the pitch flexure and the droop wedge. With blade droop present, this method of blade pitch change will introduce a small amount of blade sweep equal to the product of the blade pitch angle and the droop angle. This sweep effect is accounted for in the theory.

## Model Test Stand

The blades and associated hub components were mounted on a rigid test stand, figure 6, powered by a 60 hp variable frequency motor. The motor power was transmitted to the rotor shaft through a flexible belt drive. The upper truss framework which houses the drive shaft is attached to the circular mounting plate by two flexures. The lead-lag mode was excited by oscillating the upper structure about the flexures with a 220 N electromagnetic shaker. The shaker, located on the floor below the mounting plate, is attached to a forward arm of the upper truss framework by a hollow aluminum pushrod. Once sufficient lead-lag motion of the blade was obtained, the shaker excitation was terminated while simultaneously activating a pneumatic clamp to lock

the upper structure. Frequency and damping were obtained from the transient decay of the blade motions.

In order to preclude dynamic coupling between the test stand and the rotor blade lead-lag motion from contaminating isolated blade damping and frequency measurements, the test stand structure was stiffened sufficient to raise the lowest natural frequency to twice that of the rotor blade frequency. The fixed system lead-lag natural frequency of the rotor is equal to the rotating system lead-lag natural frequency plus the rotor speed which, at a nominal rotor speed of 1000 rpm, corresponds to a range of frequencies for this model from 35 to 42 Hz. The lowest test stand natural frequency was measured at 86 Hz. It is not expected, therefore, that the stand flexibility will significantly influence the measured damping and frequency values.

## Instrumentation

Most of the data obtained during this study was derived from measurements of blade strain using surface mounted strain gages located near the blade root at 12% blade radius for the flap and lead-lag gages and 14% blade radius for the torsion gages. These gages were installed in a conventional bridge arrangement to measure blade flapping, lead-lag, and torsional moments. In addition, the soft pitch flexures were each gaged to measure torsional moments. The strain gage leads were routed through the inside of the hollow drive shaft to a 40-channel slip ring set mounted beneath the upper truss structure. Rotor speed was determined both by an inductive pickup from a 60-tooth gear which provided a 60/rev signal, and by a Hall effect switch which provided a 1/rev pulse. All signals were conditioned and amplified and then routed to a computer for digitizing and online analysis. In addition, the analog blade signals were recorded on magnetic tape for offline analysis.

## TEST PROCEDURES

### Nonrotating Tests

Nonrotating tests were conducted for each configuration to determine nonrotating modal frequencies and lead-lag structural damping. With the upper stand clamped, each mode was manually excited and the natural frequencies of the resulting blade oscillations were measured. In addition, with the stand unlocked, the differential lead-lag mode was excited at its natural frequency with the electromagnetic shaker. When a sufficient signal level was reached, the clamp was engaged, the shaker input terminated, and the transient decay recorded. Additional discussion of the nonrotating frequencies is provided in Appendix A.

## Rotating Tests

Rotating tests were performed to determine both lead-lag stability characteristics and steady state bending moments. The model rotor speed was varied up to and including the nominal value of 1000 rpm. Most configurations were investigated at rotor speeds of 0, 600, 900, and 1000 rpm, although the bulk of the data was taken at 1000 rpm. Data acquisition was virtually impossible for some cases in the 625- to 875-rpm range due to the close proximity of the rotating lead-lag frequency to the rotor 2/rev frequency. The limiting blade pitch angle for each configuration was determined from the blade bending stresses at the nominal rpm. In a few cases it was possible to test in the blade stall regime. The test matrix for blade set 1 and an expanded test matrix for blade set 2 are shown in table 1. In all cases, the lead-lag mode was excited by the electromagnetic shaker at the progressing mode frequency.

## DATA ANALYSIS

For each test condition, four seconds of transient data were digitized and six channels of data were displayed on an on-line interactive computer display, figure 7(a). The lead-lag signal from each blade primarily consists of the response of two rotor modes: the collective lead-lag and the differential lead-lag modes. The collective lead-lag mode represents the two blades moving in phase and this mode couples with the drive system. The differential lead-lag mode is a torqueless mode, that is, the two blades move out of phase in opposite directions without involving drive system motion. This differential mode is, therefore, a good representation of the isolated blade of the theory in which the blade is assumed to be mounted on a rigid hub with infinite drive system impedance. For data analysis then, the two lead-lag bending moment signals are differenced which eliminates the collective mode, and the resulting differential lead-lag mode was analyzed.

The differential lead-lag mode, shown as channel 4 in figure 7(a), is processed to obtain the FFT shown in figure 7(b). The lead-lag frequency is identified from this display and then the modal damping is obtained using the moving-block analysis (described in ref. 8) as shown in figure 7(c).

Blade surface mounted strain gages were used to obtain steady state bending and torsion moments as well as stability data. A description of the strain gage calibrations and interactions between flap, lead-lag and torsional moments and the resulting interaction matrix are presented in Appendix A. The mean values of the blade bending moments were acquired at the same time as the transient decay stability data. The strain gage outputs of blade bending and torsion were multiplied by the calibration interaction matrix thereby providing uncoupled bending and torsional moments. In addition to the blade gages, the soft pitch flexure strain gage bridges were used to measure the torsion moment. However, steady flexure data were not successfully recorded for all cases tested.

## RESULTS

Frequency and damping data are tabulated for all test conditions in tables 2 through 20. For each configuration defined by pitch flexure stiffness, precone angle, and droop angle these tables include the blade pitch angle, the rotor speed in rpm, and the frequency and damping of lead-lag transient decays as determined by the moving block analysis. Two measurements are usually included for each test rotor speed. The zero rpm data was obtained as described in the section on nonrotating tests. The tests results that will be discussed herein consist primarily of damping measurements made at the nominal test speed of 1000 rpm.

### Blade Frequencies

The experimental frequency measurements for the case with zero blade pitch angle, zero precone, and zero droop are compared with the theory for the full range of rotor speeds tested in figure 8(a) for the stiff pitch flexure, and figure 8(b) for the soft pitch flexure. It was possible to successfully measure four modal frequencies in the nonrotating condition but only the first lead-lag mode with the rotor spinning. Agreement between experiment and theory for lead-lag frequency is quite good for the stiff pitch flexure configuration but only fair for the soft pitch flexure configuration. The over-prediction of the lead-lag frequency is due in part to the inaccuracy of the theoretical modeling of the lead-lag stiffness inboard of the blade. The theoretical model represents this section as infinitely stiff while the experimental model was shown to have a small amount of flexibility in the lead-lag direction. This difference is not evident for the low frequency flap mode due to a much higher stiffness ratio between the flexure and blade. Calculations for the first and second flap modes and the first torsion mode are also shown in figure 8. Attempts to determine experimentally these rotating frequencies were not practical with existing equipment, and only the experimental nonrotating frequencies for those modes are compared with the theory.

### Lead-Lag Damping

Before presenting the experimental results, a brief discussion on the isolated blade lead-lag damping is in order. This damping is derived from four primary sources: 1) blade

structural damping; 2) aerodynamic damping from both constant values of lift and drag coefficients and their change of slope with respect to angle of attack; 3) flap-lag coupling owing to structural or kinematic couplings; 4) pitch-flap and pitch-lag coupling owing to blade torsion and/or control system flexibility. These damping sources, which can be quite complex and often interrelated, are discussed in detail in references 2-4.

A brief description of damping sources will be given here, making use of typical theoretical results. Figure 9 shows lead-lag damping as a function of blade pitch angle for several different intermediate blade configurations. At zero blade pitch angle, the damping is due to blade internal structural damping, and aerodynamic profile drag damping of the blade airfoil. These two contributions are essentially invariant with pitch angle, except when the profile drag increases at blade stall, which is not shown in this example. For a blade without torsional flexibility, coupled flap and lead-lag bending produce an increment in lead-lag damping as pitch angle increases, which is caused by aerodynamic and inertial coupling of the bending motions. The magnitude of this coupling is a function of the equilibrium flap bending of the blade.

In addition to aerodynamic and inertial coupling of flap and lead-lag bending, there is a structural coupling of flap and lead-lag bending deflections if the principal elastic axes of bending are not aligned parallel and perpendicular to the plane of rotation. This coupling, therefore, increases as the blade pitch angle is increased and typically provides a large increment in lead-lag damping. The aerodynamic, inertial, and structural flap-lag coupling contributions to lead-lag damping of coupled flap and lead-lag bending are illustrated in figure 9 by the curve labeled "flap-lag without torsion."

With blade torsional flexibility, including both elastic torsion of the blade and motion of the pitch flexure to simulate control system flexibility, other sources of lead-lag damping exist. For blade configurations without chordwise offsets between the aerodynamic center, mass center, and elastic axis, the principal effect is that blades of unequal flap and lead-lag bending stiffness will experience torsional deflections as a consequence of combined flap and lead-lag bending. This structural bending torsion coupling can be represented as effective pitch-lag and pitch-flap couplings and the magnitude of these couplings is essentially proportional to the equilibrium flap bending and lead-lag bending of the blade, respectively.

It is known that the lead-lag damping of hingeless rotor blades is sensitive to such couplings, particularly the pitch-lag coupling. Furthermore, blade stability is dependent on blade pitch angle, precone, and droop because these parameters all influence the equilibrium flap bending deflection of the blade. For the simple case without precone or droop (fig. 9), the effects of elastic blade torsion and pitch flexibility on lead-lag damping are illustrated by the curve labeled

"flap-lag-torsion with soft pitch flexure." This effect increases as the torsional stiffness is reduced.

The experimental lead-lag damping results for each configuration investigated are presented by showing lead-lag damping as a function of blade pitch angle. The experimental results are compared to the theoretical predictions. For configurations where both rotor blade sets were tested, both sets of experimental data are included; but only the theoretical results for blade set 2 are shown. In order to provide a comprehensive overview of the effects of precone and droop on lead-lag damping, all of the damping results are presented in two summary figures, figure 10 for the stiff pitch flexure configuration and figure 11 for the soft pitch flexure configuration. Figures 10(a) and 11(a) first show lead-lag damping as a function of pitch angle for the configuration with no precone or droop. Figures 10(b) and (c) and 11(b) and (c) show the results for ±2.5° and ±5° of droop and figures 10(d) and (e) and 11(d) and (e) show the results for 2.5° and 5° of precone.

*Stiff pitch flexure*– Lead-lag damping data is shown in figure 10(a) as a function of both positive and negative blade pitch angles for the stiff pitch flexures with zero precone and droop. Both experiment and theory show that the damping is a minimum at zero pitch angle with the damping increasing as the absolute value of pitch angle increases. In the low range of blade pitch settings, the agreement between experiment and the theory is good. Above 4° to 6° the theoretically predicted increase in damping with blade pitch is not evident in the experimental results which show a much smaller increase in damping as blade pitch is increased. This difference between the theory and experimental results occurred for nearly all configurations tested. This difference is strongly suggestive of similar results reported in reference 6 for a torsionally rigid blade. In that study, the inclusion of nonlinear airfoil section lift and drag coefficients was able to account for the differences between the measurements and the theory with linear aerodynamics. In addition, it is worth noting that where direct comparisons can be made, the experimental data of the two blade sets are in good agreement.

Figure 10(b) shows the effect of droop on the torsionally stiff configurations by presenting lead-lag damping vs pitch angle for configurations having droop angles of ±2.5° in combination with the stiff pitch flexures. Both configurations show a change in the predicted pitch angle for minimum lead-lag damping. This minimum occurred at the zero pitch angle for the configuration without blade droop; figure 10(b) shows that with 2.5° of positive droop the minimum damping point moves to about -3° pitch angle. With 2.5° of negative blade droop angle, the minimum damping occurs at about +3° pitch angle. The experimental data for these two configurations are for blade set 1 that was tested only at positive blade pitch angles. For the positively

drooped case, blade pitch angles greater than 6° were not tested owing to conservative blade stress limits. Correlation with theory for both cases at the lower blade pitch settings is good.

Figure 10(c) shows lead-lag damping versus blade pitch angle for droop configurations of ±5°. With increased blade droop angles, each configuration experiences a further shift in the pitch angle for minimum damping and a reduction in the minimum damping. The experimental data in figure 10(c) confirm this shift and agreement between theory and experiment is good at low blade pitch angles, but only fair at the higher settings. Test data were not obtained for positive pitch angles for the positive 5° droop configuration or negative pitch angles for the negative 5° droop configuration, because of blade stress limits. For the ±5° droop configurations, the effect of droop is sufficiently large that the trends of the theoretical predictions are clearly apparent in the experimental results. Note that for the one case where it was possible to operate at $\theta_O$ = -16°, the lead-lag damping decreases with increased pitch angle change. It is believed that this is stall related as noted above and described in reference 6.

The effect of rotor precone in combination with the stiff pitch flexures is shown in figures 10(d) and 10(e) for precone angles of 2.5° and 5°, respectively. Both theory and experiment show behavior that is very similar to the corresponding configurations with negative droop. Thus, figure 10(d), with a precone angle of 2.5°, is found to have the same lead-lag damping characteristics as the configuration with a blade droop angle of 2.5° shown in figure 10(b). Similarly, the configuration with a precone angle of 5° shown in figure 10(e) is the same as the 5° droop angle case of figure 10(c). This demonstrates, as would be expected, that precone and negative droop are equivalent when there is no control system flexibility. Correlation between theory and experiment for precone of 2.5°, figure 10(d), is good at low blade pitch angles but poor at the higher values. The correlation for the 5° precone case is reasonably good for the pitch angle range tested.

The stiff pitch flexure results show that, where direct comparisons can be made, the experimental data of the two blade sets are in good agreement.

*Soft pitch flexure–* The configuration with soft pitch flexures and with zero precone and droop was tested over a greater range of pitch angles than the case with stiff pitch flexures. The damping results are shown in figure 11 in the same format as figure 10. As discussed above, the increased torsional flexibility provided by the soft pitch flexure increases the effects on lead-lag damping due to bending-torsion coupling. Therefore, larger variations in lead-lag damping for pitch angle, precone, and droop variations are to be expected.

The lead-lag damping without precone or droop is shown in figure 11(a) as a function of both positive and negative pitch angles. Damping predictions, as with the stiff pitch flexures, are found to be good for small blade pitch angles of either sign, and become progressively poorer as the absolute value of pitch angle is increased. There is no discernible difference in the damping data obtained with two different blade sets. As discussed in Appendix A, the match in blade properties was improved between the blade set 1 and blade set 2 test entries; the good match in the data seen here suggests that the damping is not especially sensitive to the differences between the properties of blade set 1.

Both theory and experimental results show the point of minimum damping for the soft pitch flexure configuration without precone or droop occurs at the zero blade pitch angle. However, the theory predicts the damping values to be symmetric with pitch angle; the experimental data, on the other hand, show a small but distinct asymmetry. This asymmetry also appeared, but to a lesser extent, for the stiff pitch flexure configuration without precone or droop (fig. 10(a)). It is possible that the more pronounced asymmetry on the soft pitch flexure configuration may be attributed to the increased torsional flexibility. These asymmetries in lead-lag measurements for positive and negative pitch angles appear to be related to some asymmetry in the experimental apparatus. Comparing the positive pitch angle case thrusting upward and the wake moving downward with the negative pitch angle case thrusting down and the wake moving upward, the only apparent differences are the aerodynamic effect due to test chamber recirculation and stand interference, or the blade weight which reduces blade coning for the positive pitch angle case and increases the coning for negative blade pitch angles. The possibility of aerodynamic asymmetries was investigated and will be discussed later in the report.

The lead-lag damping as a function of blade pitch angle is shown in figures 11(b) and 11(c) for the configurations with soft pitch flexures and droop angles of ±2.5° and ±5°, respectively. Correlation of the theory with experimental results for each case is again quite good for low pitch angles and poor at high pitch. The point of minimum damping follows closely the characteristics found with the stiff pitch flexure configuration. In the case in which experimental data was obtained for both blade sets (i.e., the 2.5° droop configuration), there is very good agreement between the two data sets.

In figure 11(d) and (e), the lead-lag damping is shown for the soft pitch flexure configuration with 2.5° and 5° of precone. These results confirm that precone has a stronger effect on lead-lag stability than droop when control system flexibility is present. For the 2.5° precone configuration, both theory and experiment show the lead-lag mode to be just slightly stable for pitch angles between 2° and 3°. At this pitch setting the lead-lag damping is reduced to about one half the value experienced at zero degrees pitch angle, and is significantly less than the equivalent case with the stiff flexures. In the low negative pitch angle range, the damping is seen to increase rapidly due to the dominance of structural

pitch-lag coupling. Correlation between theory and the experimental data is very good over the entire range of pitch settings, with the exception of angles above 8°, where the theory again tends to over-estimate the lead-lag damping. In figure 11(e), for the case with 5° precone, the effect of the soft pitch flexure is shown to strongly destabilize the lead-lag mode and an instability occurs between 3° and 7° pitch angle. Comparison of the theory and experiment for this configuration is quite good. The unstable data points were obtained for this configuration by increasing the rotor speed into the unstable region, holding the speed constant for the time needed to obtain an unstable transient, and then quickly reducing the rotor speed to stabilize the rotor.

*Effects of rotor speed–* Figure 12, which shows damping as a function of rotor speed for the soft pitch flexure configuration with 5° precone, illustrates the strong gradient in damping with rpm above 700 rpm for the unstable case with $\theta_O = 4°$. The lead-lag damping for the zero precone, zero droop, and soft pitch flexure configuration originally shown in figure 11(a) is shown in figure 13 as a function of rotor speed at two pitch angles. At zero pitch angle, figure 13(a), the lead-lag damping is essentially invariant with rotor speed while for $\theta_O = 8°$ the damping increases significantly for rotor speeds above 700 rpm. The agreement between theory and experiment is seen to be good for low thrust while the agreement becomes poorer with increasing thrust although the same qualitative behavior is shown.

*Effects of precone, droop, and pitch flexure stiffness–* In order to more clearly illustrate the effects of precone, droop, and pitch flexure stiffness (simulating control system flexibility), figures 14 through 20 are presented. A comparison of the damping characteristics for several configurations are shown in figures 14 through 16, and cross plots of previously presented data are shown in figures 17 through 20. In order to clarify the experimental results for these figures, the several values of lead-lag damping measured at each blade pitch angle have been combined and only the resulting average values are plotted.

The effect of the pitch flexure on configurations without precone and droop is shown in figure 14. Both theory and experiment show slightly greater damping for the soft pitch flexure configuration than for the stiff one. This, as previously discussed, is due to the increased effective pitch-lag coupling resulting from the increased torsional flexibility.

A comparison of the effects of precone and droop for configurations without and with simulated control system flexibility are shown in figures 15 and 16, respectively. It is clearly shown that not only do precone and droop modify the basic lead-lag damping characteristics, but without control system flexibility (fig. 15), the effects of precone and droop are virtually identical. When control system flexibility is introduced, as shown in figure 16 with the soft pitch flexure, the effects of precone and droop are different. Both

configurations are seen to have reduced minimum lead-lag damping and a shifting of the minimum damping value that was evident for the configuration with no precone or droop. The soft pitch flexure configuration is stable with 5° negative droop and unstable with 5° of precone.

Because it is clear that the theory is not capable of predicting the lead-lag damping at high blade pitch angles, the validity of the theory for predicting the aeroelastic effects of blade bending, torsion, precone, and droop can be properly tested only for low blade pitch angles. For this reason, the lead-lag damping data have been plotted as a function of the blade precone and droop angles for a pitch angle of 2° for the stiff pitch flexure, figure 17, and for the soft pitch flexure, figure 18. The data points with solid symbols indicate data taken at -2° pitch angle in which the sign of the precone and droop angle were reversed for these figures. For the stiff pitch flexures, figure 17, the theory is shown to predict identical results for precone and droop. For the soft pitch flexures, figure 18, the theory predicts quite different results for precone than for droop. The close agreement between the measured and calculated results in both of these figures confirm the accuracy of the basic theory when the effects of airfoil stall are not present.

To emphasize the consistently good agreement between theory and experiment at low blade pitch angles and the deterioration in the correlation as the pitch angle is increased, figure 19 for the stiff pitch flexure, and figure 20 for the soft pitch flexure, are shown. On the left hand side of each figure, the lead-lag damping is plotted against negative droop in order that an easy comparison can be made with the opposing right hand side where damping is plotted against precone angle. Each figure contains results for three different pitch angles: 0°, 4°, and 8°. These results clearly show the deterioration of the agreement between theory and experiment as the pitch angle increases.

### Asymmetry in Lead-Lag Damping with Pitch Angle

The asymmetry of lead-lag damping between positive and negative pitch angles that was discussed previously will be investigated here. Because the blade had a symmetric airfoil section, the only apparent cause for differences in damping between positive and negative pitch angles would be aerodynamic asymmetry of induced flow, or the effect of blade weight. Asymmetric induced velocity conditions for up and down thrust conditions would be expected to arise from the different flow blockage created by the support stand for the two different thrust conditions. In the normal up thrust condition, the stand is located in the high velocity downwash region of the rotor; in the down thrust condition the stand is located in the relatively low velocity inflow region. Therefore, the stand might be expected to have a smaller influence on the rotor induced velocity in the down thrust condition. The effect of gravity on the magnitude of equilibrium blade

flapwise deflections will be reversed for the up and down thrust directions; in the former, gravity will counteract deflections produced by rotor thrust; in the latter, blade deflections will be increased by gravity. Since the lead-lag damping is dependent on both the induced velocity and blade equilibrium deflections, these asymmetries were investigated in some detail.

The theoretical predictions were made assuming the model rotor was operating out of ground effect, but as seen in figure 21, this is only approximately true. The upper mounting plate, the floor, and the walls will all modify the induced flow pattern. Two test stand modifications were introduced to study the effects of large changes in induced flow on lead-lag damping. First, a 2.43 m diameter ground plane was installed flush with the upper mounting plate, figure 22(a), and second, a "mirror image" ground plane was also installed above the rotor, figure 22(b). The rotor induced velocities and lead-lag damping were measured and then compared to the basic system without the ground planes.

*Induced velocity measurements*— The axial component of the induced velocity was measured at discrete radial locations with a traversing hot wire probe. By illuminating the blade with a stroboscopic light source, and viewing it through a surveying transit, the probe could be positioned within 1 cm below the blade regardless of the equilibrium deflection position. Surveys were made at 1.0, 2.5, and 5.0 cm below the blade. All data were taken at a rotor speed of 1000 rpm for the soft pitch flexure blade configuration without precone or droop. Figure 23 shows the induced velocity profiles for three different blade pitch angles, at a distance of 5 cm below the blade position (2.5 cm for $\theta_O = 10°$). Variations in the probe position from 1 to 5 cm below the blade were found to have only a minor effect on induced velocity. The pronounced peak in velocity near the blade tip is due to the tip vortex.

To determine if the induced velocity varied asymmetrically with thrust direction, measurements were made for positive and negative pitch angles. The results, shown in figure 24, show no significant difference except near the blade tip in the vicinity of the tip vortex. For the positive pitch angle case, the tip vortex passed through the hot wire located below the rotor disk. For negative pitch, the tip vortex is convected upward and no longer intersects the hot wire probe, still located below the rotor.

To investigate how large a reduction in induced inflow could be produced by the influence of the test stand, a large diameter ground plane was added to the test stand. Figure 25 compares the induced velocities measured with and without the ground plane and a reduction of roughly 25% in inflow is observed for the 10° blade pitch angle. The induced inflow with the double ground plane was not measured because the hot wire probe traverse mechanism could not be used with the double ground plane.

*Effect of induced inflow variations on lead-lag damping*— The lead-lag damping measurements with and without the ground plane are shown in figure 26. Although the differences are quite small, the lead-lag damping is slightly higher with the ground plane. Two theoretical results are also included in figure 26 that compare predicted lead-lag damping with normal out-of-ground-effect inflow and without any induced inflow; they show that decreasing the inflow increases the damping. If the effect of the ground plane is assumed to cause a reduction in inflow of approximately 25% as observed in figure 25, then the effect of the ground plane on the predicted lead-lag damping is consistent with the observed effect of the ground plane on the measured damping. It should be noted that this discussion does not address the large differences between theoretical and measured damping at high blade pitch angles; as stated this is attributed to nonlinear airfoil section lift and drag characteristics not included in the theory.

With respect to the asymmetry in measured lead-lag damping for the positive and negative pitch angles, figure 24 showed the measured inflow to be essentially independent of thrust direction. This indicates that the asymmetric damping is not caused by asymmetric inflow. The measurements with the double ground plane provide further evidence to support this conclusion. The double ground plane effectively enforces symmetry of inflow for the positive and negative thrust conditions. However, the lead-lag damping measurements with the double ground plane shown in figure 27 exhibit the same asymmetry as the results without the ground plane.

As the results of these investigations are inconclusive, the cause of the asymmetric damping cannot be established. The effect of blade weight on equilibrium blade deflection or an undetected asymmetry in rotor blade airfoil section characteristics remain as possible but unproven causes.

## Steady State Blade Loads

The largest contribution to the lead-lag damping of a hingeless rotor is derived from the aeroelastic couplings associated with the structural characteristics of cantilevered blades. These couplings are the result of the blade equilibrium elastic deformations caused by combined steady state aerodynamic and inertial loading. For the experimental model, the first mode flapping, lead-lag, and torsional deformations may be approximated by measuring the strain of the blade with surface mounted strain gages located near the blade root. The steady strain gage signals, suitably calibrated to measure flapping, lead-lag, and torsional moments, were recorded at the same time as the transient decay records. The interaction between flapping, lead-lag, and torsion were removed by multiplying the individual strain gage signals by a carefully determined interaction matrix, described in Appendix A.

In addition to the moment interactions, an unexpected tensile load interaction was encountered that is described in detail in Appendix A. It was concluded that the centrifugal force induced tensile interaction primarily influenced only the lead-lag moment measurements. The basic effect of the tensile loading was to cause a static offset (or tare) of the lead-lag strain gage output. At the nominal 1000 rpm operating condition, this tare was determined to be −4.02 N-m. All experimental steady state lead-lag bending moment data presented in this report has been corrected by removing this tare moment.

The experimental data was measured for blade set 2 at the 1000 rpm rotor speed. The flap bending, lead-lag bending, and torsion moments are presented in figures 28 through 38 as a function of blade pitch angle. The flap and lead-lag moments were measured at the 12% blade radial location and the torsion moment at 14%. For most of the soft pitch flexure configurations, the pitch flexure moment is also presented. The theoretical predictions described in Appendix B are also included, and are shown as solid lines in the figures.

Results for the stiff and soft pitch flexure configurations without precone or droop are shown in figures 28 and 29. The results are similar for both configurations. The flap bending moments are in very good agreement with theory indicating that for the pitch angles tested, the lift coefficient characteristics of the airfoil are close to the linear approximation assumed in the theory. The lead-lag bending moments are in good agreement with the theory except for increasing deviation as the pitch angle increases. This is consistent with a nonlinear drag rise typical of low Reynolds number airfoil aerodynamic characteristics. A negative torsion moment variation linear with pitch angle is produced by the inertial tennis-racket effect acting to twist the blade chord in a direction toward the plane of rotation. An opposing nonlinear torsion moment is produced by bending torsion coupling; for the small pitch angle range tested here, the inertial effect is dominant. The theory assumes no aerodynamic moment for the symmetrical airfoil, therefore the difference between measured and predicted torsion moment is a reasonable indication of nonlinear airfoil pitching moment characteristics. Results in figure 29, and results presented below, show pronounced asymmetric variations at the largest positive and negative pitch angles tested.

The effects of precone and droop for the stiff pitch flexure configuration are shown in figures 30-32. With 5° of precone, figure 30 shows the large negative flap bending moment increment caused by centrifugal force acting to bend the blade into the plane of rotation. Even for the largest pitch angle tested, the positive flap moment generated by aerodynamic lift has not overcome the negative centrifugal flap moment. The effect of precone produces a large negative gradient of lead-lag bending moment with pitch angle. This is caused by the combined effect of precone and flap-lag structural coupling. At a positive pitch angle, $\theta_O$, the centrifugally induced downward flap bending of the pre-

coned blade imparts a lead displacement of the blade proportional to the product of $\theta_O$ times the flap bending. Centrifugal force acting to lag the blade back to a radial direction imparts a negative lead-lag bending moment. This effect is evident in both the measured data and the theoretical results.

The torsion moments are also affected by the bending torsion structural coupling. Since for this configuration precone generates large flap and lead-lag bending moments, the structural torsion moment that is proportional to the product of these two moments is large. Since this moment is negative and therefore augments the tennis-racket effect, the torsion moment with precone is considerably larger than in figure 28 without precone. The structural torsion moment, since it depends on the product of flap and lead-lag bending, will vanish when either the flap or lead-lag bending moments are small. This occurs for $\theta_O \cong -2°$ where the lead-lag bending vanishes and for $\theta_O \cong 14°$ where the flap bending moment vanishes. This nonlinear behavior can be observed by the curvature in the torsion moment theoretical result which would be essentially coincident with the zero precone torsion moment at $\theta_O \cong 14°$. Although the measured torsion moments show trends similar to theory in figure 30, the absolute level of agreement is relatively poor.

For the configuration with 5° of negative droop shown in figure 31, the same basic effects are evident as for the 5° precone configuration. However, there are some perceptible differences. First, the flap-bending moments are virtually identical to the precone configuration. The lead-lag bending moments with negative droop are reduced compared to those with precone although the reduction is much more pronounced for the theoretical results than the measurements. As noted previously, the kinematics of blade pitch change introduce a lead-lag displacement in the case of blade droop but not for precone. Positive blade-pitch angles produce a corresponding lag displacement and centrifugal force acts to lead the blade back to a radial direction imparting a positive increment in lead-lag bending moment. The combined effects are partly compensating in the case of the torsion moment. For both the lead-lag bending moment and the torsion moment the comparison between theory and measured data is relatively poor, although trends are correct.

The final stiff pitch flexure configuration with 5° of positive droop is shown in figure 32. Positive droop produces a large positive flap-bending moment as centrifugal force acts to bend the blade in an upward direction parallel to the plane of rotation. The structural coupling effects again have a pronounced effect on lead-lag and torsion moments. The trends compared to the configuration without droop in figure 28 are correct but the comparison of theory and measured data is relatively poor.

The effects of precone and droop for the soft pitch flexure configuration are shown in figures 33-38. Figure 33 shows the effects of 2.5° of precone, figure 34 the effects of 2.5° of negative droop, and figure 35 the effects of 2.5° of positive droop. Figures 36-38 are repeated with 5° of

precone and droop. Since the effects with the 5° precone and droop exhibit similar, but more pronounced, characteristics than the 2.5° precone and droop, only the former results will be discussed. Compared to the results with the stiff pitch flexure and 5° precone and droop, the soft pitch flexure has very little effect on the equilibrium bending and torsion moments. Since the soft pitch flexure was strain gaged to measure pitch moments, these results show both the blade torsion moment and pitch flexure moments. In the case of 5° precone, figure 36, the two moments are nearly identical since the blade root torsion axis is parallel to the pitch flexure axis. In the case of 5° positive or negative droop, the two axes are not parallel and the principal effect is to introduce a component of lead-lag bending moment into the pitch flexure moment. The pitch flexure moments of figures 37 and 38 clearly show that negative droop at positive pitch angles and positive droop at negative pitch angles produce large positive and negative increments respectively from the torsion moments. The theory clearly shows the same trends as the measured data; however, the absolute agreement is only fair.

## CONCLUSIONS

The experimental testing of a small scale model has provided hingeless rotor stability data that can be used for validation of theoretical models. The results cover a variety of hub configurations and test conditions. The following conclusions are drawn:

1. The experimental data generally verified theoretical predictions indicating that precone, droop, and pitch control flexibility have a large impact on lead-lag damping.

2. At large pitch angles, the theory substantially overpredicts the lead-lag damping. This difference is attributed to effects of nonlinear airfoil aerodynamics which are not included in the theory.

3. The asymmetry in lead-lag damping observed at equal but opposite blade-pitch angles was extensively investigated. It is concluded that the asymmetry is not caused by asymmetrical inflow, but more likely is due to blade weight or asymmetrical airfoil characteristics.

4. At low blade-pitch angles where the theory is believed to be valid, the predicted effects of precone, droop, and pitch flexure stiffness are in close agreement with the data, confirming the validity of the elastic bending torsion coupling represented in the theory and the assumption of linear quasi-steady aerodynamics.

5. It was shown that the large structural couplings due to precone or droop are destabilizing at low blade-pitch angles. The theoretical lead-lag instability of configurations with both large precone and pitch control flexibility was experimentally demonstrated.

6. The effects of small differences between two blade sets did not greatly influence the experimental results. The experimental data from the two blade sets tested were in close agreement.

7. Agreement between predicted and measured data for rotor blade steady state bending and torsion moments was generally good including trends for the influence of precone and droop. The flap bending moments were very accurately predicted. The lead-lag bending moments corrected for the tension axis offset were predicted with fair to good accuracy. The torsion moments were predicted with fair to poor accuracy.

Ames Research Center
  National Aeronautics and Space Administration
    Moffett Field, California, April 1, 1985

# APPENDIX A

## EXPERIMENTAL MODEL PROPERTIES

### David L. Sharpe and Scott C. Ingram

The blades and hub hardware were designed and built to match the uniform blade of the theory as closely as possible. Prior to the experimental investigation, an extensive bench-test program was undertaken to measure the blade properties and to obtain the best matched set of blades. In some cases, more than one method was used to determine a specific blade property. Alternative methods of measurement were not always in agreement, and their relative accuracy is discussed below. Certain parameters that could not be effectively determined by experimental means were calculated. The radial station of each component of the model is shown in figure 39. The basic geometric properties of the experimental model are shown in table 21. The mass and stiffness properties plus the measured isolated blade frequencies for each blade are shown in table 22.

Although the blades were designed to be untwisted as indicated in table 2, a small amount of twist did exist on blade set 1; +2.3° on blade A and -0.7° on blade B. This twist is believed to be the result of blade warping during fabrication due to premature removal of the blades from the mold. Blade set 2 had zero measured twist due in part to improved fabrication techniques.

## Blade Mass Properties

The weight and chordwise center of gravity were determined for each blade. The full length blade and the fiberglass root plug (without the blade root cuff) were measured as a unit. The result for the uniform section has been experimentally determined by subtracting the mass properties of the root plug. Two different methods were used in locating the center of gravity. The first method was to simply balance the blade on a knife edge. The results from this method were considered good, i.e., within ±0.5%. For the second method, a fixture was constructed that allowed the blade to be supported while an analytical balance measured the downward force of one side of the fixture (see fig. 40). The resultant balance reading and fixture dimensions were used to calculate the location of the center of gravity. Although the resulting accuracy was about the same, the second method was found to work better for a full length blade. The weight and center of gravity for each blade are given in table 22.

The blade polar mass moment of inertia about its elastic axis was measured by swinging the blade as a pendulum about its trailing edge. The accuracy of this measurement depends on the precision of the pendular frequency measurement. The blade was suspended from tape at two locations along the trailing edge and was oscillated as shown in figure 41. A light source about the trailing edge triggered a photo cell located below the leading edge as the blade swung in and out of the light path. The frequency was determined with an electric counter connected to the photo cell output. The mass moment of inertia about the elastic axis was then calculated as:

$$\left. \begin{array}{l} I_{TE} = W r_1 / \omega^2 \\[2mm] I_{CG} = I_{TE} - \dfrac{W}{g} r_1^2 \\[2mm] I_{EA} = I_{CG} + \dfrac{W}{g} d^2 \end{array} \right\} \qquad (A1)$$

The polar moment of inertia of the fiberglass root plug was determined separately and the results were subtracted from the measured result for the combined blade and plug. This yields the inertia values for the uniform section given in table 22.

## Blade Elastic Axis

The chordwise elastic axis is defined as the position along the chord line where a force applied normal to the chord line causes no torsional deflection. For the elastic axis determination, the blade was mounted vertically with the root end clamped in a fixture, figure 42. A small mirror was mounted on the leading edge near the blade tip, perpendicular to the chord line. An auto collimator was aligned with the mirror and a slide table with a mounted pointer was used to deflect the blade in the flap direction. The reflection of the cross hairs was observed in the auto collimator as the slide table was moved to deflect the blade with the pointer applied at different chord positions. The observed image of the cross hairs indicated the true magnitude of the blade torsional deformation. The slide table chordwise position was changed until a chord location was found at which the pointer deflected the blade about the flap axis only, with no torsional deflection present. The elastic axis for each blade is given in table 22.

## Nonrotating Blade Frequencies

The nonrotating blade, flap, chord, and torsional frequencies were measured for each isolated blade. The blades were mounted vertically on a solid plate at the blade root cuff flange with the tips up. The blades were manually excited and modal frequencies were derived from the blade surface mounted strain gage signals that were analyzed on a spectral analyzer. The first mode flapping, chord, and torsional frequencies for each blade are given in table 22.

## Blade Stiffness

The flapping stiffness $EI_\beta$, chord stiffness $EI_\zeta$, and torsional stiffness $GJ$, were determined using two approaches. The first was the moment-deflection method. This method of stiffness determination begins with the blade mounted in a clamp fixture and suspended vertically. A micrometer slide table was positioned so that a load cell mounted on the table would deflect the blade and measure the applied force as the slide table was moved toward the blade. A linear motion transducer measured the amount of travel of the table. The electrical output of the load cell and motion transducer was recorded by a data acquisition system and a real time plot of force, $F$, vs deflection, $\delta$, was made. The slope of this curve and the free length, $L'$, the distance from the fixed attachment to the point that the load cell contacted the blade, were used in a simple beam theory calculation to determine blade stiffness.

$$EI = \frac{F(L')^3}{3\delta} \tag{A2}$$

For the flap stiffness measurement, figure 43, the load cell probe contacted the blade at the quarter chord position. The slide table motion deflected the blade tip in the flap direction to a maximum of approximately 3 cm with a force of about 2.67 N. For the chord stiffness measurements, the slide table and the load cell were positioned to direct the applied force along the chord line. Because of the higher stiffness in the chord direction, the maximum applied calibration load was of the order of 5.71 N with resultant deflections of approximately 0.33 cm. A possible source of error in this measurement was root rotation of the clamp fixture which held the blade. For the chord measurement, the applied load is relatively large and hence the potential error is larger. These measurements were repeated after the blade root had been bonded into the aluminum blade root cuff. However, root rotation was not measured and it remains a possible source of error. A second possible source of error, which could only be minimized and not entirely eliminated, was due to the higher chord stiffness compared to flap and torsion. This made it difficult to apply pure chord loads with resultant pure chord deflections.

The determination of torsional stiffness was made with the blade mounted the same as in the case of flap and chord. The slide table, however, was replaced with a rotary table with a torque cell attached. The table was then positioned such that a fixture mounted on top of the torque cell could be clamped on the tip of the blade without deflecting the blade. The rotary table was positioned so the torsional axis was at the 25% chord position. The electrical outputs from the torque cell and rotary table were recorded by the data system and plotted as torque, $M_\theta$, versus angular deflection, $\theta$. The slope of the curve and the measured free length of the blade, $L'$, were used to calculate torsional stiffness from beam theory.

$$GJ = \frac{M_\theta}{\theta} L' \tag{A3}$$

The second, and possibly more accurate, method of evaluating blade stiffness used the measured frequencies and blade mass properties. Frequencies can easily be measured within ±1%, and blade weight may also be determined with this accuracy. The stiffness can then be derived from elementary beam and rod theory as follows:

$$EI_\beta = (1/12.4)\mu L^4 \omega_{\beta NR}^2 \tag{A4}$$

$$EI_\zeta = (1/12.4)\mu L^4 \omega_{\zeta NR}^2 \tag{A5}$$

$$GJ = \left(\frac{2\omega_{\theta NR}}{\pi}\right)^2 I_{EA} L \tag{A6}$$

Even though the accuracy of the measured torsional frequency, $\omega_{\theta NR}$, is considered to be as good as the flap and chord frequency measurements, the confidence level in stiffness determination by this method is not as high. The required polar mass moment of inertia property used in the equation (A6) is not as easily and precisely determined as the blade weight.

The stiffness values obtained from the frequency and mass property measurements are shown in table 22 and are used for the theoretical predictions. A comparison of stiffness values determined by the two methods is shown in table 23 for each of the four blades used in the experiment. The percent differences in stiffness as derived by these two methods are also shown.

## Pitch Flexure Stiffness

The pitch flexure torsional stiffness, $K_\theta$, was first determined for each of the soft pitch flexures by applying a series of known moments, $M_{\theta F}$, to the free end of a bench mounted flexure, figure 44, and recording the angular

deflection, $\theta$, of the free end. These measurements were then used to calculate $K_\theta$ by:

$$K_\theta = \frac{M_\theta F}{\theta} \qquad (A7)$$

This method provided an experimental value of $K_\theta$ = 36.39 N-m/rad. It is believed that some inaccuracy might exist in these measurements owing to the small angles involved.

A second method was used to determine this spring constant by mounting the flexure as the spring element in a torsional pendulum. Assuming a single degree of freedom, the relationship between the torsional stiffness and the pendular frequency and inertia is:

$$K_\theta = I\omega^2 \qquad (A8)$$

This method used a steel disk and a rectangular cross-section steel bar, two simple geometric solids whose polar moments of inertia were easily calculated. The frequency was measured using the signals from the torsional strain gages located on the flexure webs. The pitch flexure spring constants determined from the bar and the disk agreed within less than 2%. The final value of the torsional spring stiffness was determined to be $K_\theta$ = 41.21 N-m/rad, approximately 12% greater than that measured by the moment-deflection method. The frequency-inertia results are considered to be the more accurate results.

The torsional stiffness of the stiff pitch flexure and the bending stiffness of both stiff and soft pitch flexures were calculated from geometric characteristics given in figure 45. These calculated results and the frequency derived experimental value of the torsional stiffness for the soft pitch flexure are summarized in table 24.

#### Hub Hardware Mass and Inertia

The mass and stiffness properties of the components outboard of the torsional flexure shown in figure 46 have been calculated or experimentally determined to provide the best description of each component for the theoretical predictions. The hub components outboard of the pitch flexure were weighed on an electronic balance; the mass of the outboard flange of the pitch flexure was calculated. The polar moment of inertia about the quarter chord of each component outboard of the soft pitch flexure could have been calculated, but an experimental method was considered more accurate. Each component of the hub hardware was secured, separately and in combination, to the soft pitch flexure, figure 47. The inboard flange of the pitch flexure was rigidly clamped to a surface plate and the assembly manually excited. From the torsional spring constant $K_\theta$ established earlier, and the measured frequency, the polar moment of

inertia for each component was found. The mass and inertia for all hub components are given in table 25.

#### Rotor Blade Mass and Stiffness Summary

The results of the mass and stiffness property determination of the blade, pitch flexure, and hub hardware are summarized as a function of blade span in tables 26 and 27. Table 26 contains mass per unit length and polar moment of inertia distributions and table 27 contains flap bending stiffness, chord bending stiffness, and torsional rigidity distributions. The mass and stiffness values for the pitch flexure web span pertain to the soft pitch flexure only.

#### Strain Gage Interaction Calibration

The surface mounted strain gages used to measure both dynamic and steady state response were attached to each individual blade in the conventional fashion. Each strain gage bridge, consisting of four gages, was attached to both upper and lower surfaces of the blade and was electrically connected so that each independent bridge measured, as nearly as possible, only that strain resulting from a uniaxially applied moment. Because interactions between the flap, lead-lag and torsion moments cannot be totally eliminated, an interaction matrix for each blade was determined by precisely loading the blades in one direction at a time and then recording output voltages on all three strain gage bridges. This yielded a set of calibrated interaction equations described by the matrix relationship:

$$\begin{Bmatrix} V_\beta \\ V_\zeta \\ V_\theta \end{Bmatrix} = \begin{bmatrix} \partial V_\beta/\partial M_\beta & \partial V_\beta/\partial M_\zeta & \partial V_\beta/\partial M_\theta \\ \partial V_\zeta/\partial M_\beta & \partial V_\zeta/\partial M_\zeta & \partial V_\zeta/\partial M_\theta \\ \partial M_\theta/\partial M_\beta & \partial V_\theta/\partial M_\zeta & \partial V_\theta/\partial M_\theta \end{bmatrix} \begin{Bmatrix} M_\beta \\ M_\zeta \\ M_\theta \end{Bmatrix} \qquad (A9)$$

or

$$\{V\} = [C]\{M\} \qquad (A10)$$

giving

$$\{M\} = [C]^{-1}\{V\} \qquad (A11)$$

The coefficients of $[C]^{-1}$ were obtained for each blade by individual calibrations. These matrices, stored in the data analysis computer program, were then multiplied by voltage outputs from the three strain gage bridges to give uncoupled flap, lead-lag, and torsion steady moments.

### Lead-Lag Bending Moment and Blade Tension Interaction

Although the correlation between theory and experiment was fair to good for flap bending and torsion moments, initially the correlation of the lead-lag moments was found to be quite poor, with the experiment showing more than seven times the predicted value at zero blade-pitch angle. A typical example is shown in figure 48. The discrepancy in lead-lag moment is approximately 4 N-m. All blades used during the experiment showed the same magnitude of lead-lag moment and the discrepancy was observed to be a function of the square of the rotor speed. Thus, it appeared that this discrepancy was the result of a centrifugally induced moment unaccounted for.

Two potential sources were examined: 1) an offset of the blade section mass center forward of a radial line from the hub center such that centrifugal force will create a negative lead-lag bending moment, and 2) structural interactions within the blade due to centrifugal loading. The hub components were precisely measured and revealed no spurious chordwise offset or sweep of the blade. The blade itself was carefully measured along the leading-edge to determine if any residual sweep existed from bonding the root cuff to the blade. For blade A, the root to tip offset was found to be 1.016 mm which is equivalent to an angular sweep of 0.067°. The centrifugally induced lead-lag bending moment resulting from blade sweep can be calculated from the following equation:

$$M_\zeta = -\Omega^2 \, \frac{WeR^2}{2g} \, \zeta \qquad (A12)$$

The resulting lead-lag moment of –0.147 N-m is insufficient to account for the difference between theory and measurement.

To determine the effect of centrifugal loading on lead-lag bending moments, several static loading tests were performed. To eliminate bending which is due to improper loading, the rotor blade was suspended vertically, tip down, by a steel cable approximately 6 m in length. A fixture was bonded to the blade tip, and a weight pan attached so that the tensile force would act through the quarter chord. The blade was incrementally loaded up to the centrifugal force at 1000 rpm of 1779 N. The lead-lag bending versus tensile loading is shown in figure 49. The magnitude of lead-lag bending due to the tensile load at 1779 N is nearly identical to the difference between the experimental measurements and the theoretical predictions.

Although the blades were designed to place the tension axis (or chordwise neutral axis) at the section quarter chord location, the results of the tensile loading test gave strong indication that the tension axis was in fact offset from the intended location. Additional tensile loading tests were performed to determine the location of the tension axis. The blade was loaded as described previously; however, the blade root and tip loading fixtures were modified so that the load could be applied at chordwise locations other than the quarter chord. The results of these tests are shown in figure 50 for three different chordwise loading locations: 25, 27, and 27.4%. For the load at 27.4% chord, a near zero lead-lag moment interaction with tensile load is evident. The chord location where zero lead-lag bending/tensile loading interaction occurs defines the tension axis. Extrapolating the loading measurements to this condition yields a tension axis location of 27.45% chord.

This empirically determined tension axis was used to correct the measured steady lead-lag bending moments. The tension axis displacement from the blade chordwise center of gravity, 0.0245 c, multiplied by the centrifugal force at the operating rpm, in combination with the measured blade sweep contribution of equation (A12) is used to calculate the value of the lead-lag bending moment tare correction discussed above.

# APPENDIX B

# THEORETICAL MODEL

The theoretical methods used to predict stability results presented in this report are developed and described in references 1-4. This theory specifically addresses the structural, dynamic, and aeroelastic characteristics of elastic cantilevered rotor blades, particularly the nonlinear coupling between bending and torsion motions of such blades. The analysis is specialized to treat blades having uniform radial distributions of mass and stiffness properties.

Reference 1 presents the development of the basic structural dynamic equations of motion for bending and torsion of rotating cantilever blades including precone. Reference 2 extended the theory to include structural coupling of flap and lead-lag bending, and a derivation of the aerodynamic forces required for aeroelastic stability analysis in the hovering flight condition. The nonlinear equations of reference 2 were solved by first transforming the partial differential equations to nonlinear ordinary differential equations using Galerkin's method. The resulting nonlinear equations for the modal amplitudes were linearized for small perturbation motions about the steady state equilibrium operating condition and these linear equations were then solved by standard eigenanalysis techniques to yield the frequency and damping of each modal degree of freedom. The nonlinear algebraic equilibrium equations were iteratively solved to yield the equilibrium modal deflections of the blade since these results were required to evaluate the coefficients of linearized perturbation equations. Reference 2 presented equilibrium and stability results for a variety of rotor blade configurations. The theory was further extended in reference 3 to include additional structural details. These details included a blade pitch degree of freedom with spring restraint to represent pitch link or control system flexibility, blade twist, blade droop, torque offset, and hub offset. Typical results for such configurations were presented in reference 4.

The aerodynamic theory used for references 2-4 was limited to the hover flight condition and was based on a two-dimensional blade element strip theory analysis. The unsteady aerodynamic lift and moment acting on the blade are based on Greenberg's extension of Theodorsen's theory for an airfoil undergoing sinusoidal motion in a pulsating incompressible flow. A quasi-steady approximation of the unsteady theory for low reduced frequency is employed where the Theodorsen function is taken to be unity. The airfoil drag characteristics are represented by constant profile drag coefficient. The steady induced inflow for the rotor is calculated from classical momentum theory.

Although the experiment was designed to achieve as close a match as possible between the physical model rotor system and the theoretical representation, the theory was incomplete in several respects. It does not include:

1. Gravitational forces that produce small changes in the equilibrium deflection of the blade and that may indirectly influence the lead-lag damping.

2. The effects of aerodynamic center, mass center, elastic axis, or tension axis offsets from the airfoil quarter chord location. These offsets were designed to be as small as possible in the present experiment.

3. The effects of nonlinear airfoil section aerodynamics. At low Reynolds numbers, the profile drag and lift coefficients depart from constant and linear behavior, respectively, even at low angles of attack. The theory is not considered applicable for the present experimental results for moderate or large blade-pitch angles.

4. The theory does not account for bending flexibility of blade or hub structure inboard of the point where the flexible blade portion begins. These components, including the pitch flexures, were treated as infinitely stiff in bending.

The theoretical results for the steady state blade bending and torsion moments presented herein were not calculated using the nonlinear equilibrium equations developed in references 2 and 3. The modal solution technique is sufficiently accurate for calculating displacements, but is generally not reliable for calculating bending moments unless a very large number of modes are included or other precautions are taken. Therefore, the theoretical predictions for steady state moments were obtained using an alternative method. This method is based on a finite element analysis using variable order nonlinear beam elements currently under development at the Aeromechanics Laboratory. Although the technique for solving the equations is substantially different from the Galerkin analysis described above, the underlying structural dynamic and aerodynamic theory of the finite element approach is identical with the former analysis. Therefore, the comparison of theoretical and experimental results for steady state loads is considered to be a valid test of the structural dynamic and aerodynamic theory developed in references 1-3. Although the finite element analysis has not yet been published, related early results preceding this development may be found in references 9 and 10.

The measured physical properties of the model rotor components were presented in tables 21-27. These property values were used to calculate the specific dimensionless configuration parameters required for the coefficients of the theoretical equations of reference 3. A collection of these dimensionless parameters is given in table 28. Several adjustments to the theory were made to accommodate inconsistencies between the theoretical and experimental configurations.

The theory was modified to include the inertial effect on the blade torsional frequency of the blade root components outboard of the pitch flexure. The measured torsional stiffness of the pitch flexures was analytically corrected to account for centrifugal stiffening according to the following equation:

$$f_{rot} = f + 2.974\bar{\Omega}^2 \qquad (B1)$$

Table 28 presents parameter values for both blade sets. In case of differences between the two blades in each set, the values were combined within each blade set. The theoretical results were calculated using the parameter values of blade set 2 unless otherwise noted. The steady state loads were calculated using properties for blade A of blade set 2.

# REFERENCES

1. Hodges, D. H.; and Dowell, E. H.: Nonlinear Equations of Motion for the Elastic Bending and Torsion of Twisted Nonuniform Rotor Blades, NASA TN D-7818, 1974.

2. Hodges, D. H.; and Ormiston, R. A.: Stability of Elastic Bending and Torsion of Uniform Cantilever Rotor Blades in Hover with Variable Structural Coupling, NASA TN D-8192, April 1976.

3. Hodges, D. H.: Nonlinear Equations of Motion for Cantilever Rotor Blades in Hover With Pitch Link Flexibility, Twist, Precone, Droop, Sweep, Torque Offset, and Blade Root Droop, NASA TM X-73,112, May 1976.

4. Hodges, Dewey H.; and Ormiston, R. A.: Stability of Hingeless Rotor Blades in Hover with Pitch-Link Flexibility, AIAA Journal, vol. 15, no. 4, Apr. 1977, pp. 476-482.

5. Ormiston, R. A.; and Bousman, W. G.: A Theoretical and Experimental Investigation of Flap-Lag Stability of Hingeless Helicopter Rotor Blades, NASA TM X-62,179, Aug. 1972.

6. Ormiston, R. A.; and Bousman, W. G.: A Study of Stall Induced Flap-Lag Instability of Hingeless Rotors, J. Am. Helicop. Soc., vol. 29, no. 1, Jan. 1975, pp. 20-30.

7. Bousman, W. G.; Sharpe, D. L.; and Ormiston, R. A.: An Experimental Study of Techniques for Increasing the Lead-Lag Damping of Soft Inplane Hingeless Rotors, Preprint no. 1035, Proceedings AHS 32nd National Forum, Washington, D.C., May 1976.

8. Bousman, William G.; and Winkler, Diana J.: Application of the Moving-Block Analysis, Proceedings, AIAA/ASME/ASCE/AHS 22nd Structures, Structural Dynamics, and Materials Conference, Atlanta, Ga., Apr. 1981, pp. 755-763.

9. Hodges, Dewey H.: Vibration and Response of Nonuniform Rotating Beams with Discontinuities, J. Am. Helicop. Soc., vol. 33, no. 4, Oct. 1979, pp. 43-50.

10. Hodges, Dewey H.; and Rutkowski, Michael J.: Free-Vibration Analysis of Beams by a Variable-Order Finite-Element Method, AIAA Journal, vol. 19, no. 11, Nov. 1981, pp. 1459-1466.

## TABLE 1. TEST MATRIX (BLADE SET 1 ----, BLADE SET 2 —— )

| PITCH FLEXURE | PRECONE ANGLE, deg | DROOP ANGLE, deg | BLADE PITCH ANGLE, deg |
|---|---|---|---|
| STIFF | 0 | 0 | |
| | 0 | -2.5 | |
| | 0 | -5.0 | |
| | 0 | 2.5 | |
| | 0 | 5.0 | |
| | 2.5 | 0 | |
| | 5.0 | 0 | |
| SOFT | 0 | 0 | |
| | 0 | -2.5 | |
| | 0 | -5.0 | |
| | 0 | 2.5 | |
| | 0 | 5.0 | |
| | 2.5 | 0 | |
| | 5.0 | 0 | |

Blade pitch angle scale: -16  -14  -12  -10  -8  -6  -4  -2  0  2  4  6  8  10  12  14  16

### TABLE 2.– MEASURED LEAD-LAG FREQUENCY AND DAMPING, BLADE SET 1, $\beta_{pc} = 0°, \beta_d = 0°$, STIFF PITCH FLEXURE

| Blade pitch angle, deg | rpm | Lead-lag frequency, Hz | Lead-Lag damping, rad/sec | Blade pitch angle, deg | rpm | Lead-lag frequency, Hz | Lead-lag damping, rad/sec |
|---|---|---|---|---|---|---|---|
| 0 | 0 | 24.50 | -1.305 | 4 | 1000 | 25.60 | -1.969 |
| 0 | 500 | 24.81 | -1.426 | 4 | 1000 | 25.60 | -1.950 |
| 0 | 500 | 24.81 | -1.521 | 4 | 1000 | 25.60 | -2.172 |
| 0 | 550 | 24.81 | -1.371 | 6 | 0 | 24.24 | -1.163 |
| 0 | 550 | 24.81 | -1.403 | 6 | 0 | 24.24 | -1.166 |
| 0 | 600 | 24.87 | -1.417 | 6 | 600 | 24.64 | -1.259 |
| 0 | 600 | 24.81 | -1.472 | 6 | 600 | 24.62 | -1.057 |
| 0 | 650 | 25.00 | -1.448 | 6 | 600 | 24.62 | -1.103 |
| 0 | 650 | 24.81 | -1.340 | 6 | 750 | 25.00 | -0.694 |
| 0 | 700 | 25.02 | -1.420 | 6 | 750 | 25.20 | -0.694 |
| 0 | 700 | 25.00 | -1.531 | 6 | 900 | 25.40 | -1.738 |
| 0 | 750 | 25.09 | -1.486 | 6 | 900 | 25.40 | -1.704 |
| 0 | 750 | 25.00 | -1.586 | 6 | 1000 | 25.60 | -1.731 |
| 0 | 800 | 25.20 | -1.847 | 6 | 1000 | 25.60 | -2.258 |
| 0 | 800 | 25.20 | -1.821 | 8 | 0 | 24.24 | -1.173 |
| 0 | 850 | 25.20 | -1.767 | 8 | 600 | 24.43 | -1.035 |
| 0 | 850 | 25.20 | -1.699 | 8 | 600 | 24.43 | -1.296 |
| 0 | 900 | 25.20 | -1.670 | 8 | 0 | 24.20 | -1.225 |
| 0 | 900 | 25.40 | -1.694 | 8 | 600 | 24.43 | -0.837 |
| 0 | 950 | 25.40 | -1.694 | 8 | 600 | 24.43 | -0.952 |
| 0 | 950 | 25.40 | -1.948 | 8 | 900 | 25.60 | -1.571 |
| 0 | 1000 | 25.40 | -1.703 | 8 | 900 | 25.60 | -1.796 |
| 0 | 1000 | 25.40 | -1.609 | 8 | 1000 | 25.95 | -1.513 |
| 2 | 0 | 24.40 | -1.426 | 8 | 1000 | 25.95 | -2.134 |
| 2 | 600 | 24.81 | -1.402 | 10 | 0 | 24.19 | -1.177 |
| 2 | 600 | 24.81 | -1.321 | 10 | 0 | 24.19 | -0.962 |
| 2 | 750 | 24.81 | -1.575 | 10 | 600 | 24.22 | -0.898 |
| 2 | 750 | 24.81 | -0.837 | 10 | 800 | 24.90 | -0.898 |
| 2 | 1000 | 25.50 | -1.728 | 10 | 800 | 24.90 | -1.368 |
| 2 | 1000 | 25.40 | -2.050 | 10 | 1000 | 25.95 | -2.151 |
| 2 | 900 | 25.40 | -1.725 | 10 | 1000 | 25.95 | -2.083 |
| 2 | 900 | 25.20 | -1.765 | 10 | 0 | 24.24 | -1.230 |
| 4 | 0 | 24.42 | -1.137 | 10 | 600 | 24.25 | -1.025 |
| 4 | 600 | 24.10 | -1.493 | 10 | 600 | 24.43 | -0.878 |
| 4 | 600 | 24.81 | -1.246 | 10 | 900 | 25.69 | -1.623 |
| 4 | 750 | 24.98 | -2.157 | 10 | 900 | 25.60 | -1.271 |
| 4 | 900 | 25.40 | -1.784 | 10 | 1000 | 26.15 | -1.984 |
| 4 | 900 | 25.40 | -1.746 | 10 | 1000 | 26.15 | -1.831 |

TABLE 3.– MEASURED LEAD-LAG FREQUENCY AND DAMPING, BLADE SET 1,
$\beta_{pc} = 0°, \beta_d = -2.5°$, STIFF PITCH FLEXURE

| Blade pitch angle, deg | rpm | Lead-lag frequency, Hz | Lead-Lag damping, rad/sec | Blade pitch angle, deg | rpm | Lead-lag frequency, Hz | Lead-lag damping, rad/sec |
|---|---|---|---|---|---|---|---|
| 0 | 0 | 24.20 | -1.205 | 6 | 1000 | 25.40 | -1.489 |
| 0 | 0 | 24.19 | -1.213 | 8 | 0 | 24.19 | -1.217 |
| 0 | 600 | 24.29 | -1.678 | 8 | 600 | 24.60 | -1.292 |
| 0 | 600 | 24.24 | -1.580 | 8 | 600 | 24.62 | -1.198 |
| 0 | 900 | 24.53 | -1.717 | 8 | 900 | 25.40 | -1.411 |
| 0 | 900 | 24.43 | -1.709 | 8 | 900 | 25.20 | -1.593 |
| 0 | 1000 | 24.68 | -1.588 | 8 | 1000 | 25.60 | -2.021 |
| 0 | 1000 | 24.61 | -1.467 | 8 | 1000 | 25.60 | -2.122 |
| 2 | 0 | 24.19 | -1.239 | 10 | 0 | 24.08 | -1.179 |
| 2 | 600 | 24.24 | -1.723 | 10 | 600 | 24.43 | -1.216 |
| 2 | 600 | 24.43 | -1.394 | 10 | 600 | 24.43 | -1.089 |
| 2 | 900 | 24.62 | -1.589 | 10 | 900 | 25.39 | -1.668 |
| 2 | 900 | 24.62 | -1.494 | 10 | 900 | 25.39 | -1.533 |
| 2 | 1000 | 24.62 | -1.297 | 10 | 1000 | 25.81 | -1.519 |
| 2 | 1000 | 24.62 | -1.445 | 10 | 1000 | 25.81 | -1.923 |
| 4 | 0 | 24.00 | -1.310 | 12 | 0 | 24.00 | -1.180 |
| 4 | 0 | 24.00 | -1.291 | 12 | 600 | 24.24 | -1.088 |
| 4 | 600 | 24.43 | -1.370 | 12 | 600 | 24.43 | -0.981 |
| 4 | 600 | 24.43 | -1.486 | 12 | 900 | 25.40 | -1.427 |
| 4 | 900 | 24.62 | -1.477 | 12 | 900 | 25.40 | -1.507 |
| 4 | 900 | 24.62 | -1.459 | 12 | 1000 | 25.76 | -2.152 |
| 4 | 1000 | 24.81 | -1.459 | 14 | 0 | 23.81 | -1.254 |
| 4 | 1000 | 24.81 | -1.548 | 14 | 600 | 24.18 | -1.166 |
| 6 | 0 | 24.00 | -1.208 | 14 | 600 | 24.18 | -1.044 |
| 6 | 600 | 24.62 | -1.219 | 14 | 900 | 25.40 | -1.174 |
| 6 | 600 | 24.62 | -1.056 | 14 | 900 | 25.40 | -1.198 |
| 6 | 900 | 25.20 | -1.419 | 14 | 1000 | 26.15 | -1.192 |
| 6 | 900 | 25.20 | -1.518 | 14 | 1000 | 25.95 | -1.651 |
| 6 | 1000 | 25.40 | -1.630 | | | | |

TABLE 4.— MEASURED LEAD-LAG FREQUENCY AND DAMPING, BLADE SET 1,
$\beta_{pc} = 0°, \beta_d = -5.0°$, STIFF PITCH FLEXURE

| Blade pitch angle, deg | rpm | Lead-lag frequency, Hz | Lead-Lag damping, rad/sec | Blade pitch angle, deg | rpm | Lead-lag frequency, Hz | Lead-lag damping, rad/sec |
|---|---|---|---|---|---|---|---|
| 10 | 0 | 24.00 | -1.124 | 6 | 1000 | 25.00 | -1.729 |
| 10 | 600 | 24.43 | -1.527 | 4 | 0 | 24.00 | -1.164 |
| 10 | 600 | 24.62 | -1.448 | 4 | 600 | 24.19 | -1.834 |
| 10 | 900 | 25.00 | -1.703 | 4 | 600 | 24.20 | -1.763 |
| 10 | 900 | 25.00 | -1.558 | 4 | 900 | 24.62 | -1.831 |
| 10 | 1000 | 25.40 | -2.332 | 4 | 900 | 24.62 | -1.851 |
| 10 | 1000 | 25.40 | -2.211 | 4 | 1000 | 24.81 | -1.707 |
| 12 | 0 | 24.00 | -1.154 | 4 | 1000 | 24.81 | -1.640 |
| 12 | 0 | 24.00 | -1.137 | 2 | 0 | 24.00 | -1.239 |
| 12 | 600 | 24.43 | -1.174 | 2 | 600 | 24.00 | -1.915 |
| 12 | 600 | 24.43 | -1.121 | 2 | 600 | 24.19 | -1.858 |
| 12 | 900 | 25.40 | -1.464 | 2 | 900 | 24.43 | -1.953 |
| 12 | 900 | 25.40 | -2.001 | 2 | 900 | 24.62 | -1.985 |
| 12 | 1000 | 25.60 | -1.472 | 2 | 1000 | 24.62 | -1.758 |
| 12 | 1000 | 25.76 | -1.279 | 2 | 1000 | 24.62 | -1.741 |
| 8 | 0 | 24.00 | -1.206 | 0- | 0 | 24.19 | -1.147 |
| 8 | 0 | 24.00 | -1.182 | 0 | 600 | 24.00 | -1.906 |
| 8 | 600 | 24.62 | -1.402 | 0 | 900 | 24.00 | -1.883 |
| 8 | 600 | 24.43 | -1.597 | 0 | 900 | 24.43 | -2.621 |
| 8 | 900 | 25.00 | -1.693 | 0 | 1000 | 24.62 | -2.516 |
| 8 | 900 | 25.00 | -1.645 | 0 | 1000 | 24.62 | -2.198 |
| 8 | 1000 | 25.20 | -2.116 | 0 | 1000 | 24.62 | -2.294 |
| 8 | 1000 | 25.40 | -1.622 | 14 | 0 | 23.81 | -1.129 |
| 6 | 0 | 24.00 | -1.217 | 14 | 600 | 24.43 | -1.088 |
| 6 | 600 | 24.43 | -1.757 | 14 | 600 | 24.43 | -1.103 |
| 6 | 600 | 24.43 | -1.781 | 14 | 900 | 25.48 | -1.480 |
| 6 | 900 | 24.81 | -1.749 | 14 | 900 | 25.40 | -1.234 |
| 6 | 900 | 24.81 | -1.661 | 14 | 1000 | 25.95 | -1.050 |
| 6 | 1000 | 25.00 | -1.873 | 14 | 1000 | 25.95 | -2.122 |

TABLE 5.– MEASURED LEAD-LAG FREQUENCY AND DAMPING, BLADE SET 1,
$\beta_{pc} = 0°, \beta_d = 2.5°$, STIFF PITCH FLEXURE

| Blade pitch angle, deg | rpm | Lead-lag frequency, Hz | Lead-Lag damping, rad/sec | Blade pitch angle, deg | rpm | Lead-lag frequency, Hz | Lead-lag damping, rad/sec |
|---|---|---|---|---|---|---|---|
| 0 | 0 | 24.43 | -1.572 | 2 | 1000 | 25.40 | -2.011 |
| 0 | 600 | 24.43 | -1.653 | 4 | 0 | 24.43 | -1.189 |
| 0 | 700 | 24.62 | -1.507 | 4 | 600 | 24.43 | -1.141 |
| 0 | 700 | 24.62 | -1.808 | 4 | 600 | 24.43 | -1.108 |
| 0 | 800 | 24.81 | -1.683 | 4 | 900 | 25.20 | -1.835 |
| 0 | 800 | 24.81 | -1.572 | 4 | 900 | 25.20 | -1.959 |
| 0 | 900 | 25.00 | -1.494 | 4 | 1000 | 25.40 | -2.252 |
| 0 | 900 | 25.00 | -1.551 | 4 | 1000 | 25.40 | -2.236 |
| 0 | 1000 | 25.20 | -1.488 | 6 | 0 | 25.28 | -1.316 |
| 0 | 1000 | 25.20 | -1.388 | 6 | 0 | 24.24 | -1.133 |
| 2 | 0 | 24.24 | -1.244 | 6 | 600 | 24.24 | -0.880 |
| 2 | 600 | 24.43 | -1.276 | 6 | 900 | 25.20 | -1.905 |
| 2 | 600 | 24.43 | -1.609 | 6 | 900 | 25.20 | -2.267 |
| 2 | 900 | 25.27 | -1.951 | 6 | 1000 | 25.60 | -2.126 |
| 2 | 900 | 25.00 | -1.872 | 6 | 1000 | 25.60 | -2.655 |
| 2 | 1000 | 25.40 | -2.074 | | | | |

TABLE 6.– MEASURED LEAD-LAG FREQUENCY AND DAMPING, BLADE SET 1,
$\beta_{pc} = 2.5°, \beta_d = 0°$, STIFF PITCH FLEXURE

| Blade pitch angle, deg | rpm | Lead-lag frequency, Hz | Lead-Lag damping, rad/sec | Blade pitch angle, deg | rpm | Lead-lag frequency, Hz | Lead-lag damping, rad/sec |
|---|---|---|---|---|---|---|---|
| 0 | 0 | 24.19 | -1.272 | 8 | 1000 | 25.60 | -1.789 |
| 0 | 600 | 24.43 | -1.484 | 8 | 1000 | 25.60 | -1.810 |
| 0 | 900 | 25.00 | -2.259 | 10 | 0 | 24.00 | -1.218 |
| 0 | 1000 | 25.19 | -1.889 | 10 | 600 | 24.43 | -1.123 |
| 2 | 0 | 24.19 | -1.299 | 10 | 900 | 25.40 | -1.437 |
| 2 | 600 | 24.62 | -1.503 | 10 | 1000 | 25.81 | -1.775 |
| 2 | 900 | 25.00 | -1.846 | 10 | 1000 | 25.81 | -1.884 |
| 2 | 1000 | 25.20 | -1.679 | 10 | 600 | 24.43 | -1.689 |
| 2 | 1000 | 25.20 | -1.638 | 12 | 0 | 23.89 | -1.249 |
| 4 | 0 | 24.19 | -1.247 | 12 | 600 | 24.24 | -1.069 |
| 4 | 600 | 24.62 | -1.447 | 12 | 900 | 25.40 | -1.197 |
| 4 | 900 | 25.20 | -1.692 | 12 | 1000 | 25.95 | -1.697 |
| 4 | 1000 | 25.20 | -1.735 | 12 | 1000 | 25.95 | -1.782 |
| 6 | 0 | 24.00 | -1.272 | 14 | 0 | 23.81 | -1.185 |
| 6 | 600 | 24.62 | -1.361 | 14 | 600 | 24.19 | -1.102 |
| 6 | 900 | 25.19 | -1.671 | 14 | 900 | 25.43 | -1.109 |
| 6 | 1000 | 25.40 | -1.708 | 14 | 1000 | 25.64 | -1.815 |
| 6 | 1000 | 25.40 | -1.793 | 14 | 1000 | 26.15 | -1.494 |
| 8 | 0 | 24.00 | -1.221 | 16 | 0 | 23.81 | -1.187 |
| 8 | 600 | 24.41 | -1.281 | 16 | 600 | 23.93 | -1.952 |
| 8 | 900 | 25.20 | -1.684 | | | | |

## TABLE 7.— MEASURED LEAD-LAG FREQUENCY AND DAMPING, BLADE SET 1, $\beta_{pc} = 0°, \beta_d = 0°$, SOFT PITCH FLEXURE

| Blade pitch angle, deg | rpm | Lead-lag frequency, Hz | Lead-Lag damping, rad/sec | Blade pitch angle, deg | rpm | Lead-lag frequency, Hz | Lead-lag damping, rad/sec |
|---|---|---|---|---|---|---|---|
| 0 | 0 | 22.05 | -1.145 | 8 | 600 | 22.05 | -1.031 |
| 0 | 600 | 22.40 | -1.204 | 8 | 900 | 23.26 | -2.155 |
| 0 | 600 | 22.40 | -1.178 | 8 | 900 | 23.26 | -2.020 |
| 0 | 900 | 22.73 | -1.188 | 8 | 1000 | 23.62 | -3.166 |
| 0 | 900 | 22.73 | -1.163 | 8 | 1000 | 23.62 | -3.247 |
| 0 | 1000 | 22.90 | -1.113 | 10 | 0 | 22.05 | -1.085 |
| 0 | 1000 | 22.91 | -1.110 | 10 | 600 | 22.71 | -1.225 |
| 2 | 0 | 22.05 | -1.183 | 10 | 600 | 22.88 | -1.158 |
| 2 | 600 | 22.40 | -1.189 | 10 | 900 | 23.27 | -2.396 |
| 2 | 600 | 22.40 | -1.191 | 10 | 900 | 23.26 | -2.119 |
| 2 | 900 | 22.71 | -1.485 | 10 | 1000 | 24.00 | -2.616 |
| 2 | 900 | 22.73 | -1.407 | 10 | 1000 | 24.00 | -3.130 |
| 2 | 1000 | 22.90 | -1.631 | -10 | 0 | 22.06 | -1.123 |
| 2 | 1000 | 22.90 | -1.603 | -10 | 600 | 22.06 | -1.067 |
| 4 | 0 | 22.00 | -1.120 | -10 | 600 | 22.05 | -1.023 |
| 4 | 600 | 22.40 | -1.050 | -10 | 900 | 23.00 | -3.275 |
| 4 | 600 | 22.40 | -1.035 | -10 | 1000 | 23.38 | -4.248 |
| 4 | 900 | 22.95 | -1.579 | -10 | 1000 | 23.44 | -3.993 |
| 4 | 900 | 22.90 | -1.632 | -12 | 0 | 22.06 | -1.234 |
| 4 | 1000 | 23.15 | -2.175 | -12 | 600 | 22.06 | -1.222 |
| 4 | 1000 | 23.08 | -2.185 | -12 | 600 | 21.71 | -1.401 |
| 6 | 0 | 22.05 | -1.082 | -12 | 900 | 23.08 | -3.947 |
| 6 | 600 | 22.40 | -0.978 | -12 | 900 | 23.08 | -4.460 |
| 6 | 600 | 22.40 | -0.961 | -12 | 1000 | 23.81 | -4.460 |
| 6 | 900 | 23.08 | -2.058 | -12 | 1000 | 24.13 | -5.000 |
| 6 | 900 | 23.08 | -1.908 | 12 | 0 | 22.11 | -1.235 |
| 6 | 1000 | 23.44 | -2.611 | 12 | 600 | 22.50 | -1.500 |
| 6 | 1000 | 23.44 | -2.527 | 12 | 600 | 22.50 | -1.382 |
| 8 | 0 | 22.05 | -1.088 | 12 | 900 | 23.22 | -2.052 |
| 8 | 600 | 22.10 | -1.075 | 12 | 1000 | 24.25 | -3.525 |

## TABLE 8.– MEASURED LEAD-LAG FREQUENCY AND DAMPING, BLADE SET 1, $\beta_{pc} = 0°, \beta_d = -2.5°$, SOFT PITCH FLEXURE

| Blade pitch angle, deg | rpm | Lead-lag frequency, Hz | Lead-Lag damping, rad/sec | Blade pitch angle, deg | rpm | Lead-lag frequency, Hz | Lead-lag damping, rad/sec |
|---|---|---|---|---|---|---|---|
| 0 | 0 | 21.71 | -1.374 | 10 | 0 | 21.71 | -1.324 |
| 0 | 600 | 22.25 | -1.222 | 10 | 600 | 21.37 | -1.214 |
| 0 | 600 | 22.22 | -1.195 | 10 | 600 | 21.37 | -1.149 |
| 0 | 900 | 22.40 | -1.315 | 10 | 900 | 22.90 | -1.965 |
| 0 | 900 | 22.40 | -1.328 | 10 | 900 | 22.90 | -1.849 |
| 0 | 900 | 22.40 | -1.318 | 10 | 1000 | 23.52 | -2.795 |
| 0 | 900 | 22.40 | -1.338 | 10 | 1000 | 23.44 | -2.761 |
| 0 | 1000 | 22.60 | -1.251 | 12 | 1000 | 23.62 | -2.548 |
| 0 | 1000 | 22.58 | -1.249 | 12 | 1000 | 23.81 | -2.225 |
| 2 | 0 | 21.71 | -1.311 | 14 | 0 | 21.55 | -1.254 |
| 2 | 600 | 22.22 | -1.225 | 14 | 600 | 20.47 | -1.350 |
| 2 | 600 | 22.22 | -1.219 | 14 | 600 | 20.47 | -1.559 |
| 2 | 900 | 22.58 | -1.280 | 14 | 900 | 22.79 | -1.974 |
| 2 | 900 | 22.58 | -1.296 | 14 | 900 | 22.73 | -2.277 |
| 2 | 1000 | 22.68 | -1.439 | 14 | 1000 | 23.69 | -2.907 |
| 2 | 1000 | 22.73 | -1.384 | 0 | 0 | 21.73 | -1.408 |
| 4 | 0 | 21.71 | -1.331 | 0 | 600 | 22.22 | -1.203 |
| 4 | 600 | 22.05 | -1.133 | 0 | 600 | 22.22 | -1.286 |
| 4 | 600 | 22.05 | -1.079 | 0 | 900 | 22.58 | -1.371 |
| 4 | 900 | 22.58 | -1.596 | 0 | 900 | 22.58 | -1.380 |
| 4 | 900 | 22.58 | -1.564 | 0 | 1000 | 22.73 | -1.396 |
| 4 | 1000 | 22.73 | -1.910 | 0 | 1000 | 22.73 | -1.431 |
| 4 | 1000 | 22.73 | -1.895 | 0 | 1000 | 22.73 | -1.442 |
| 6 | 0 | 21.71 | -1.361 | 4 | 0 | 21.73 | -1.389 |
| 6 | 600 | 21.88 | -1.016 | 4 | 600 | 22.21 | -1.187 |
| 6 | 900 | 22.73 | -1.557 | 4 | 600 | 22.05 | -1.175 |
| 6 | 900 | 22.58 | -1.710 | 4 | 900 | 22.75 | -1.776 |
| 6 | 1000 | 23.00 | -2.126 | 4 | 900 | 22.73 | -1.794 |
| 6 | 1000 | 23.08 | -2.078 | 4 | 1000 | 22.94 | -2.283 |
| 6 | 600 | 21.86 | -1.036 | 4 | 1000 | 22.90 | -2.426 |
| 8 | 0 | 21.54 | -1.215 | 8 | 0 | 21.62 | -1.318 |
| 8 | 0 | 21.71 | -1.292 | 8 | 600 | 21.88 | -0.985 |
| 8 | 600 | 21.71 | -0.914 | 8 | 600 | 21.88 | -1.007 |
| 8 | 600 | 21.71 | -0.876 | 8 | 900 | 22.90 | -2.509 |
| 8 | 900 | 22.73 | -1.920 | 8 | 900 | 22.90 | -2.252 |
| 8 | 900 | 22.73 | -1.740 | 8 | 1000 | 23.26 | -3.095 |
| 8 | 1000 | 23.26 | -2.803 | 8 | 1000 | 23.26 | -3.059 |
| 8 | 1000 | 23.26 | -2.755 | | | | |

## TABLE 9.– MEASURED LEAD-LAG FREQUENCY AND DAMPING, BLADE SET 1, $\beta_{pc} = 2.5°, \beta_d = 0°$, SOFT PITCH FLEXURE

| Blade pitch angle, deg | rpm | Lead-lag frequency, Hz | Lead-Lag damping, rad/sec | Blade pitch angle, deg | rpm | Lead-lag frequency, Hz | Lead-lag damping, rad/sec |
|---|---|---|---|---|---|---|---|
| 0 | 0 | 22.20 | -1.104 | 8 | 1000 | 23.26 | -2.202 |
| 0 | 600 | 22.10 | -1.730 | 8 | 1000 | 23.32 | -2.198 |
| 0 | 900 | 22.40 | -1.814 | 10 | 0 | 22.05 | -1.077 |
| 0 | 1000 | 22.45 | -1.819 | 10 | 600 | 22.40 | -0.880 |
| 0 | 1000 | 22.40 | -1.855 | 10 | 900 | 23.26 | -1.598 |
| 2 | 0 | 22.22 | -1.114 | 10 | 1000 | 23.62 | -2.174 |
| 2 | 600 | 22.22 | -1.481 | 10 | 1000 | 23.62 | -1.717 |
| 2 | 900 | 22.40 | -1.480 | 14 | 0 | 22.07 | -1.151 |
| 2 | 1000 | 22.40 | -1.271 | 14 | 600 | 22.05 | -1.063 |
| 2 | 1000 | 22.40 | -1.325 | 14 | 600 | 22.05 | -1.029 |
| 4 | 0 | 22.10 | -1.227 | 14 | 900 | 23.62 | -1.193 |
| 4 | 600 | 22.37 | -1.438 | 14 | 900 | 23.62 | -1.543 |
| 4 | 900 | 22.65 | -1.461 | 14 | 1000 | 24.32 | -1.795 |
| 4 | 1000 | 22.67 | -1.383 | 14 | 1000 | 24.18 | -2.009 |
| 4 | 1000 | 22.58 | -1.322 | 12 | 0 | 22.02 | -1.055 |
| 6 | 0 | 22.05 | -1.121 | 12 | 600 | 22.24 | -0.904 |
| 6 | 600 | 22.40 | -1.209 | 12 | 600 | 22.22 | -0.835 |
| 6 | 900 | 22.73 | -1.429 | 12 | 900 | 23.50 | -1.210 |
| 6 | 1000 | 22.90 | -1.724 | 12 | 900 | 23.44 | -1.397 |
| 6 | 1000 | 22.90 | -1.570 | 12 | 1000 | 24.19 | -2.015 |
| 8 | 0 | 22.05 | -1.046 | 12 | 1000 | 24.19 | -2.359 |
| 8 | 600 | 22.58 | -1.005 | 12 | 1000 | 24.19 | -2.238 |
| 8 | 900 | 23.08 | -1.552 | | | | |

| Blade pitch angle, deg | rpm | Lead-lag frequency, Hz | Lead-Lag damping, rad/sec | Blade pitch angle, deg | rpm | Lead-lag frequency, Hz | Lead-lag damping, rad/sec |
|---|---|---|---|---|---|---|---|
| 0 | 0 | 23.76 | -1.227 | 8 | 593 | 24.20 | -0.982 |
| 0 | 300 | 24.05 | -1.242 | 8 | 898 | 25.08 | -1.717 |
| 0 | 500 | 24.28 | -1.327 | 8 | 893 | 25.06 | -1.593 |
| 0 | 585 | 24.39 | -1.349 | 8 | 902 | 25.14 | -1.739 |
| 0 | 702 | 24.56 | -1.204 | 8 | 1006 | 25.46 | -2.142 |
| 0 | 814 | 24.82 | -1.257 | 8 | 1005 | 25.55 | -2.454 |
| 0 | 902 | 24.97 | -1.252 | 8 | 1002 | 25.54 | -2.107 |
| 0 | 1002 | 25.24 | -1.190 | 10 | 0 | 23.71 | -1.190 |
| 2 | 0 | 23.80 | -1.215 | 10 | 0 | 23.87 | -1.404 |
| 2 | 612 | 24.46 | -1.257 | 10 | 593 | 24.13 | -0.911 |
| 2 | 901 | 24.93 | -1.321 | 10 | 603 | 24.10 | -0.888 |
| 2 | 997 | 25.27 | -1.313 | 10 | 902 | 25.24 | -1.748 |
| 4 | 0 | 23.85 | -1.299 | 10 | 896 | 25.17 | -1.768 |
| 4 | 500 | 24.30 | -1.094 | 10 | 996 | 25.66 | -2.023 |
| 4 | 601 | 24.43 | -1.020 | 10 | 994 | 25.60 | -1.956 |
| 4 | 596 | 24.42 | -1.052 | -2 | 0 | 23.67 | -1.169 |
| 4 | 897 | 25.01 | -1.523 | -2 | 603 | 24.39 | -1.272 |
| 4 | 903 | 25.04 | -1.432 | -2 | 894 | 24.95 | -1.431 |
| 4 | 995 | 25.25 | -1.627 | -2 | 895 | 24.95 | -1.387 |
| 4 | 1004 | 25.28 | -1.529 | -2 | 1001 | 25.21 | -1.340 |
| 4 | 1008 | 25.28 | -1.558 | -2 | 1001 | 25.20 | -1.379 |
| 6 | 0 | 23.76 | -1.190 | -4 | 0 | 23.70 | -1.174 |
| 6 | 305 | 24.01 | -1.214 | -4 | 607 | 24.31 | -1.227 |
| 6 | 499 | 24.04 | -1.650 | -4 | 705 | 24.52 | -1.007 |
| 6 | 604 | 24.32 | -1.130 | -4 | 1000 | 25.20 | -1.878 |
| 6 | 598 | 24.32 | -1.102 | -6 | 0 | 23.84 | -1.242 |
| 6 | 694 | 24.51 | -1.143 | -6 | 600 | 24.36 | -1.114 |
| 6 | 818 | 24.77 | -1.568 | -6 | 904 | 25.10 | -1.989 |
| 6 | 900 | 25.06 | -1.491 | -6 | 1008 | 25.38 | -2.247 |
| 6 | 898 | 25.04 | -1.650 | -6 | 999 | 25.36 | -2.356 |
| 6 | 1008 | 25.40 | -1.873 | -8 | 0 | 23.77 | -1.184 |
| 6 | 1001 | 25.40 | -1.685 | -8 | 600 | 24.20 | -0.791 |
| 6 | 994 | 25.37 | -1.725 | -8 | 898 | 25.10 | -2.018 |
| 8 | 0 | 23.69 | -1.238 | -8 | 1004 | 25.34 | -2.812 |
| 8 | 590 | 24.17 | -1.012 | -8 | 993 | 25.46 | -2.551 |

TABLE 11.— MEASURED LEAD-LAG FREQUENCY AND DAMPING, BLADE SET 2, $\beta_{pc} = 0°, \beta_d = -5°$, STIFF PITCH FLEXURE

| Blade pitch angle, deg | rpm | Lead-lag frequency, Hz | Lead-Lag damping, rad/sec | Blade pitch angle, deg | rpm | Lead-lag frequency, Hz | Lead-lag damping, rad/sec |
|---|---|---|---|---|---|---|---|
| -2 | 0 | 23.52 | -1.202 | 8 | 999 | 24.50 | -2.075 |
| -2 | 1007 | 24.31 | -3.291 | 10 | 995 | 24.71 | -2.235 |
| 0 | 0 | 23.56 | -1.225 | 10 | 1004 | 24.70 | -2.305 |
| 0 | 999 | 24.24 | -1.947 | 11 | 0 | 23.31 | -1.282 |
| 0 | 1007 | 24.26 | -1.795 | 11 | 1000 | 24.65 | -2.788 |
| 0 | 1004 | 24.26 | -1.920 | 11 | 1009 | 24.65 | -2.839 |
| 2 | 0 | 23.54 | -1.288 | 12 | 0 | 23.33 | -1.139 |
| 2 | 997 | 24.14 | -1.449 | 12 | 1000 | 24.77 | -2.368 |
| 2 | 1001 | 24.21 | -1.379 | 12 | 1004 | 24.80 | -2.380 |
| 4 | 0 | 23.44 | -1.225 | 12 | 995 | 24.63 | -3.213 |
| 4 | 1003 | 24.17 | -1.381 | 13 | 0 | 23.26 | -1.268 |
| 4 | 1005 | 24.20 | -1.262 | 13 | 1004 | 24.95 | -2.927 |
| 4 | 1006 | 24.21 | -1.226 | 13 | 1004 | 24.88 | -2.938 |
| 6 | 0 | 23.50 | -1.199 | 13 | 997 | 24.84 | -3.465 |
| 6 | 1002 | 24.28 | -1.503 | 13 | 1005 | 24.89 | -2.733 |
| 6 | 1002 | 24.33 | -1.496 | 14 | 0 | 23.27 | -1.168 |
| 8 | 0 | 23.40 | -1.202 | 14 | 1005 | 25.36 | -4.072 |
| 8 | 995 | 24.43 | -2.706 | 14 | 996 | 24.99 | -3.608 |
| 8 | 1005 | 24.59 | -1.992 | 14 | 997 | 25.11 | -3.476 |

TABLE 12.— MEASURED LEAD-LAG FREQUENCY AND DAMPING, BLADE SET 2, $\beta_{pc} = 0°, \beta_d = 5°$, STIFF PITCH FLEXURE

| Blade pitch angle, deg | rpm | Lead-lag frequency, Hz | Lead-Lag damping, rad/sec | Blade pitch angle, deg | rpm | Lead-lag frequency, Hz | Lead-lag damping, rad/sec |
|---|---|---|---|---|---|---|---|
| 0 | 0 | 23.68 | -1.200 | -8 | 1007 | 24.86 | -1.575 |
| 0 | 993 | 24.60 | -1.893 | -10 | 0 | 23.52 | -1.222 |
| 0 | 1006 | 24.62 | -1.861 | -10 | 1000 | 24.96 | -1.953 |
| -2 | 0 | 23.65 | -1.209 | -10 | 1002 | 25.01 | -1.828 |
| -2 | 996 | 24.49 | -1.171 | -10 | 999 | 25.16 | -2.036 |
| -2 | 1003 | 24.52 | -1.064 | -12 | 0 | 23.42 | -1.227 |
| -2 | 999 | 24.50 | -1.073 | -12 | 1005 | 25.18 | -2.277 |
| -4 | 0 | 23.61 | -1.213 | -12 | 996 | 25.19 | -2.095 |
| -4 | 994 | 24.52 | -1.031 | -12 | 1003 | 25.19 | -2.268 |
| -4 | 1002 | 24.52 | -0.982 | -14 | 0 | 23.42 | -1.157 |
| -6 | 0 | 23.63 | -1.237 | -14 | 1000 | 25.45 | -2.863 |
| -6 | 1001 | 24.62 | -1.264 | -14 | 1005 | 25.38 | -2.997 |
| -6 | 1006 | 24.65 | -1.216 | -14 | 1002 | 25.57 | -2.815 |
| -8 | 0 | 23.57 | -1.166 | -16 | 0 | 23.36 | -1.216 |
| -8 | 996 | 24.37 | -1.475 | -16 | 991 | 25.72 | -2.026 |
| -8 | 996 | 24.89 | -1.483 | -16 | 989 | 25.73 | -2.062 |

TABLE 13.– MEASURED LEAD-LAG FREQUENCY AND DAMPING, BLADE SET 2,
$\beta_{pc} = 5°$, $\beta_d = 0°$, STIFF PITCH FLEXURE

| Blade pitch angle, deg | rpm | Lead-lag frequency, Hz | Lead-Lag damping, rad/sec | Blade pitch angle, deg | rpm | Lead-lag frequency, Hz | Lead-lag damping, rad/sec |
|---|---|---|---|---|---|---|---|
| -2 | 0 | 23.63 | -1.286 | 6 | 599 | 23.90 | -1.915 |
| -2 | 604 | 23.45 | -2.309 | 6 | 898 | 24.32 | -1.672 |
| -2 | 907 | 24.14 | -3.006 | 6 | 999 | 24.38 | -1.480 |
| -2 | 1000 | 24.44 | -3.310 | 6 | 994 | 24.39 | -1.535 |
| -2 | 997 | 24.38 | -3.247 | 8 | 0 | 23.43 | -1.358 |
| 0 | 0 | 23.67 | -1.154 | 8 | 601 | 23.94 | -1.784 |
| 0 | 607 | 23.58 | -2.202 | 8 | 897 | 24.37 | -1.666 |
| 0 | 899 | 24.15 | -2.238 | 8 | 1002 | 24.59 | -1.966 |
| 0 | 998 | 24.35 | -1.923 | 8 | 1001 | 24.59 | -2.144 |
| 0 | 1008 | 24.32 | -1.964 | 8 | 1000 | 24.61 | -1.876 |
| 2 | 0 | 23.69 | -1.250 | 9 | 0 | 23.55 | -1.150 |
| 2 | 598 | 23.64 | -2.347 | 9 | 610 | 24.05 | -1.859 |
| 2 | 891 | 24.02 | -1.999 | 9 | 896 | 24.48 | -1.651 |
| 2 | 1000 | 24.29 | -1.438 | 9 | 1005 | 24.76 | -1.865 |
| 2 | 1005 | 24.29 | -1.432 | 9 | 1002 | 24.73 | -2.066 |
| 4 | 0 | 23.66 | -1.270 | 9 | 1000 | 24.73 | -2.000 |
| 4 | 603 | 23.76 | -2.134 | 10 | 0 | 23.47 | -1.140 |
| 4 | 905 | 24.19 | -1.549 | 10 | 608 | 24.06 | -1.674 |
| 4 | 1002 | 24.30 | -1.352 | 10 | 901 | 24.54 | -1.877 |
| 4 | 1005 | 24.33 | -1.292 | 10 | 1001 | 24.81 | -2.159 |
| 6 | 0 | 23.49 | -1.430 | 10 | 1005 | 24.87 | -2.871 |
| 6 | 0 | 23.61 | -1.199 | | | | |

TABLE 14.– MEASURED LEAD-LAG FREQUENCY AND DAMPING, BLADE SET 2, $\beta_{pc} = 0°, \beta_d = 0°$, SOFT PITCH FLEXURE

| Blade pitch angle, deg | rpm | Lead-lag frequency, Hz | Lead-Lag damping, rad/sec | Blade pitch angle, deg | rpm | Lead-lag frequency, Hz | Lead-lag damping, rad/sec |
|---|---|---|---|---|---|---|---|
| 0 | 0 | 22.02 | -1.027 | 6 | 599 | 22.47 | -1.064 |
| 0 | 311 | 22.37 | -1.099 | 6 | 650 | 22.51 | -1.329 |
| 0 | 399 | 22.49 | -1.125 | 6 | 725 | 22.70 | -1.370 |
| 0 | 504 | 22.55 | -1.230 | 6 | 802 | 22.90 | -1.592 |
| 0 | 600 | 22.62 | -1.154 | 6 | 849 | 23.02 | -1.854 |
| 0 | 700 | 22.73 | -1.015 | 6 | 902 | 23.14 | -2.003 |
| 0 | 795 | 22.91 | -1.343 | 6 | 952 | 23.21 | -2.463 |
| 0 | 807 | 22.85 | -1.373 | 6 | 997 | 23.53 | -2.505 |
| 0 | 909 | 23.03 | -1.203 | 6 | 997 | 23.52 | -2.843 |
| 0 | 0 | 22.03 | -1.106 | 6 | 999 | 23.50 | -2.052 |
| 0 | 996 | 23.13 | -1.055 | 8 | 0 | 21.86 | -1.109 |
| 2 | 0 | 22.00 | -1.021 | 8 | 304 | 22.04 | -1.103 |
| 2 | 0 | 22.00 | -1.021 | 8 | 502 | 22.00 | -0.824 |
| 2 | 907 | 23.06 | -1.199 | 8 | 598 | 22.25 | -1.002 |
| 2 | 1001 | 23.18 | -1.198 | 8 | 704 | 22.52 | -2.022 |
| 2 | 0 | 22.06 | -1.047 | 8 | 704 | 22.56 | -1.095 |
| 2 | 1001 | 23.20 | -1.274 | 8 | 803 | 22.84 | -1.584 |
| 4 | 0 | 22.00 | -1.123 | 8 | 902 | 23.17 | -1.963 |
| 4 | 605 | 22.53 | -1.000 | 8 | 997 | 23.45 | -3.401 |
| 4 | 904 | 23.03 | -1.648 | 8 | 1007 | 23.76 | -3.008 |
| 4 | 999 | 23.24 | -1.892 | 8 | 1003 | 23.71 | -2.917 |
| 4 | 0 | 21.98 | -1.032 | 9 | 599 | 22.02 | -0.964 |
| 4 | 1007 | 23.24 | -1.865 | 9 | 901 | 23.02 | -2.177 |
| 6 | 0 | 21.95 | -1.093 | 9 | 1000 | 23.54 | -2.862 |
| 6 | 343 | 22.20 | -1.060 | 9 | 998 | 23.36 | -2.974 |
| 6 | 505 | 22.26 | -0.934 | 9 | 1007 | 23.57 | -2.986 |
| 6 | 548 | 22.32 | -0.872 | 9 | 1003 | 23.48 | -2.677 |

TABLE 14.-- CONCLUDED.

| Blade pitch angle, deg | rpm | Lead-lag frequency, Hz | Lead-Lag damping, rad/sec | Blade pitch angle, deg | rpm | Lead-lag frequency, Hz | Lead-lag damping, rad/sec |
|---|---|---|---|---|---|---|---|
| 10 | 0 | 22.11 | -1.114 | -4 | 0 | 22.12 | -1.106 |
| 10 | 604 | 22.10 | -1.135 | -4 | 601 | 22.60 | -1.020 |
| 10 | 598 | 22.07 | -0.851 | -4 | 902 | 23.09 | -1.770 |
| 10 | 893 | 23.35 | -1.918 | -4 | 1005 | 23.20 | -2.217 |
| 10 | 1000 | 24.28 | -3.169 | -4 | 1008 | 23.25 | -2.005 |
| 10 | 0 | 22.02 | -1.131 | -6 | 606 | 22.44 | -0.645 |
| 10 | 991 | 23.94 | -2.464 | -6 | 902 | 23.12 | -2.233 |
| 10 | 980 | 23.97 | -2.700 | -6 | 998 | 23.41 | -3.252 |
| 10 | 1004 | 23.99 | -2.786 | -6 | 1005 | 23.42 | -3.213 |
| 10 | 995 | 24.03 | -2.522 | -8 | 0 | 22.05 | -1.033 |
| 10 | 1001 | 23.96 | -3.450 | -8 | 608 | 22.40 | -0.581 |
| 10 | 1010 | 23.98 | -2.748 | -8 | 903 | 23.32 | -2.515 |
| 11 | 0 | 21.82 | -1.108 | -8 | 1001 | 23.66 | -4.207 |
| 11 | 604 | 21.75 | -1.168 | -8 | 998 | 23.82 | -3.741 |
| 11 | 998 | 23.99 | -3.761 | -8 | 998 | 23.67 | -4.069 |
| 11 | 999 | 23.92 | -3.009 | -10 | 1008 | 23.84 | -3.661 |
| 11 | 1002 | 23.99 | -3.191 | -10 | 1004 | 23.91 | -3.567 |
| 12 | 0 | 21.82 | -1.205 | -10 | 998 | 23.70 | -3.710 |
| 12 | 608 | 21.68 | -1.179 | -10 | 996 | 23.76 | -3.700 |
| 12 | 902 | 23.43 | -3.215 | -10 | 1005 | 23.78 | -3.992 |
| 12 | 997 | 24.20 | -3.321 | -12 | 0 | 21.92 | -1.226 |
| 12 | 999 | 24.15 | -3.311 | -12 | 997 | 24.02 | -4.034 |
| -2 | 0 | 22.09 | -1.125 | -12 | 1011 | 24.23 | -4.445 |
| -2 | 598 | 22.70 | -1.178 | -12 | 1001 | 24.16 | -4.174 |
| -2 | 903 | 23.12 | -1.340 | -12 | 1002 | 24.16 | -4.717 |
| -2 | 998 | 23.25 | -1.293 | -12 | 1008 | 23.96 | -4.314 |
| -2 | 1008 | 23.19 | -1.377 | -12 | 0 | 21.85 | -1.187 |

TABLE 15.– MEASURED LEAD-LAG FREQUENCY AND DAMPING, BLADE SET 2, $\beta_{pc} = 0°$, $\beta_d = 0°$, SOFT PITCH FLEXURE, WITH SINGLE GROUND PLANE

| Blade pitch angle, deg | rpm | Lead-lag frequency, Hz | Lead-Lag damping, rad/sec | Blade pitch angle, deg | rpm | Lead-lag frequency, Hz | Lead-lag damping, rad/sec |
|---|---|---|---|---|---|---|---|
| 6 | 0 | 22.17 | -1.137 | -8 | 603 | 22.05 | -0.777 |
| 6 | 0 | 22.32 | -1.252 | -8 | 899 | 23.08 | -3.036 |
| 6 | 1006 | 23.50 | -2.743 | -8 | 1006 | 23.52 | -4.024 |
| 6 | 991 | 23.50 | -2.348 | -8 | 1001 | 23.41 | -4.116 |
| 8 | 603 | 22.26 | -0.839 | -8 | 1003 | 23.37 | -4.121 |
| 8 | 906 | 23.34 | -2.245 | -10 | 1000 | 23.81 | -4.588 |
| 8 | 1001 | 23.56 | -3.414 | -10 | 1002 | 23.79 | -3.799 |
| 8 | 1006 | 23.68 | -3.674 | -10 | 1005 | 23.87 | -4.291 |
| 9 | 0 | 21.76 | -1.044 | -10 | 1007 | 23.65 | -3.930 |
| 9 | 1000 | 23.54 | -2.850 | -10 | 999 | 23.79 | -4.446 |
| 9 | 1005 | 23.46 | -2.801 | -10 | 1000 | 23.76 | -3.647 |
| 9 | 1003 | 23.60 | -3.521 | -10 | 998 | 23.63 | -4.120 |
| 9 | 1004 | 23.39 | -2.992 | -10 | 998 | 23.80 | -4.157 |
| 10 | 0 | 22.02 | -1.140 | -12 | 0 | 21.85 | -1.187 |
| 10 | 601 | 22.17 | -1.642 | -12 | 600 | 21.26 | -1.262 |
| 10 | 899 | 23.33 | -2.395 | -12 | 893 | 23.09 | -3.506 |
| 10 | 986 | 23.99 | -3.126 | -12 | 1002 | 23.79 | -4.262 |
| 10 | 991 | 23.02 | -2.567 | -12 | 1011 | 23.88 | -4.890 |
| 11 | 0 | 21.82 | -1.108 | -12 | 998 | 23.90 | -4.372 |
| 11 | 1000 | 24.10 | -3.621 | -12 | 1008 | 24.19 | -4.653 |
| 11 | 1004 | 23.54 | -3.777 | -14 | 0 | 21.87 | -1.097 |
| 12 | 0 | 21.82 | -1.205 | -14 | 599 | 22.36 | -3.545 |
| 12 | 591 | 21.61 | -1.570 | -14 | 900 | 22.96 | -3.643 |
| 12 | 901 | 23.42 | -3.230 | -14 | 1002 | 24.01 | -4.245 |
| 12 | 997 | 24.25 | -3.577 | -14 | 1005 | 23.54 | -3.877 |
| 12 | 999 | 24.17 | -4.133 | -14 | 1000 | 23.83 | -3.995 |
| 12 | 1006 | 24.60 | -3.299 | -14 | 995 | 23.60 | -3.978 |
| 12 | 1006 | 24.29 | -3.411 | -14 | 998 | 23.90 | -3.779 |
| -8 | 0 | 21.97 | -1.220 | | | | |

## TABLE 16.– MEASURED LEAD-LAG FREQUENCY AND DAMPING, BLADE SET 2, $\beta_{pc} = 0°, \beta_d = 0°$, SOFT PITCH FLEXURE, WITH DOUBLE GROUND PLANE

| Blade pitch angle, deg | rpm | Lead-lag frequency, Hz | Lead-Lag damping, rad/sec | Blade pitch angle, deg | rpm | Lead-lag frequency, Hz | Lead-lag damping, rad/sec |
|---|---|---|---|---|---|---|---|
| 8 | 0 | 21.83 | -1.122 | 10 | 1007 | 23.60 | -3.749 |
| 8 | 1000 | 23.63 | -3.294 | 10 | 1002 | 23.77 | -3.345 |
| 8 | 1005 | 23.46 | -2.516 | 10 | 999 | 23.69 | -3.551 |
| 8 | 1008 | 23.51 | -3.496 | -10 | 0 | 21.79 | -1.280 |
| 8 | 999 | 23.47 | -3.284 | -10 | 997 | 23.76 | -4.810 |
| -8 | 0 | 21.80 | -1.033 | -10 | 1006 | 23.72 | -3.514 |
| -8 | 0 | 21.85 | -1.091 | -10 | 1008 | 23.62 | -3.995 |
| -8 | 1006 | 23.54 | -4.209 | -10 | 1001 | 23.76 | -4.048 |
| -8 | 1008 | 23.42 | -3.724 | 11 | 0 | 21.55 | -1.195 |
| -8 | 1008 | 23.39 | -4.081 | 11 | 999 | 23.54 | -3.299 |
| -8 | 1002 | 23.29 | -4.141 | 11 | 996 | 23.51 | -3.465 |
| -8 | 1001 | 23.34 | -3.996 | 11 | 999 | 23.59 | -3.233 |
| 9 | 0 | 21.69 | -1.058 | -11 | 0 | 21.70 | -1.095 |
| 9 | 997 | 23.39 | -3.376 | -11 | 1002 | 23.79 | -4.302 |
| 9 | 1001 | 23.36 | -3.213 | -11 | 998 | 23.45 | -4.372 |
| 9 | 1008 | 23.39 | -3.180 | -11 | 998 | 23.67 | -4.159 |
| 9 | 1005 | 23.39 | -2.936 | 6 | 0 | 21.77 | -1.142 |
| 9 | 997 | 23.48 | -2.915 | 6 | 598 | 22.27 | -0.970 |
| 9 | 0 | 21.79 | -1.086 | 6 | 904 | 22.88 | -1.956 |
| -9 | 1005 | 23.39 | -3.891 | 6 | 1002 | 23.18 | -2.531 |
| -9 | 1002 | 23.47 | -3.992 | 6 | 990 | 23.14 | -2.447 |
| -9 | 1004 | 23.36 | -3.713 | 8 | 0 | 21.63 | -1.200 |
| -9 | 1005 | 23.46 | -4.129 | 8 | 598 | 22.11 | -1.093 |
| 10 | 0 | 21.73 | -1.137 | 8 | 899 | 22.96 | -2.047 |
| 10 | 1000 | 23.57 | -3.671 | 8 | 1008 | 23.53 | 0.000 |
| 10 | 1001 | 23.74 | -3.159 | 8 | 1006 | 23.38 | -2.917 |

## TABLE 17.— MEASURED LEAD-LAG FREQUENCY AND DAMPING, BLADE SET 2, $\beta_{pc} = 0°, \beta_d = -2.5°$, SOFT PITCH FLEXURE

| Blade pitch angle, deg | rpm | Lead-lag frequency, Hz | Lead-Lag damping, rad/sec | Blade pitch angle, deg | rpm | Lead-lag frequency, Hz | Lead-lag damping, rad/sec |
|---|---|---|---|---|---|---|---|
| 0 | 0 | 21.74 | -1.015 | 10 | 1008 | 23.49 | -3.094 |
| 0 | 1004 | 22.76 | -1.085 | 10 | 1009 | 23.41 | -2.520 |
| 0 | 1004 | 22.79 | -1.041 | 10 | 1007 | 23.44 | -2.645 |
| 2 | 0 | 21.66 | -0.928 | 12 | 0 | 21.49 | -1.014 |
| 2 | 0 | 21.65 | -0.985 | 12 | 1002 | 23.66 | -2.607 |
| 2 | 1003 | 22.77 | -1.053 | 12 | 1000 | 23.52 | -4.318 |
| 2 | 1002 | 22.76 | -1.077 | 12 | 992 | 23.38 | -2.323 |
| 4 | 0 | 21.67 | -0.993 | -2 | 0 | 21.69 | -1.006 |
| 4 | 995 | 22.82 | -1.608 | -2 | 995 | 22.79 | -1.708 |
| 4 | 1003 | 22.88 | -1.493 | -2 | 1011 | 22.82 | -1.686 |
| 4 | 1006 | 22.84 | -1.462 | -4 | 0 | 21.63 | -0.944 |
| 6 | 0 | 21.53 | -1.025 | -4 | 1007 | 22.83 | -2.832 |
| 6 | 1006 | 22.99 | -2.169 | -4 | 1002 | 22.88 | -2.701 |
| 6 | 996 | 23.03 | -2.077 | -6 | 0 | 21.60 | -0.094 |
| 6 | 1005 | 23.01 | -2.239 | -6 | 1017 | 23.12 | -4.017 |
| 6 | 1007 | 22.96 | -2.029 | -6 | 1006 | 23.18 | -3.753 |
| 8 | 0 | 21.57 | -1.039 | -6 | 1008 | 23.13 | -4.278 |
| 8 | 1005 | 23.24 | -2.747 | -8 | 0 | 21.54 | -1.003 |
| 8 | 1007 | 23.21 | -2.583 | -8 | 1001 | 23.32 | -4.641 |
| 8 | 1008 | 23.23 | -2.965 | -8 | 1003 | 23.37 | -5.098 |
| 8 | 1008 | 23.28 | -2.834 | -8 | 1003 | 23.40 | -4.664 |
| 10 | 0 | 21.51 | -0.946 | | | | |

## TABLE 18.— MEASURED LEAD-LAG FREQUENCY AND DAMPING, BLADE SET 2, $\beta_{pc} = 0°, \beta_d = -5°$, SOFT PITCH FLEXURE

| Blade pitch angle, deg | rpm | Lead-lag frequency, Hz | Lead-Lag damping, rad/sec | Blade pitch angle, deg | rpm | Lead-lag frequency, Hz | Lead-lag damping, rad/sec |
|---|---|---|---|---|---|---|---|
| 0 | 0 | 19.64 | -0.946 | 6 | 1000 | 22.54 | -2.047 |
| 0 | 997 | 22.27 | -1.225 | 6 | 1006 | 22.56 | -2.059 |
| 0 | 1007 | 22.44 | -1.212 | 6 | 1006 | 22.57 | -2.075 |
| 0 | 1006 | 22.44 | -1.298 | 8 | 0 | 19.64 | -0.886 |
| 2 | 0 | 19.73 | -1.045 | 8 | 1001 | 22.73 | -2.340 |
| 2 | 995 | 22.35 | -1.215 | 8 | 1003 | 22.82 | -2.434 |
| 2 | 1003 | 22.37 | -1.198 | 10 | 1002 | 22.88 | -2.511 |
| 2 | 1005 | 22.40 | -1.089 | 10 | 1002 | 22.77 | -3.086 |
| 4 | 0 | 19.67 | -0.842 | 10 | 993 | 22.93 | -2.522 |
| 4 | 0 | 19.68 | -0.862 | 10 | 997 | 22.87 | -2.565 |
| 4 | 997 | 22.38 | -1.410 | 12 | 0 | 19.65 | -0.859 |
| 4 | 1001 | 22.40 | -1.379 | 12 | 1004 | 23.26 | -3.452 |
| 4 | 1014 | 22.42 | -1.383 | 12 | 1001 | 22.77 | -3.108 |
| 6 | 0 | 19.73 | -0.987 | 12 | 1001 | 22.79 | -2.819 |

TABLE 19.— MEASURED LEAD-LAG FREQUENCY AND DAMPING, BLADE SET 2,
$\beta_{pc} = 0°, \beta_d = 2.5°$, SOFT PITCH FLEXURE

| Blade pitch angle, deg | rpm | Lead-lag frequency, Hz | Lead-Lag damping, rad/sec | Blade pitch angle, deg | rpm | Lead-lag frequency, Hz | Lead-lag damping, rad/sec |
|---|---|---|---|---|---|---|---|
| 0 | 0 | 20.32 | -0.911 | -2 | 998 | 22.91 | -1.168 |
| 0 | 1001 | 23.08 | -1.280 | -4 | 0 | 20.40 | -1.105 |
| 0 | 1000 | 23.02 | -1.327 | -4 | 1000 | 23.04 | 0.000 |
| 0 | 1007 | 23.08 | -1.340 | -4 | 1010 | 23.09 | -1.798 |
| 2 | 0 | 20.32 | -1.125 | -6 | 0 | 20.31 | -1.053 |
| 2 | 1000 | 23.02 | -1.517 | -6 | 1011 | 23.22 | -2.731 |
| 2 | 1006 | 23.08 | -1.587 | -8 | 0 | 20.30 | -0.905 |
| 4 | 0 | 20.33 | -1.028 | -8 | 1001 | 23.25 | -3.263 |
| 4 | 997 | 23.19 | -2.295 | -8 | 1004 | 23.35 | -3.195 |
| 4 | 1005 | 23.19 | -2.412 | -9 | 0 | 20.31 | -1.034 |
| 6 | 0 | 20.34 | -1.044 | -9 | 1008 | 23.54 | -3.109 |
| 6 | 1006 | 23.43 | -3.234 | -9 | 1000 | 23.51 | -3.069 |
| 6 | 997 | 23.33 | -3.071 | -9 | 1010 | 23.54 | -3.106 |
| 6 | 1000 | 23.44 | -3.122 | -10 | 0 | 20.32 | -1.048 |
| 8 | 0 | 20.28 | -0.978 | -10 | 1003 | 23.47 | -3.012 |
| 8 | 996 | 23.79 | -3.261 | -12 | 0 | 20.23 | -1.035 |
| 8 | 1001 | 23.86 | -3.976 | -12 | 999 | 23.83 | -3.724 |
| 8 | 1000 | 23.89 | -3.070 | -12 | 997 | 23.82 | -3.343 |
| 8 | 999 | 23.84 | -3.433 | -12 | 1004 | 23.79 | -4.084 |
| -2 | 0 | 20.35 | -1.049 | -12 | 998 | 23.74 | -3.698 |
| -2 | 999 | 22.98 | -1.189 | | | | |

TABLE 20.– MEASURED LEAD-LAG FREQUENCY AND DAMPING, BLADE SET 2, $\beta_{pc} = 0°, \beta_d = 5°$, SOFT PITCH FLEXURE

| Blade pitch angle, deg | rpm | Lead-lag frequency, Hz | Lead-Lag damping, rad/sec | Blade pitch angle, deg | rpm | Lead-lag frequency, Hz | Lead-lag damping, rad/sec |
|---|---|---|---|---|---|---|---|
| 0 | 0 | 18.18 | -1.287 | -6 | 905 | 22.39 | -1.675 |
| 0 | 0 | 18.21 | -1.294 | -6 | 1003 | 22.73 | -2.409 |
| 0 | 601 | 21.80 | -1.342 | -6 | 998 | 22.67 | -2.442 |
| 0 | 808 | 22.36 | -1.292 | -8 | 0 | 18.20 | -1.389 |
| 0 | 997 | 22.58 | -1.355 | -8 | 606 | 21.31 | -0.709 |
| 0 | 1003 | 22.58 | -1.397 | -8 | 895 | 22.28 | -1.742 |
| 0 | 1010 | 22.56 | -1.382 | -8 | 1000 | 22.90 | -2.655 |
| 0 | 0 | 17.95 | -0.748 | -8 | 1005 | 22.82 | -2.866 |
| 0 | 997 | 22.64 | -1.234 | -8 | 1004 | 22.76 | -2.894 |
| 0 | 1008 | 22.68 | -1.207 | -8 | 0 | 17.87 | -0.799 |
| -2 | 0 | 18.24 | -1.364 | -8 | 602 | 21.17 | -0.609 |
| -2 | 597 | 21.74 | -1.210 | -8 | 900 | 22.35 | -1.763 |
| -2 | 907 | 22.34 | -1.140 | -8 | 1004 | 22.89 | -2.836 |
| -2 | 994 | 22.49 | -1.075 | -8 | 998 | 22.86 | -2.609 |
| -2 | 995 | 22.51 | -1.043 | -10 | 283 | 19.51 | -1.571 |
| -2 | 0 | 17.97 | -0.817 | -10 | 505 | 20.45 | -0.607 |
| -2 | 1002 | 22.50 | -1.055 | -10 | 598 | 20.95 | -0.828 |
| -2 | 1003 | 22.66 | -1.046 | -10 | 890 | 22.42 | -1.894 |
| -4 | 0 | 18.26 | -1.304 | -10 | 1000 | 23.25 | -2.978 |
| -4 | 585 | 21.59 | -0.979 | -10 | 1000 | 23.03 | -2.614 |
| -4 | 610 | 21.66 | -0.992 | -10 | 1005 | 23.01 | -3.818 |
| -4 | 902 | 22.24 | -1.295 | -10 | 996 | 23.02 | -2.824 |
| -4 | 1000 | 22.49 | -1.400 | -10 | 0 | 17.04 | -0.771 |
| -4 | 1002 | 22.49 | -1.418 | -10 | 606 | 20.04 | -0.765 |
| -4 | 0 | 17.96 | -0.935 | -10 | 901 | 22.46 | -1.781 |
| -4 | 607 | 21.62 | -0.923 | -10 | 999 | 23.07 | -3.095 |
| -4 | 902 | 22.27 | -1.296 | -12 | 0 | 17.90 | -0.806 |
| -4 | 1009 | 22.52 | -1.462 | -12 | 900 | 22.66 | -2.615 |
| -4 | 1002 | 22.50 | -1.431 | -12 | 998 | 23.19 | -3.581 |
| -6 | 0 | 18.28 | -1.375 | -12 | 0 | 17.94 | -0.760 |
| -6 | 605 | 21.62 | -0.860 | -12 | 995 | 23.57 | -3.572 |
| -6 | 900 | 22.47 | -1.694 | -14 | 0 | 17.94 | -0.737 |
| -6 | 1005 | 22.78 | -1.967 | -14 | 999 | 23.47 | -5.154 |
| -6 | 998 | 22.73 | -2.331 | -14 | 1002 | 23.97 | -5.142 |
| -6 | 1005 | 22.73 | -2.363 | -14 | 1004 | 24.33 | -5.360 |
| -6 | 0 | 17.87 | -0.822 | -14 | 0 | 20.30 | -0.916 |
| -6 | 600 | 21.37 | -0.721 | | | | |

## TABLE 21.– MEASURED LEAD-LAG FREQUENCY AND DAMPING, BLADE SET 2, $\beta_{pc} = 2.5°, \beta_d = 0°$, SOFT PITCH FLEXURE

| Blade pitch angle, deg | rpm | Lead-lag frequency, Hz | Lead-Lag damping, rad/sec | Blade pitch angle, deg | rpm | Lead-lag frequency, Hz | Lead-lag damping, rad/sec |
|---|---|---|---|---|---|---|---|
| 0 | 0 | 21.95 | -1.228 | 10 | 900 | 23.05 | -1.730 |
| 0 | 608 | 21.87 | -1.963 | 10 | 1000 | 23.35 | -2.220 |
| 0 | 902 | 22.17 | -1.642 | 10 | 1000 | 23.32 | -2.455 |
| 0 | 1001 | 22.37 | -1.364 | 10 | 995 | 23.24 | -2.536 |
| 0 | 1004 | 22.36 | -1.370 | 10 | 0 | 21.87 | -1.141 |
| 0 | 0 | 21.90 | -1.073 | 10 | 599 | 22.41 | -1.230 |
| 0 | 998 | 22.24 | -1.190 | 10 | 901 | 22.97 | -1.743 |
| 0 | 1000 | 22.25 | -1.277 | 10 | 901 | 23.02 | -1.554 |
| 2 | 0 | 21.93 | -1.121 | 10 | 991 | 23.24 | -2.516 |
| 2 | 602 | 21.93 | -1.932 | 10 | 991 | 23.22 | -2.339 |
| 2 | 902 | 22.12 | -1.000 | 10 | 1003 | 23.27 | -2.087 |
| 2 | 1003 | 22.25 | -0.579 | 10 | 1002 | 23.33 | -2.261 |
| 2 | 1000 | 22.23 | -0.571 | 10 | 0 | 21.88 | -1.076 |
| 4 | 0 | 21.93 | -1.183 | 10 | 0 | 21.85 | -1.127 |
| 4 | 600 | 22.12 | -1.724 | 10 | 602 | 22.50 | -1.243 |
| 4 | 896 | 22.40 | -1.212 | 10 | 1002 | 23.12 | -2.090 |
| 4 | 998 | 22.42 | -0.864 | 10 | 1000 | 23.22 | -2.090 |
| 4 | 0 | 21.94 | -1.247 | -2 | 0 | 22.04 | -1.215 |
| 4 | 1007 | 22.30 | -0.844 | -2 | 598 | 21.78 | -2.089 |
| 4 | 1002 | 22.44 | -0.885 | -2 | 904 | 22.32 | -2.829 |
| 6 | 0 | 21.92 | -1.103 | -2 | 992 | 22.53 | -3.104 |
| 6 | 0 | 21.95 | -1.180 | -2 | 1000 | 22.49 | -2.832 |
| 6 | 604 | 22.33 | -1.476 | -2 | 1002 | 22.50 | -3.458 |
| 6 | 902 | 22.52 | -1.295 | -2 | 0 | 22.03 | -1.177 |
| 6 | 988 | 22.60 | -1.307 | -2 | 609 | 21.83 | -2.087 |
| 6 | 1002 | 22.62 | -1.309 | -2 | 606 | 21.78 | -2.109 |
| 6 | 1000 | 22.58 | -1.439 | -2 | 897 | 22.31 | -2.646 |
| 6 | 0 | 21.88 | -1.264 | -2 | 999 | 22.44 | -2.982 |
| 6 | 1008 | 22.62 | -1.680 | -2 | 1002 | 22.52 | -2.846 |
| 6 | 996 | 22.58 | -1.565 | -4 | 0 | 21.98 | -1.170 |
| 8 | 0 | 21.79 | -1.075 | -4 | 608 | 21.62 | -1.614 |
| 8 | 598 | 22.35 | -1.145 | -4 | 890 | 22.30 | -3.530 |
| 8 | 898 | 22.69 | -1.560 | -4 | 995 | 22.51 | -4.619 |
| 8 | 998 | 22.82 | -2.159 | -4 | 996 | 22.56 | -4.505 |
| 8 | 1000 | 22.82 | -1.875 | -4 | 994 | 22.53 | -4.532 |
| 8 | 0 | 21.88 | -1.210 | -6 | 0 | 21.97 | -1.193 |
| 8 | 1006 | 22.87 | -2.093 | -6 | 0 | 22.00 | -1.221 |
| 8 | 1006 | 22.79 | -2.346 | -6 | 626 | 21.50 | -1.947 |
| 8 | 1014 | 22.91 | -2.166 | -6 | 903 | 22.41 | -4.563 |
| 10 | 0 | 21.93 | -1.194 | -6 | 1003 | 22.73 | -6.298 |
| 10 | 600 | 22.49 | -1.031 | -6 | 1003 | 22.82 | -6.324 |
| 10 | 900 | 23.01 | -1.680 | -6 | 1005 | 23.01 | -6.726 |

TABLE 22.- MEASURED LEAD-LAG FREQUENCY AND DAMPING, BLADE SET 2,
$\beta_{pc} = 5°, \beta_d = 0°$, SOFT PITCH FLEXURE

| Blade pitch angle, deg | rpm | Lead-lag frequency, Hz | Lead-Lag damping, rad/sec | Blade pitch angle, deg | rpm | Lead-lag frequency, Hz | Lead-lag damping, rad/sec |
|---|---|---|---|---|---|---|---|
| -2 | 0 | 22.03 | -1.175 | 6 | 0 | 21.97 | -1.161 |
| -2 | 600 | 19.99 | -3.474 | 6 | 596 | 21.46 | -2.665 |
| -2 | 899 | 21.03 | -4.117 | 6 | 803 | 21.39 | -4.117 |
| -2 | 1000 | 21.27 | -4.838 | 6 | 904 | 21.37 | -1.190 |
| -2 | 1004 | 21.30 | -4.922 | 6 | 949 | 21.21 | -0.756 |
| 0 | 0 | 22.08 | -1.084 | 6 | 975 | 21.32 | -0.517 |
| 0 | 606 | 20.68 | -3.083 | 6 | 988 | 21.26 | -0.120 |
| 0 | 905 | 21.04 | -2.158 | 6 | 997 | 21.25 | 0.229 |
| 0 | 1000 | 21.25 | -1.669 | 8 | 0 | 21.97 | -1.167 |
| 0 | 1008 | 21.20 | -1.570 | 8 | 0 | 21.98 | -1.161 |
| 0 | 1007 | 21.26 | -1.549 | 8 | 600 | 21.96 | -1.987 |
| 2 | 0 | 22.06 | -1.211 | 8 | 901 | 21.79 | -1.708 |
| 2 | 604 | 20.81 | -3.280 | 8 | 999 | 21.70 | -0.930 |
| 2 | 904 | 21.01 | -1.368 | 8 | 1003 | 21.65 | -1.436 |
| 2 | 1003 | 21.09 | -0.446 | 8 | 997 | 21.64 | -0.940 |
| 2 | 1003 | 21.11 | -0.434 | 8 | 1000 | 21.67 | -0.965 |
| 2 | 993 | 21.13 | -0.541 | 10 | 0 | 21.09 | -1.180 |
| 3 | 0 | 22.04 | -1.137 | 10 | 603 | 21.97 | -2.491 |
| 3 | 608 | 20.94 | -2.917 | 10 | 897 | 22.17 | -2.242 |
| 3 | 904 | 21.09 | -1.180 | 10 | 897 | 22.17 | -2.052 |
| 3 | 1000 | 20.98 | 0.096 | 10 | 995 | 22.13 | -1.804 |
| 4 | 0 | 22.04 | -1.206 | 10 | 991 | 22.03 | -2.156 |
| 4 | 607 | 21.10 | -2.753 | 10 | 1002 | 22.12 | -1.734 |
| 4 | 851 | 21.11 | -1.526 | 12 | 0 | 21.11 | -1.526 |
| 4 | 906 | 21.17 | -0.953 | 12 | 600 | 22.17 | -1.692 |
| 4 | 917 | 21.18 | -0.847 | 12 | 898 | 22.55 | -2.524 |
| 4 | 954 | 21.20 | -0.507 | 12 | 997 | 22.49 | -2.759 |
| 4 | 974 | 21.14 | -0.250 | 12 | 997 | 22.78 | -2.790 |
| 4 | 993 | 21.35 | 0.131 | 12 | 1001 | 22.32 | -1.903 |

TABLE 23.– BLADE GEOMETRIC PROPERTIES

| Parameter | Symbol | Units | |
|---|---|---|---|
| Rotor diameter | $2R$ | m | 1.923 |
| Blade length | $L$ | m | 0.87 |
| Hub offset | $e$ | %R | 9.51 |
| Chord | $c$ | m | 0.0864 |
| Taper | --- | --- | 0 |
| Twist | --- | --- | 0 |
| Airfoil | --- | --- | NACA 0012 |
| Number of blades | $b$ | --- | 2 |
| Tip Reynolds number, 1000 rpm | --- | --- | 600,000 |

TABLE 24.– INDIVIDUAL BLADE MASS PROPERTIES, NONROTATING FREQUENCIES, AND STIFFNESS PROPERTIES

| Parameters | Symbol | Units | Blade set 1 | | Blade set 2 | |
|---|---|---|---|---|---|---|
| | | | Blade 1A | Blade 1B | Blade 2A | Blade 2B |
| Mass/unit length | $\mu$ | kg/m | $3.52 \times 10^{-1}$ | $3.25 \times 10^{-1}$ | $3.45 \times 10^{-1}$ | $3.41 \times 10^{-1}$ |
| Chordwise center of gravity | --- | %c | 24.9 | 25.5 | 24.8 | 24.7 |
| Polar moment of inertia | $I_{EA}$ | kg-m² | $1.911 \times 10^{-4}$ | $1.823 \times 10^{-4}$ | $1.744 \times 10^{-4}$ | $1.844 \times 10^{-4}$ |
| Elastic axis | --- | %c | 25.4 | 24.4 | 24.8 | 25.8 |
| Nonrotating flap frequency | $\omega_{\beta NR}$ | Hz | 5.20 | 5.30 | 5.22 | 5.15 |
| Nonrotating lead-lag frequency | $\omega_{\zeta NR}$ | Hz | 25.20 | 24.00 | 23.79 | 22.97 |
| Nonrotating torsional frequency | $\omega_{\theta NR}$ | Hz | 48.75 | 48.00 | 45.89 | 44.33 |
| Flap bending stiffness | $EI_{\beta}$ | N-m² | 17.37 | 16.66 | 17.22 | 16.49 |
| Chord bending stiffness | $EI_{\zeta}$ | N-m² | 407.7 | 341.5 | 357.8 | 328.1 |
| Torsional rigidity | $GJ$ | N-m² | 6.32 | 5.83 | 5.10 | 5.05 |

TABLE 25.— COMPARISON OF BLADE STIFFNESS
USING TWO METHODS OF MEASUREMENT

| Blade | Method | $EI_\beta$, N-m² | $EI_\zeta$, N-m² | $GJ$, N-m² |
|---|---|---|---|---|
| 1A | Moment-deflection | 18.20 | 340.84 | 6.151 |
| | Frequency-mass | 17.37 | 407.7 | 6.319 |
| | Percent-difference | -4.7 | 16.8 | 2.7 |
| 1B | Moment-deflection | 16.80 | 320.4 | 5.031 |
| | Frequency-mass | 16.66 | 341.5 | 5.834 |
| | Percent-difference | -0.8 | 6.1 | 3.8 |
| 2A | Moment-deflection | 16.38 | 307.2 | 5.085 |
| | Frequency-mass | 17.22 | 357.6 | 5.099 |
| | Percent-difference | 5.0 | 14.1 | 0.3 |
| 2B | Moment-deflection | 16.09 | 295.7 | 4.870 |
| | Frequency-mass | 16.49 | 328.1 | 5.054 |
| | Percent-difference | 2.5 | 10.0 | 3.6 |

TABLE 26.— PITCH FLEXURE STIFFNESS

| Pitch flexure | $K_\beta$, N-m/rad | $K_\zeta$, N-m/rad | $K_\theta$, N-m/rad |
|---|---|---|---|
| Stiff | $3.06 \times 10^5$ | $3.06 \times 10^5$ | $5.87 \times 10^4$ |
| Soft | $2.12 \times 10^4$ | $2.71 \times 10^4$ | 41.21 |

TABLE 27.– HUB COMPONENT MASS PROPERTIES

| Hub component | Mass, kg | Polar moment of inertia, kg-m$^2$ |
|---|---|---|
| Flexure flange | $4.54 \times 10^{-2}$ | $1.60 \times 10^{-5}$ |
| Clamp ring | $2.95 \times 10^{-2}$ | $3.37 \times 10^{-5}$ |
| Droop wedge | $9.39 \times 10^{-2}$ | $6.02 \times 10^{-5}$ |
| Blade root cuff | $7.48 \times 10^{-2}$ | $7.49 \times 10^{-5}$ |
| Cuff plug | $3.22 \times 10^{-2}$ | $1.78 \times 10^{-5}$ |
| | | |
| Total | $2.76 \times 10^{-1}$ | $2.03 \times 10^{-4}$ |

TABLE 28.– ROTOR BLADE STIFFNESS DISTRIBUTION; VALUES FOR THE PITCH FLEXURE WEB SPAN PERTAIN TO THE SOFT PITCH FLEXURE ONLY

| Inboard station, $r/R$ | Outboard station, $r/R$ | Mass length, kg/m | Polar moment of inertial/length, kg-m$^2$/m |
|---|---|---|---|
| 0.0185 | 0.0215 | 5.214 | --- |
| .0215 | .0374 | .214 | --- |
| .0374 | .0407 | 5.418 | $5.827 \times 10^{-3}$ |
| .0407 | .0440 | 10.010 | $7.073 \times 10^{-3}$ |
| .0440 | .0456 | 12.745 | $4.715 \times 10^{-3}$ |
| .0456 | .0555 | 9.969 | $6.317 \times 10^{-3}$ |
| .0555 | .0608 | 5.265 | $1.468 \times 10^{-3}$ |
| .0608 | .0634 | 2.663 | $2.082 \times 10^{-3}$ |
| .0634 | .0951 | 2.429 | $2.082 \times 10^{-3}$ |
| .0951 | 1.0000 | .343 | $2.062 \times 10^{-4}$ |

TABLE 29.– ROTOR BLADE STIFFNESS DISTRIBUTION; VALUES FOR THE PITCH FLEXURE WEB SPAN PERTAIN TO THE SOFT PITCH FLEXURE ONLY

| Inboard station, $r/R$ | Outborad station, $r/R$ | $EI_\beta$, $10^3$ N-m$^2$ | $EI_\zeta$, $10^3$ N-m$^2$ | $GJ$, $10^2$ N-m$^2$ |
|---|---|---|---|---|
| 0 | 0.0192 | 57.3831 | 57.3831 | 562.4 |
| .0192 | .0430 | .4834 | .6178 | .0094 |
| .0430 | .0456 | 62.8345 | 62.8345 | 562.4 |
| .0456 | .0555 | 78.0409 | 78.0409 | 568.1 |
| .0555 | .0608 | 52.2186 | 52.2186 | 208.9 |
| .0608 | .0634 | .8607 | 86.9555 | 51.6 |
| .0634 | .0951 | .6955 | 62.6135 | 47.6 |
| .0951 | 1.0000 | .01690 | .34378 | .0508 |

## TABLE 30.– ROTOR MATH MODEL PARAMETER VALUES

| Parameter | Symbol | Blade | |
|---|---|---|---|
| | | Set 1 | Set 2 |
| Nominal rotor speed | $\Omega_o$ | 1000 rpm | 1000 rpm |
| Airfoil section lift curve slope | $a$ | 6.283 | 6.283 |
| Profile drag coefficient | $c_{d_o}$ | 0.0079 | 0.0079 |
| Rotor solidity | $\sigma_S$ | .0572 | .0572 |
| Hub offset ratio | $e_1$ | .1051 | .1051 |
| Nonrotating lead-lag structural damping for soft flexures | $\zeta_{LL}$ | .00826 | .007423 |
| Lock number | $\gamma$ | 5.115 | 5.042 |
| Normalized nonrotating flapping frequency | $\omega_{\beta NR}$ | .3150 | .3114 |
| Normalized nonrotating lead-lag frequency | $\omega_{\zeta NR}$ | 1.4760 | 1.4028 |
| Dimensionless torsional rigidity | $\kappa$ | .00286 | .00235 |
| Dimensionless hub component mass moment of inertia | $i_p$ | .000908 | .000892 |
| Dimensionless blade polar mass moment of inertia ratio | $I_{EA}$ | .02891 | .02811 |
| Static torsional stiffness ratio | $f$ | 5.899 soft | 7.062 soft |
| | | 8404 stiff | 10059 stiff |
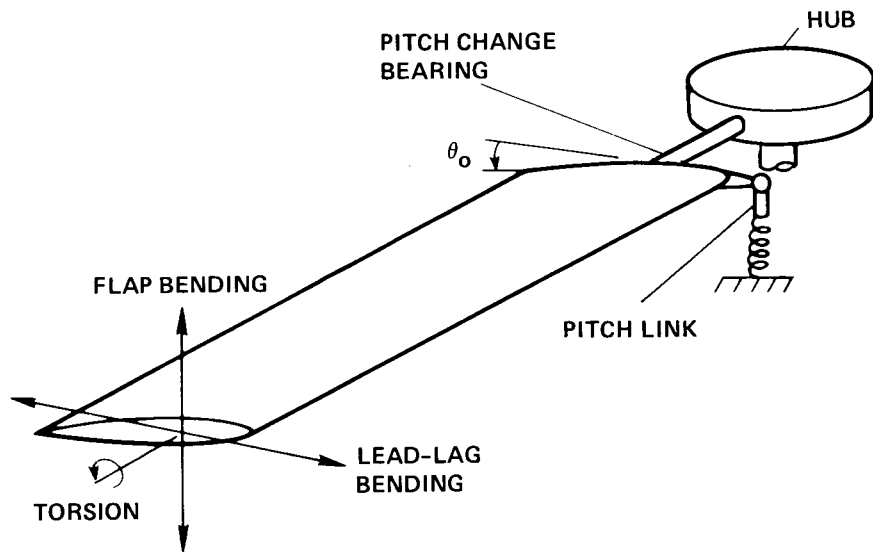
Figure 1.– Schematic of model rotor blade.
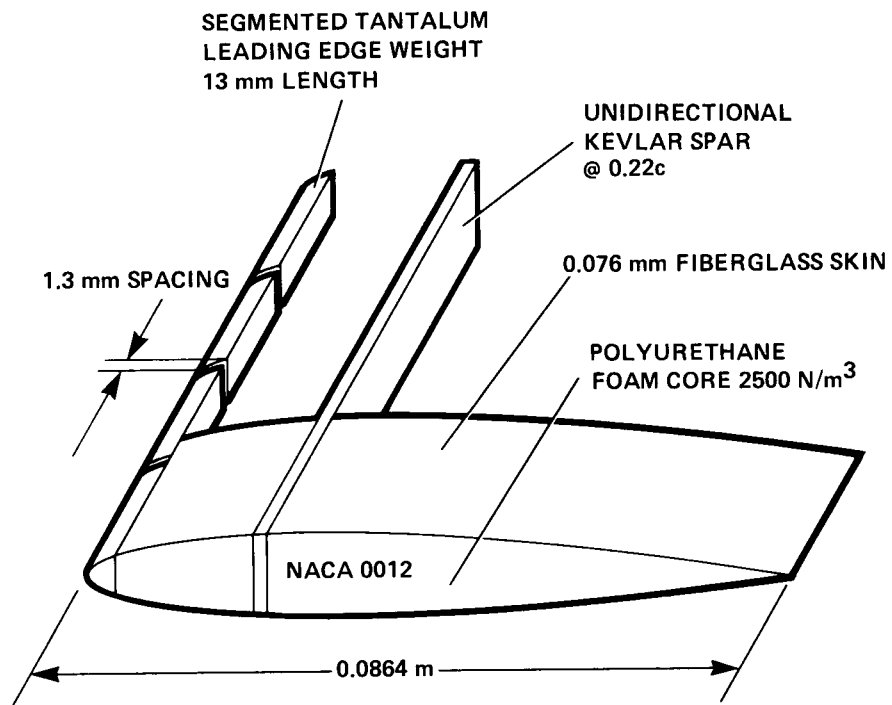


Figure 2.– Experimental model blade design.
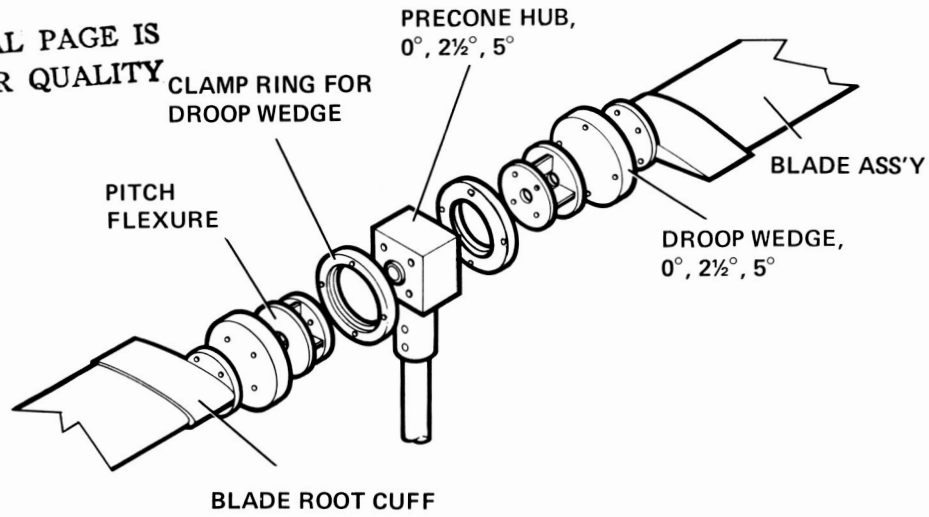
Figure 3.– Experimental model rotor hub design.
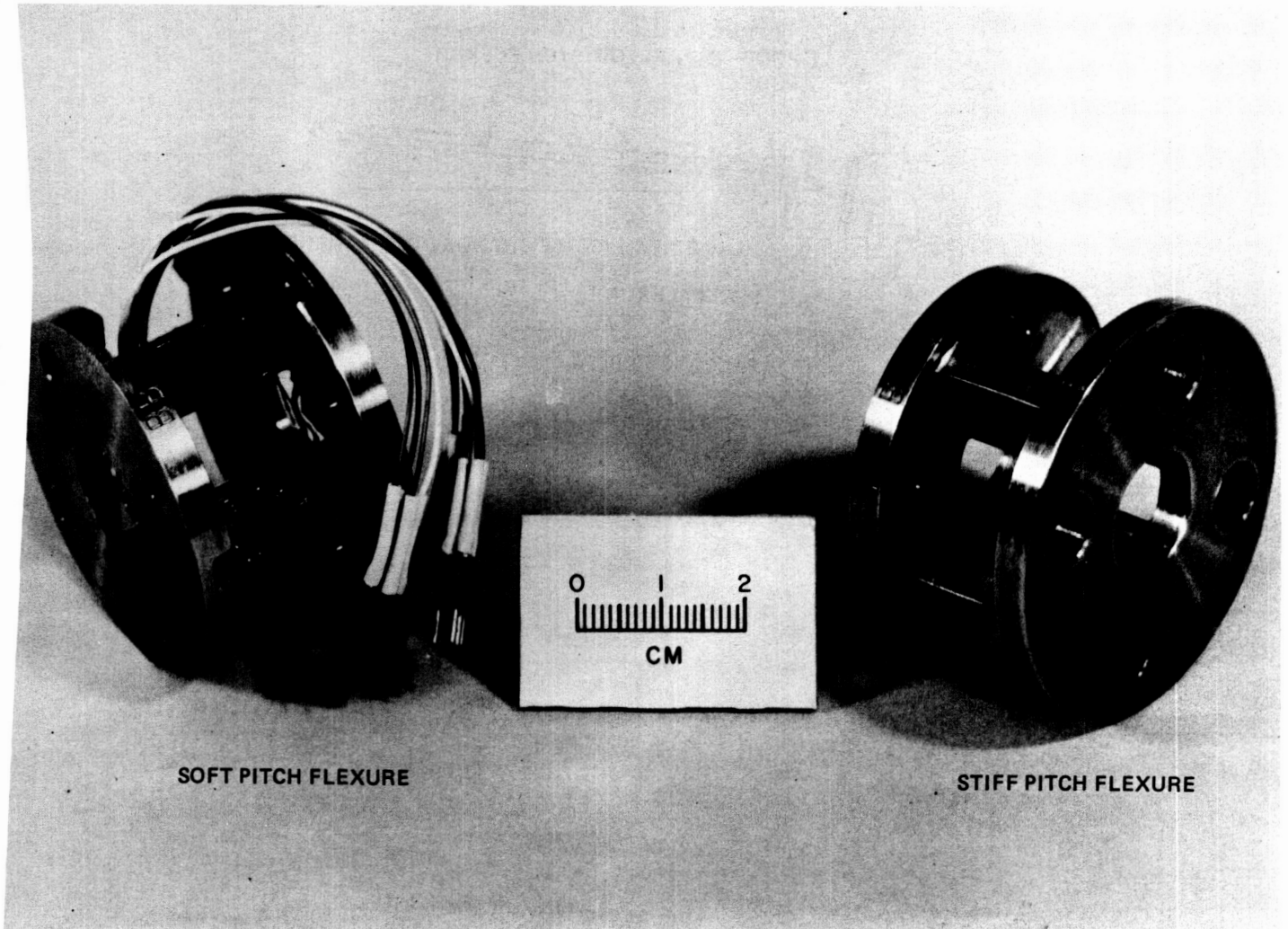
Figure 4.– Experimental model pitch flexures.
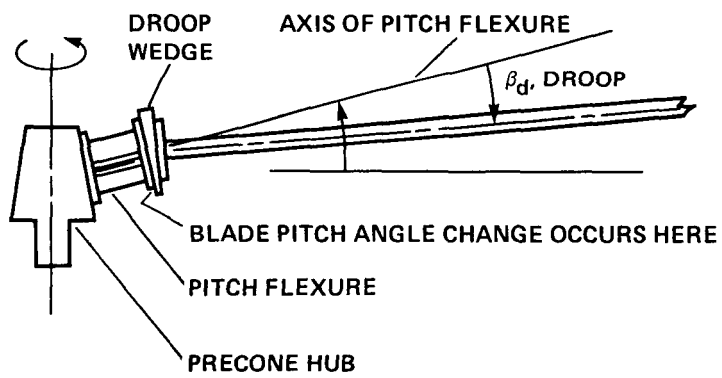
Figure 5.— Orientation of precone and droop, positive angles shown.
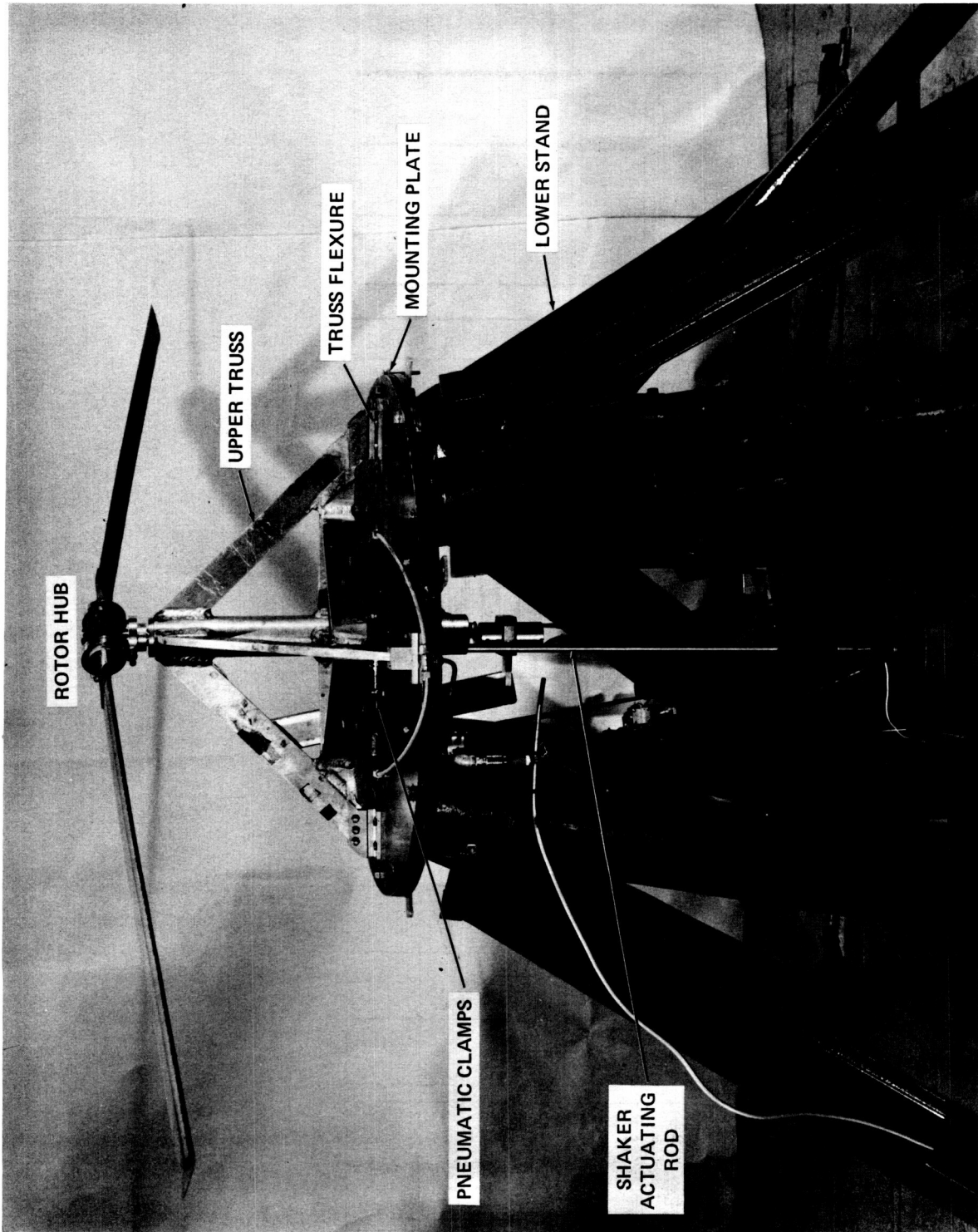
Figure 6.— Experimental model rotor test stand.

ROTOR HUB

UPPER TRUSS

TRUSS FLEXURE

MOUNTING PLATE

LOWER STAND

PNEUMATIC CLAMPS

SHAKER ACTUATING ROD
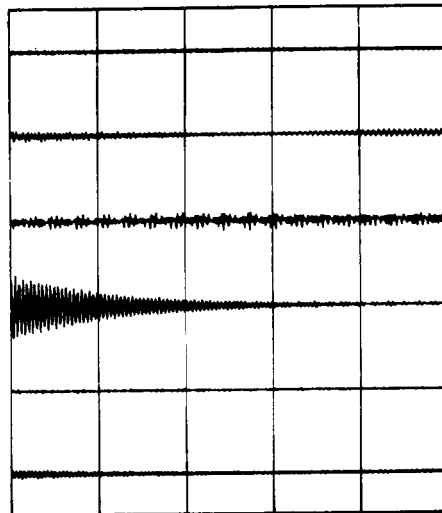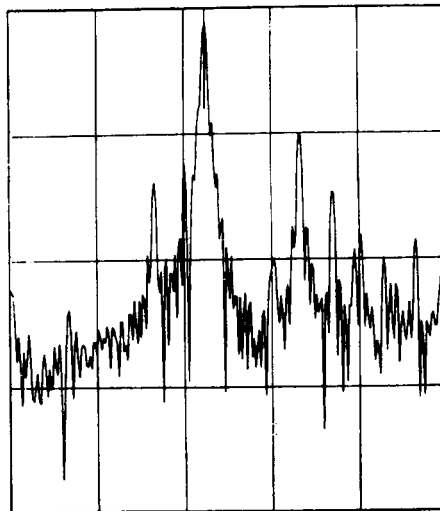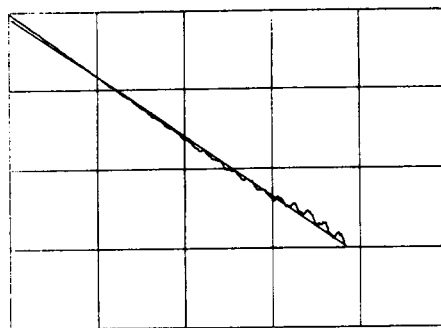
Figure 7.— Online data analysis display; a) Six channel data display mode, b) FFT of differential lead-lag mode signal,
c) Modal damping display using moving block analysis.
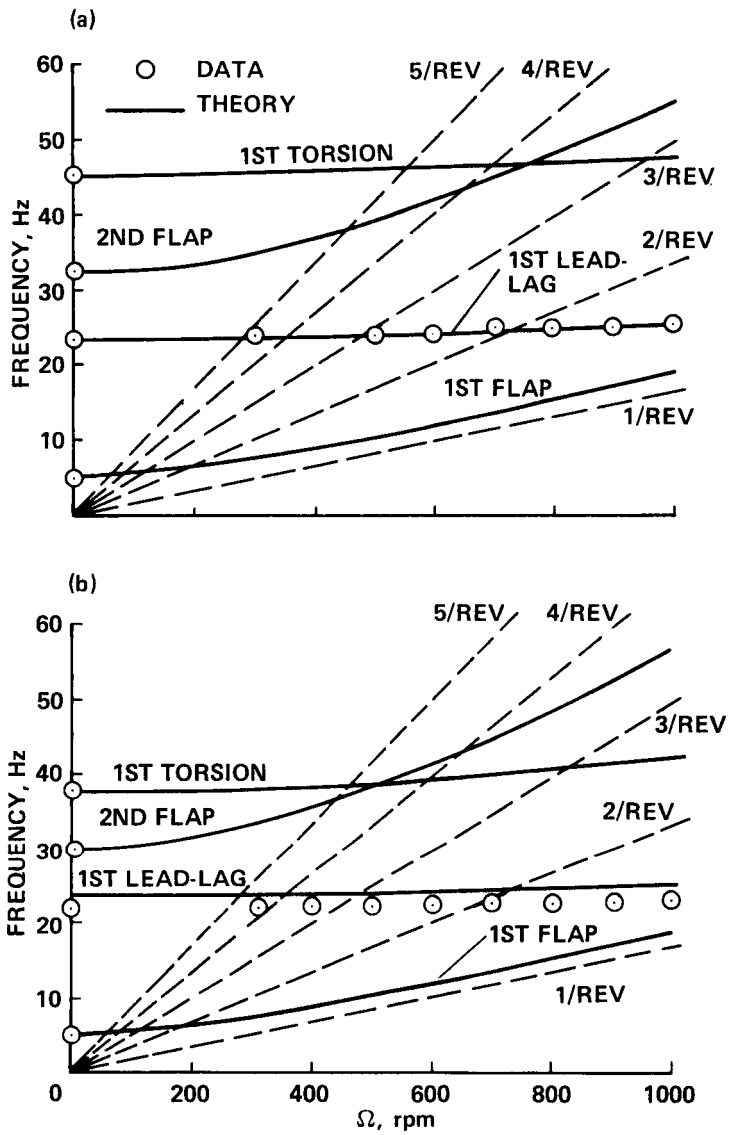
Figure 8.— Measured modal frequencies as compared with theory for blade set 2; a) Stiff pitch flexures, b) Soft pitch flexures.
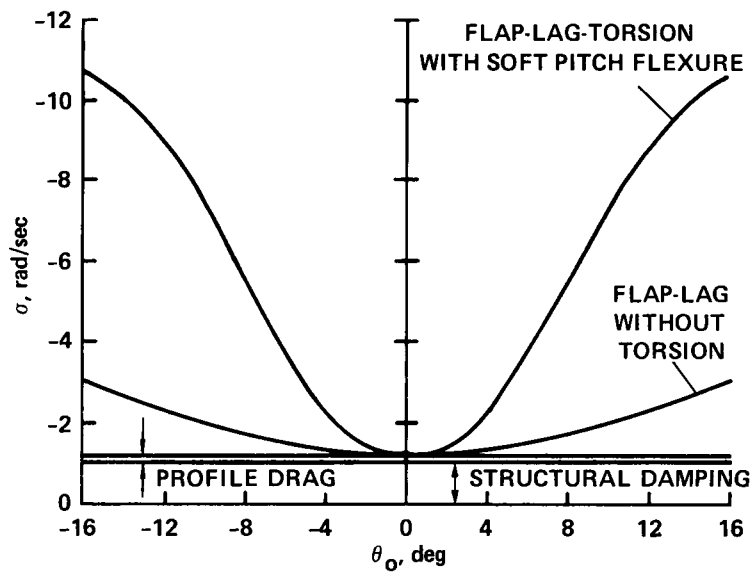
Figure 9.— Theoretical prediction of the relative magnitude of various contributions to rotor blade lead-lag damping, no precone or droop.
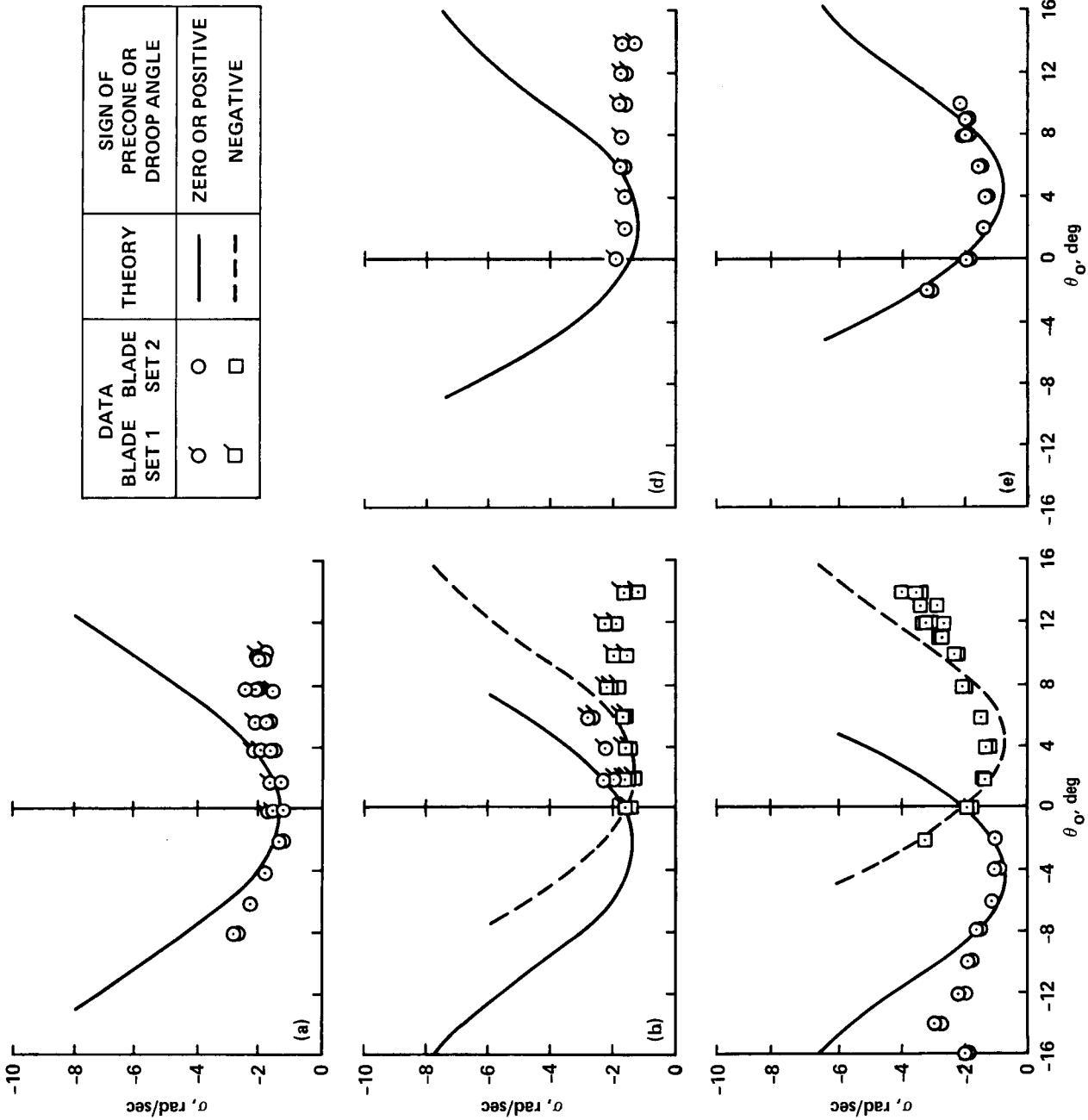
Figure 10.– Effect of precone and droop; lead-lag damping versus blade pitch angle, stiff pitch flexure; a) Without precone or droop, b) 2.5° droop, c) 5° droop, d) 2.5° precone, e) 5° precone.

49
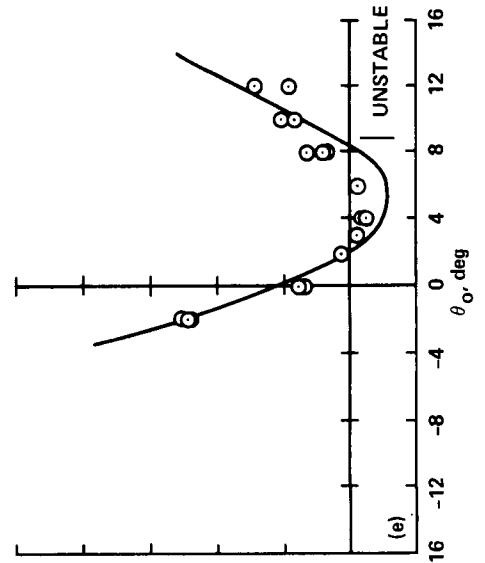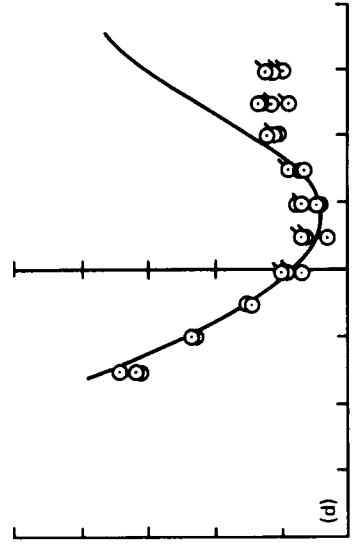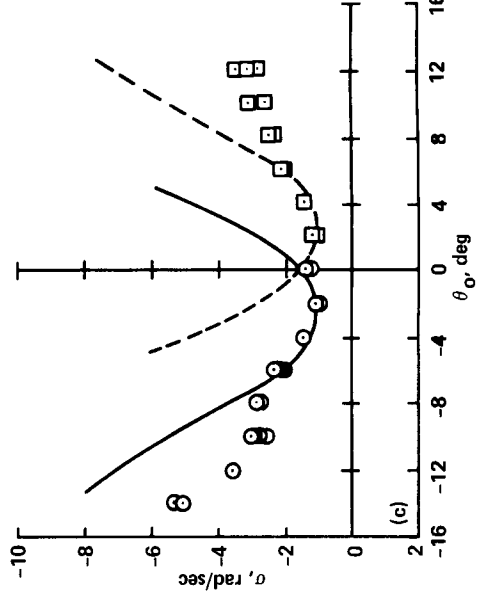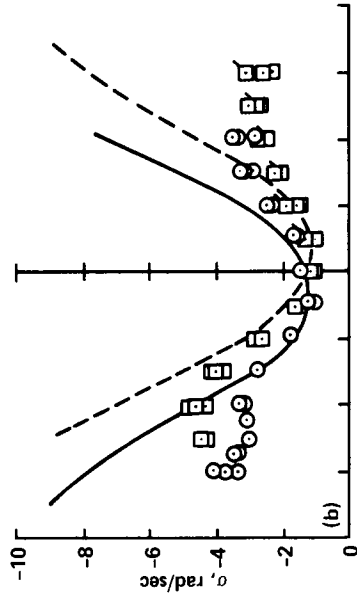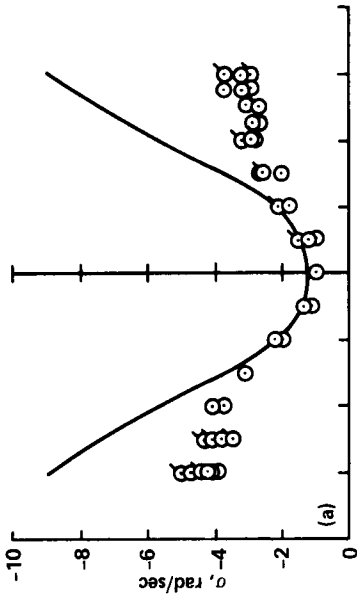
Figure 11.— Effect of precone and droop; lead-lag damping versus blade pitch angle, soft pitch flexure; a) Without precone or droop, b) 2.5° droop, c) 5° droop, d) 2.5° precone, e) 5° precone.
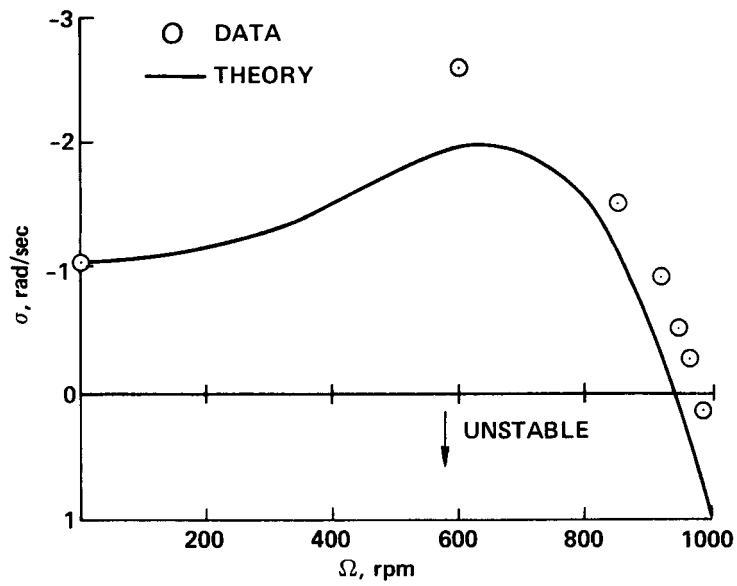
Figure 12.— Lead-lag damping versus rpm; $5°$ precone, $0°$ droop, $\theta_O = 4°$, soft pitch flexure, blade set 2.
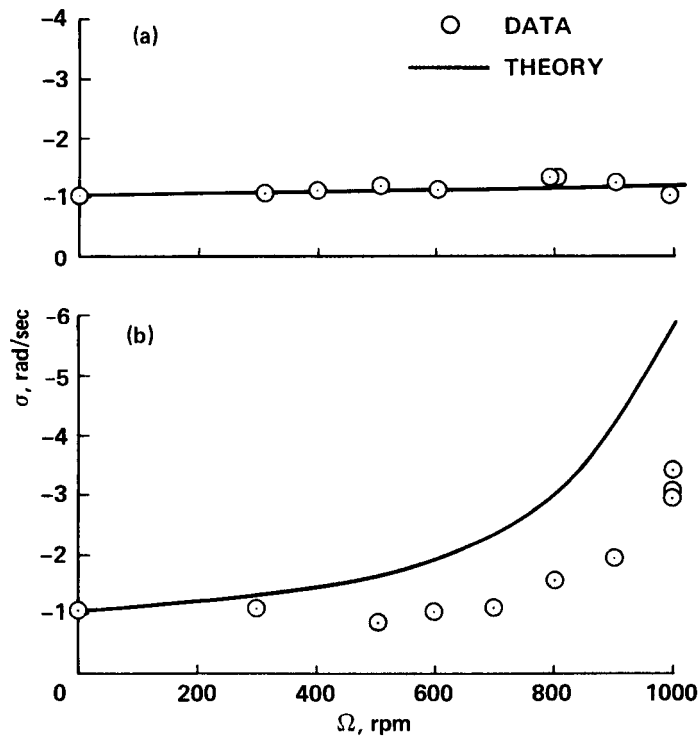


Figure 13.— Lead-lag damping versus rpm, without precone or droop, soft pitch flexures blade set 2;
a) $\theta_O = 0°$, b) $\theta_O = 8°$.
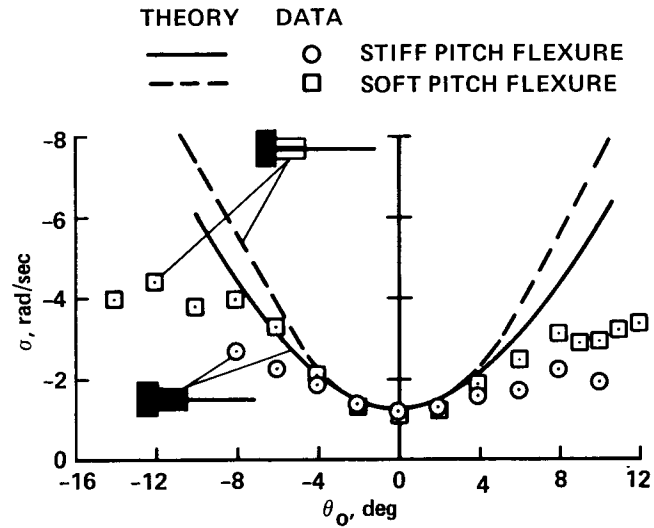
Figure 14.— Effect of pitch flexure stiffness on lead-lag damping variation with pitch angle, without precone or droop.
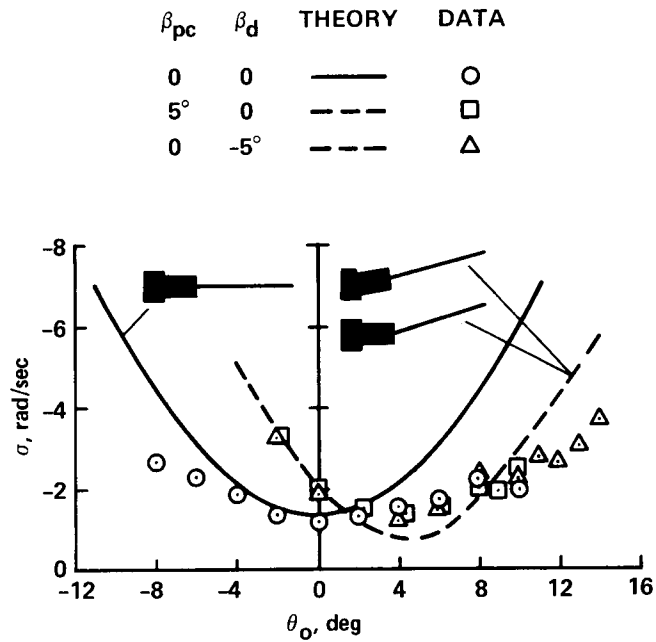


Figure 15.— Effect of precone and droop on lead-lag damping variation with pitch angle, stiff pitch flexure.
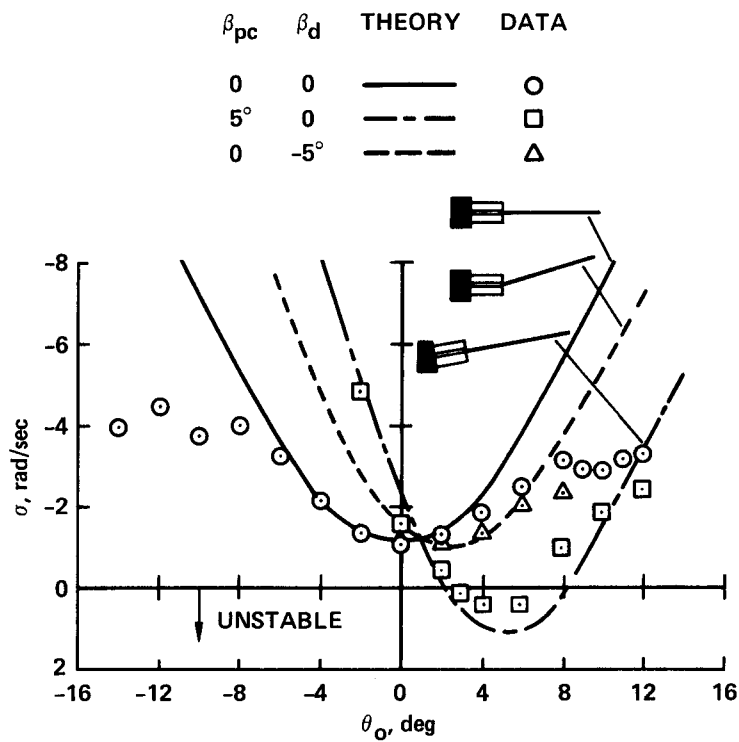
Figure 16.— Effect of precone and droop on lead-lag damping variation with pitch angle, soft pitch flexure.
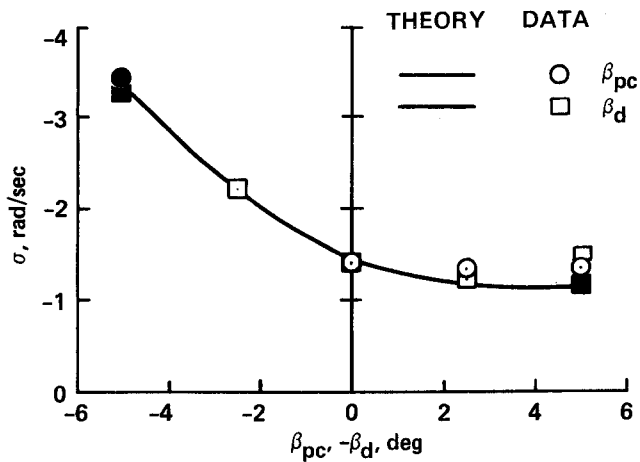


Figure 17.— Variation of lead-lag damping with precone and droop, $\theta_O = 2°$, stiff pitch flexures (for solid dymbols, $\theta_O = -2°$ and the sign of the precone or droop angle has been reversed).

53
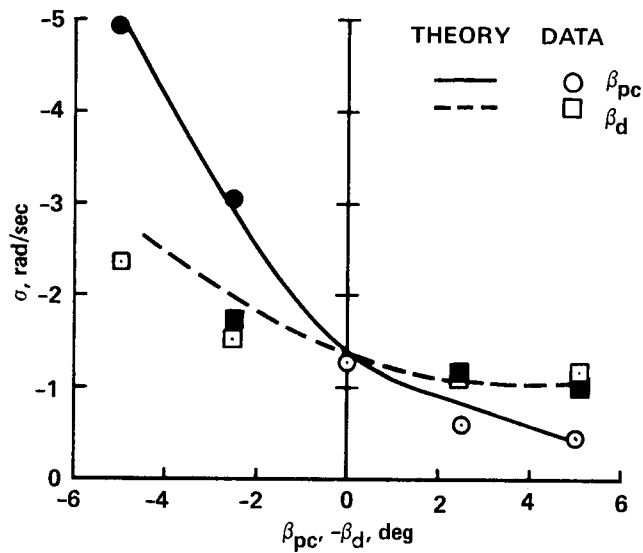
Figure 18.— Variation of lead-lag damping with precone and droop, $\theta_O = -2°$, soft pitch flexure (for solid symbols, $\theta_O = -2°$ and the sign of the precone or droop angle has been reversed).
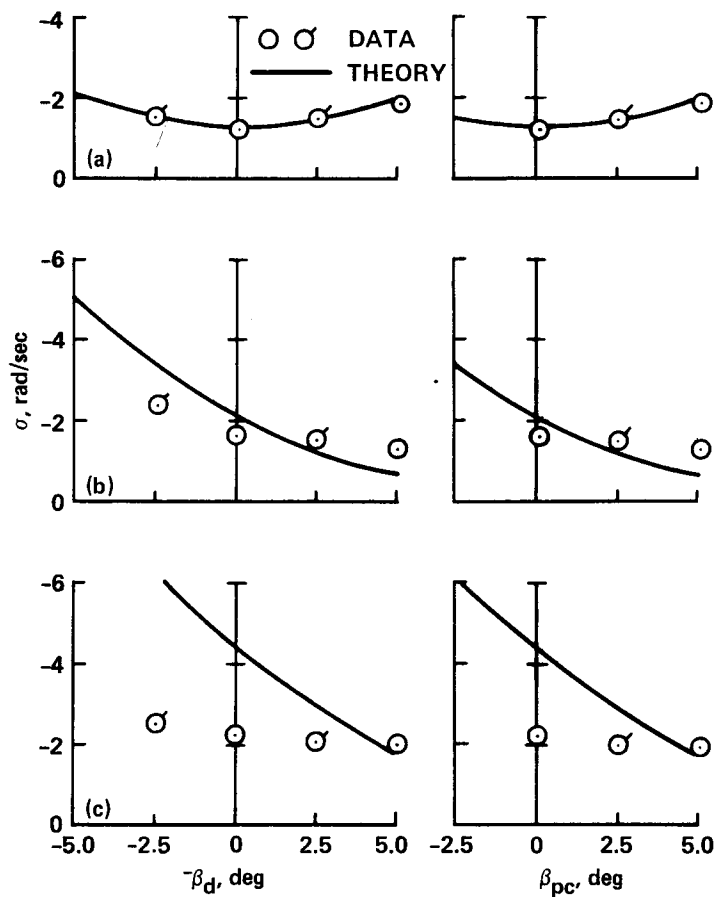


Figure 19.— Precone and droop effect on lead-lag damping at various pitch angles, stiff pitch flexure (flagged symbols represent blade set 1 data); a) $\theta_O = 0°$, b) $\theta_O = 4°$, c) $\theta_O = 8°$.
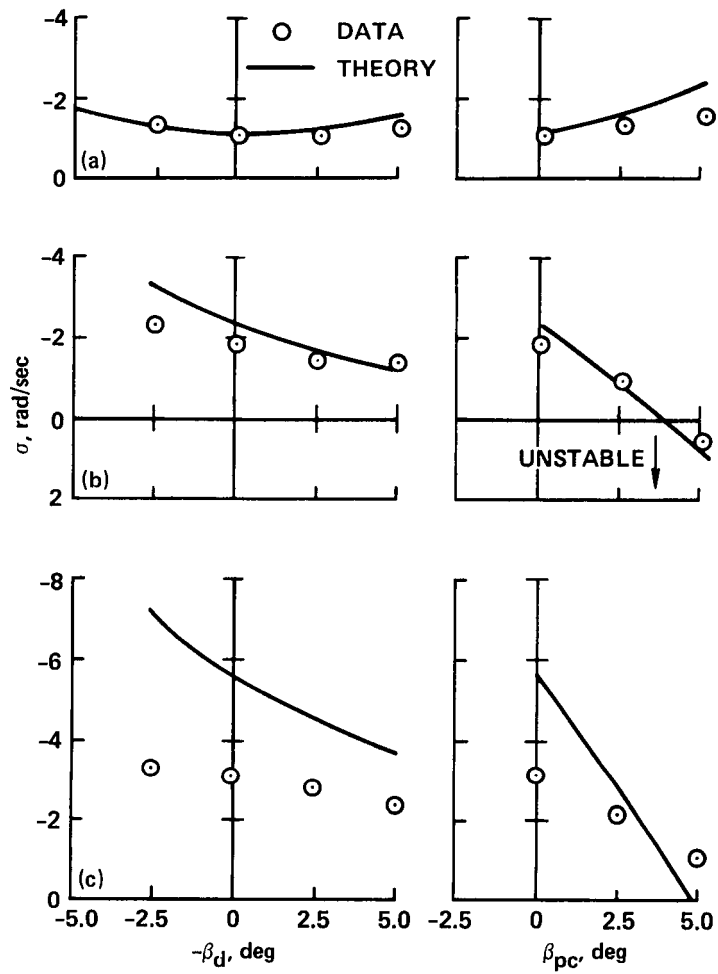
Figure 20.— Precone and droop effect on lead-lag damping at various pitch angles, soft pitch flexure; a) $\theta_O = 0°$, b) $\theta_O = 4°$, c) $\theta_O = 8°$.
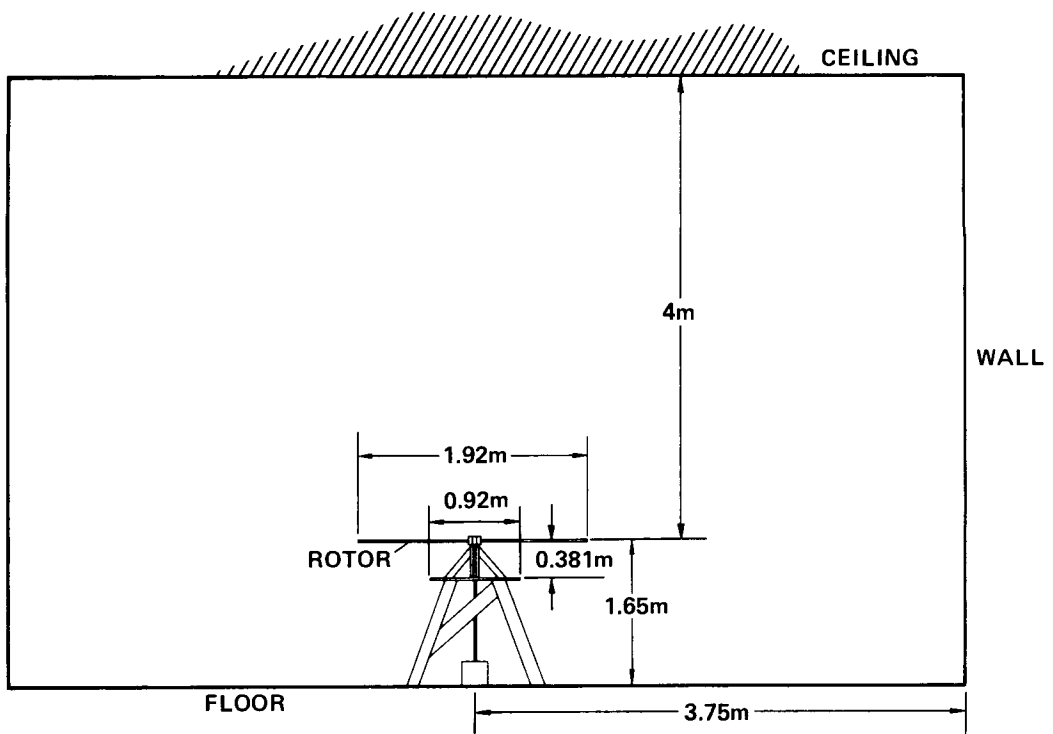
Figure 21.— Schematic of rotor stand in test facility.
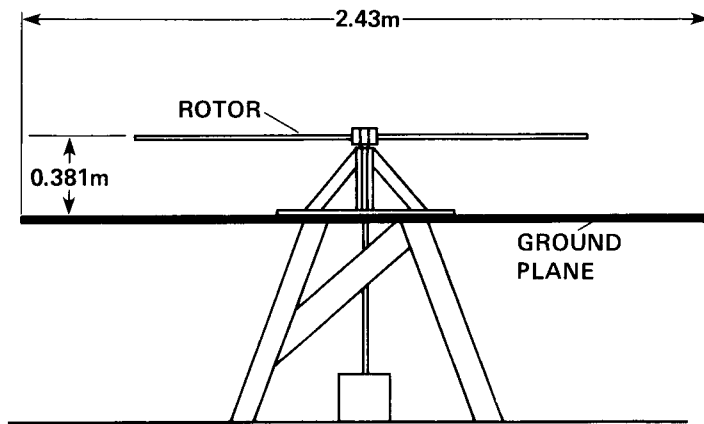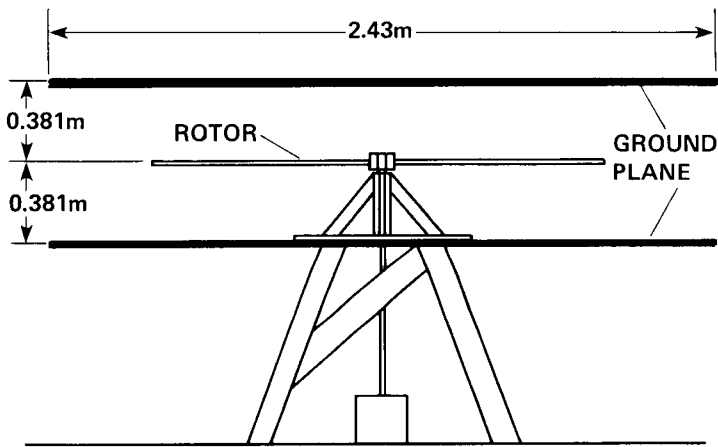
Figure 22.— Rotor stand with ground plane installations; a) Single ground plane, b) Double ground plane.
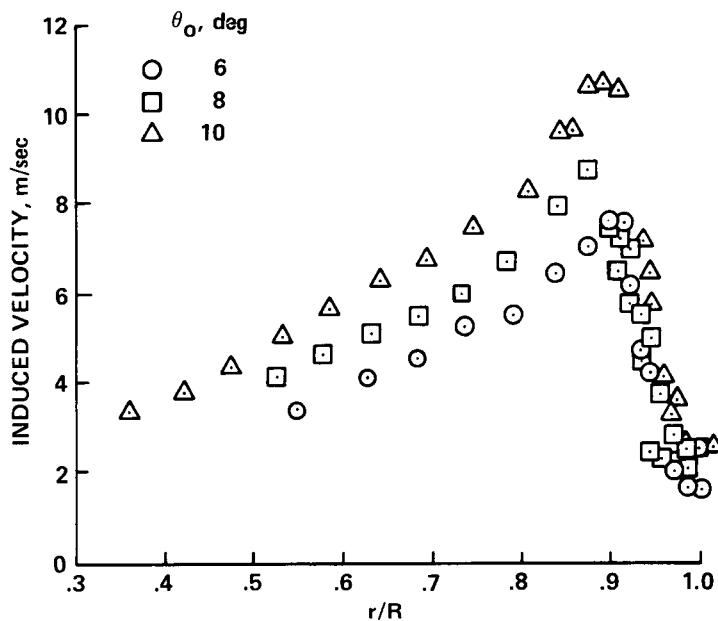
Figure 23.— Rotor induced velocity profile without ground planes, induced velocity versus radial station (for $\theta_O = 6°$ and $8°$, $h = 5$ cm; for $\theta_O = 10°, h = 2.5$ cm).
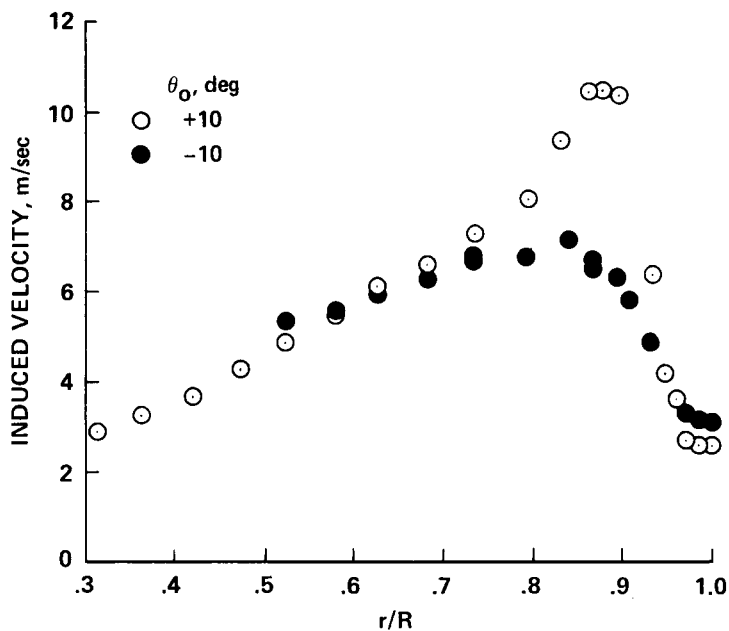


Figure 24.— Comparison of rotor induced velocity at positive and negative thrust setting without ground planes, induced velocity versus radial station, $h = 5$ cm.
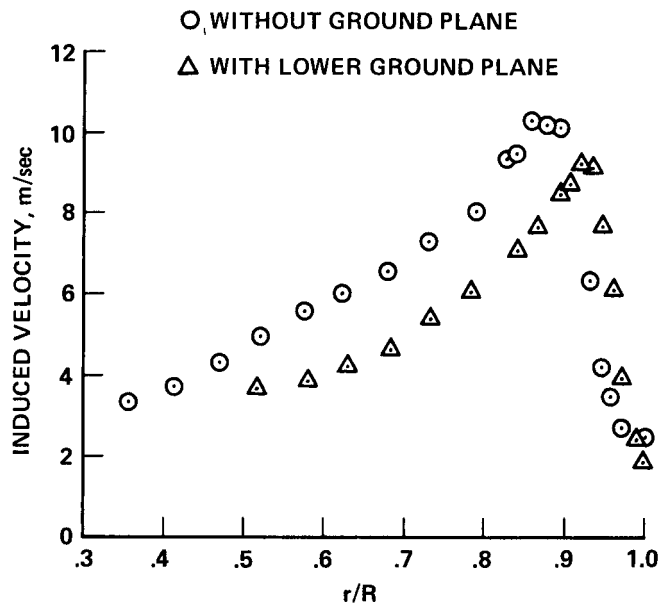
Figure 25.— Comparison of rotor induced velocity with and without ground plane, induced velocity versus radial station, $\theta_O = 10°, h = 2.5$ cm.
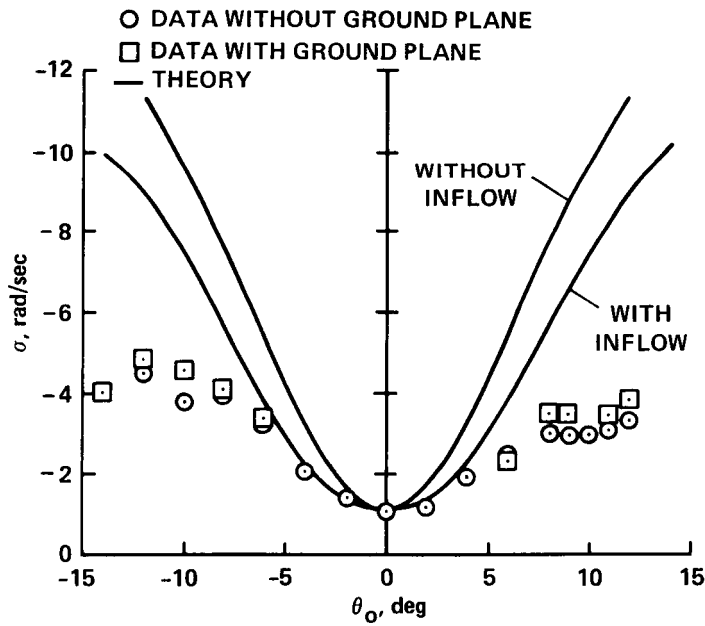


Figure 26.— Comparison of lead-lag damping with and without single ground plane, lead-lag damping versus blade pitch angle, soft pitch flexure, no precone or droop.

59
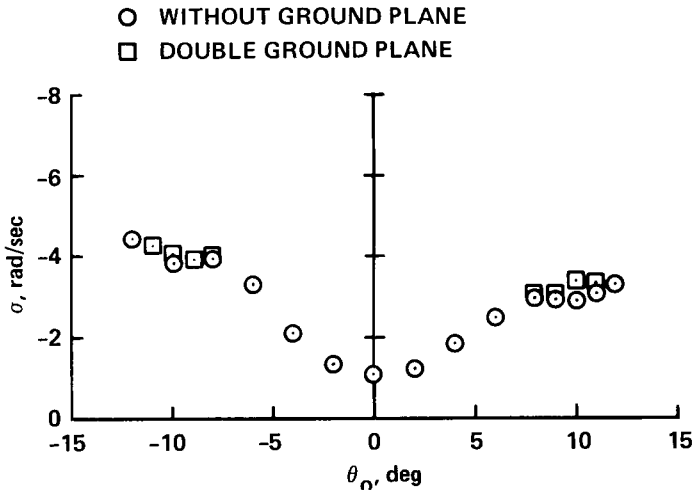
Figure 27.— Comparison of measured lead-lag damping with and without the double ground plane, lead-lag damping versus blade pitch angle, soft pitch flexure, no precone or droop.
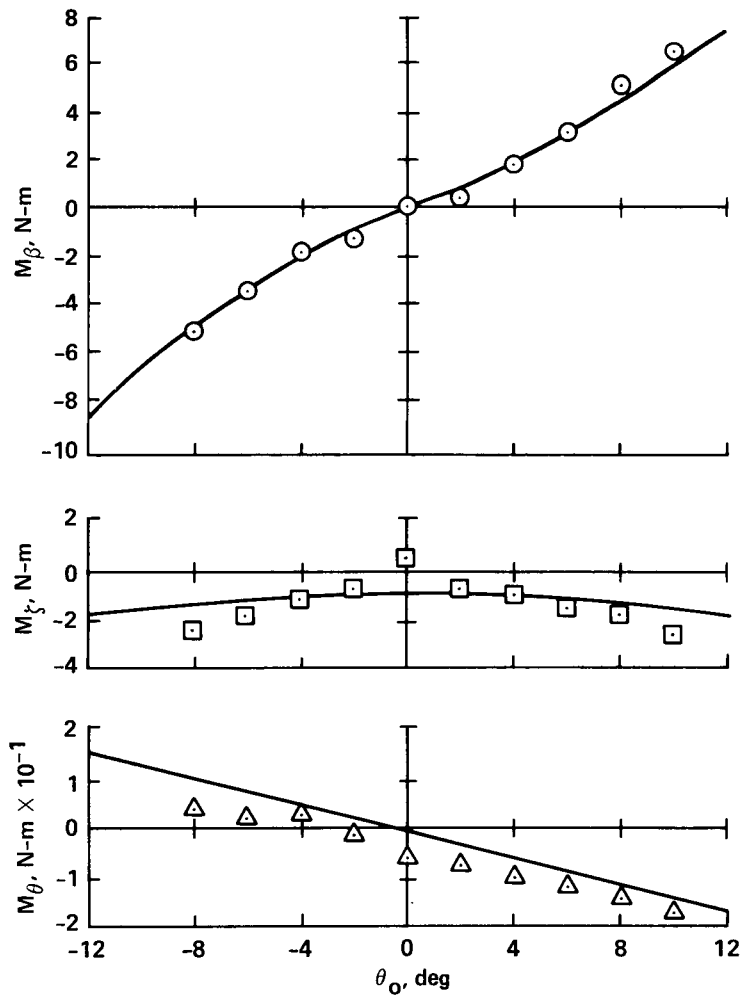


Figure 28.— Steady blade moments versus blade pitch angle, no precone or droop, stiff pitch flexure.
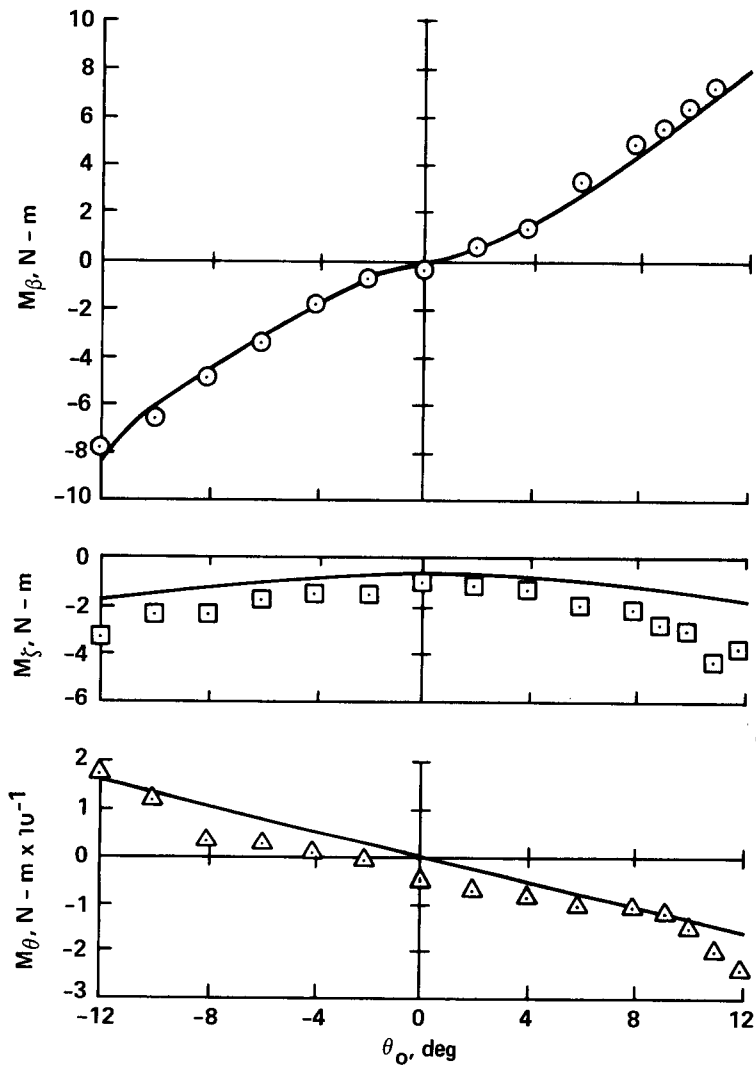
Figure 29.— Steady blade moments versus blade pitch angle, no precone or droop, soft pitch flexure.
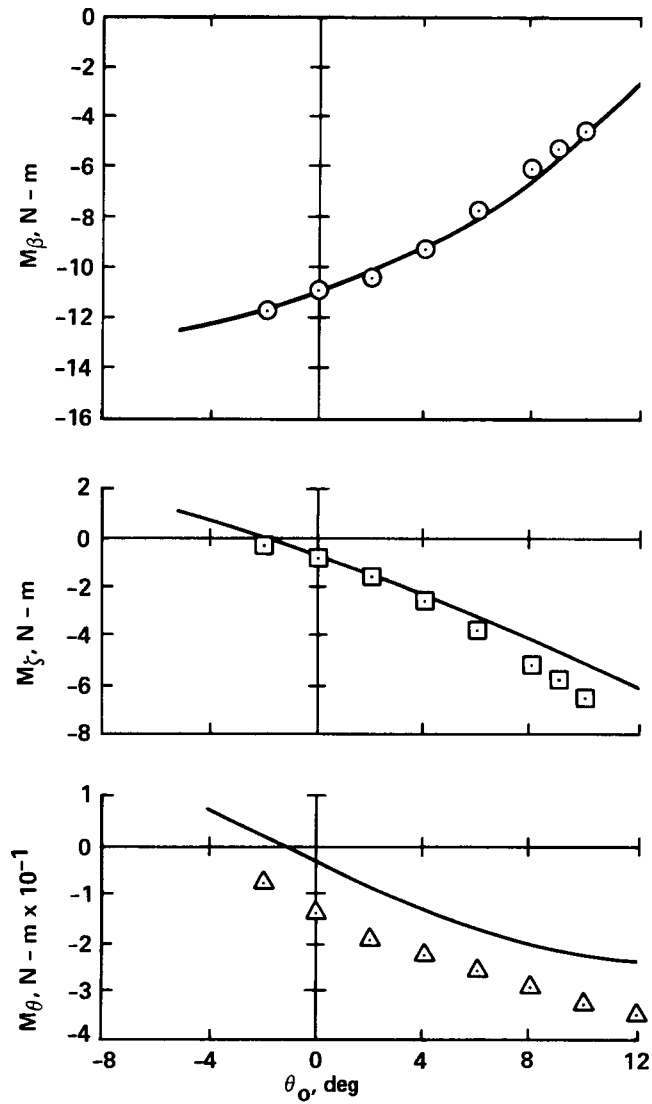
Figure 30.— Steady blade moments versus blade pitch angle, 5° precone, 0° droop, stiff pitch flexure.
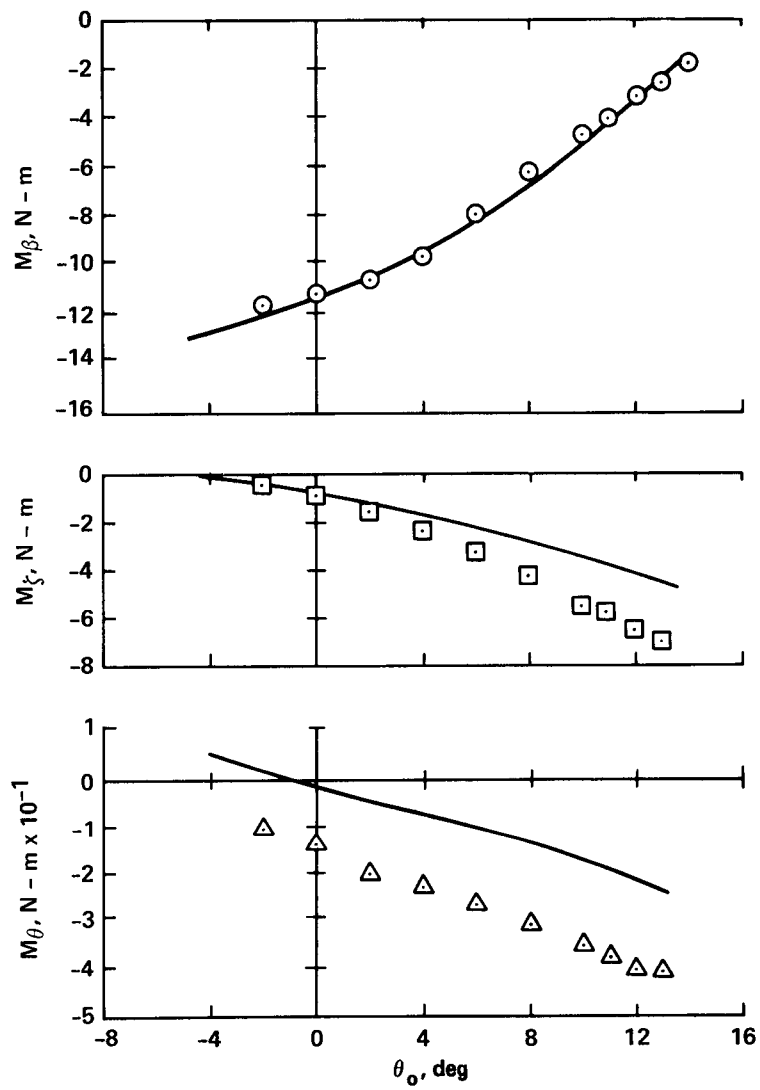
Figure 31.— Steady blade moments versus blade pitch angle, 0° precone, -5° droop, stiff pitch flexure.
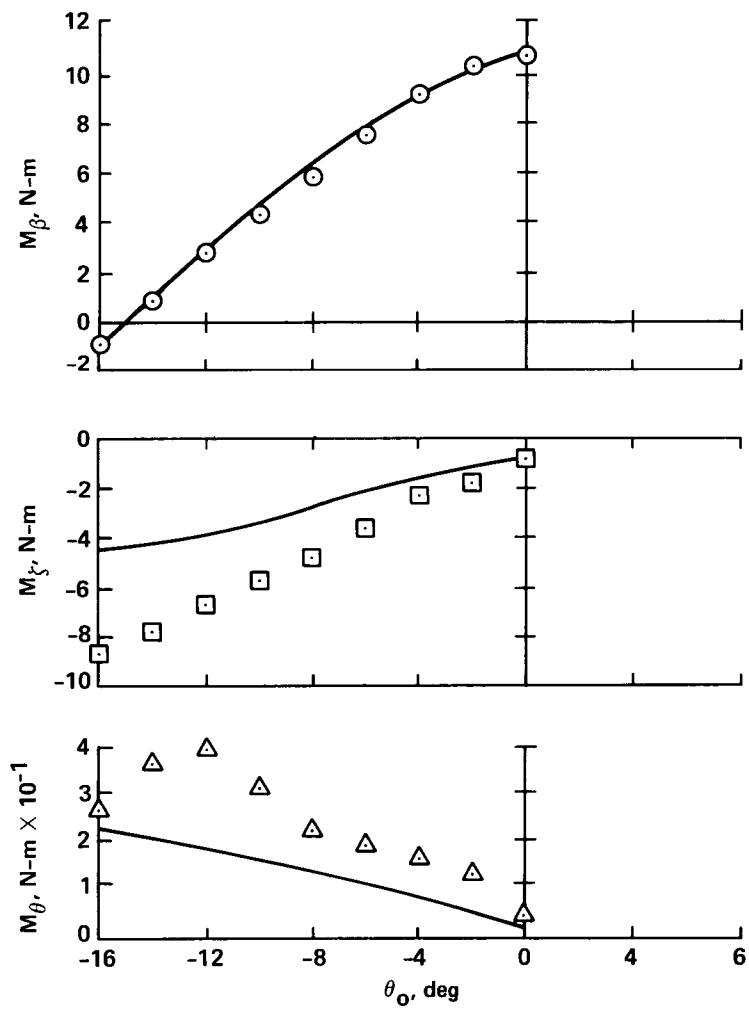
Figure 32.— Steady blade moments versus blade pitch angle, $0°$ precone, $+5°$ droop, stiff pitch flexure.
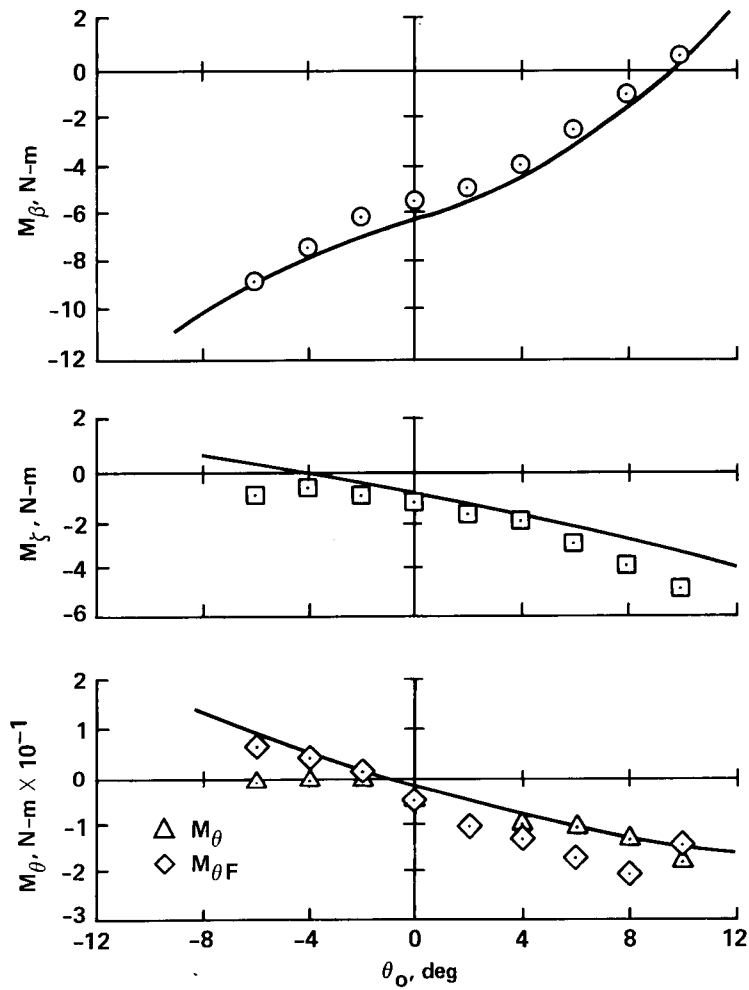
Figure 33.— Steady blade moment versus blade pitch angle, 2.5° precone, 0° droop, soft pitch flexure.
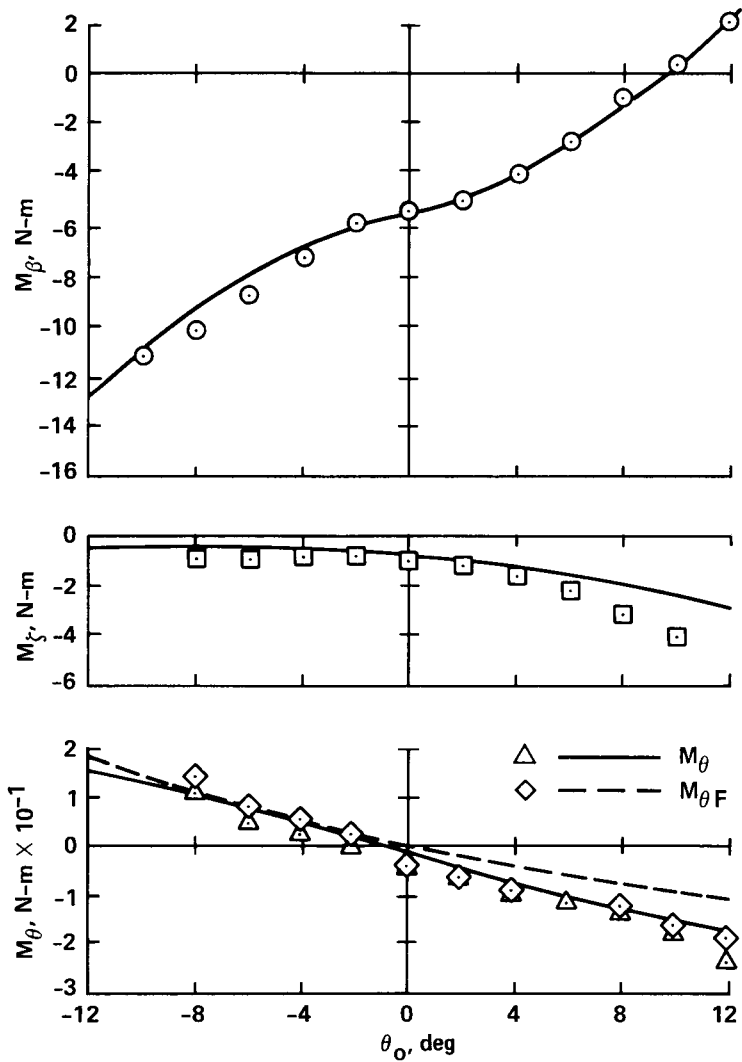
Figure 34.— Steady blade moment versus blade pitch angle, $0°$ precone, $-2.5°$ droop, soft pitch flexure.
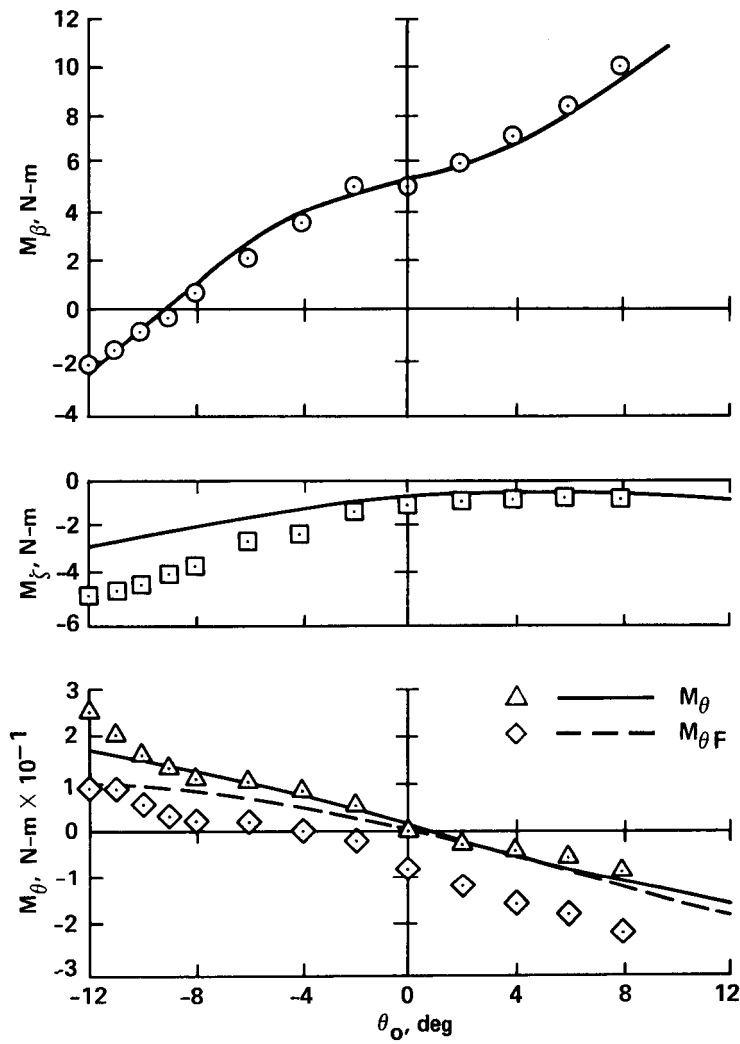
Figure 35.— Steady blade moment versus blade pitch angle, 0° precone, 2.5° droop, soft pitch flexure.
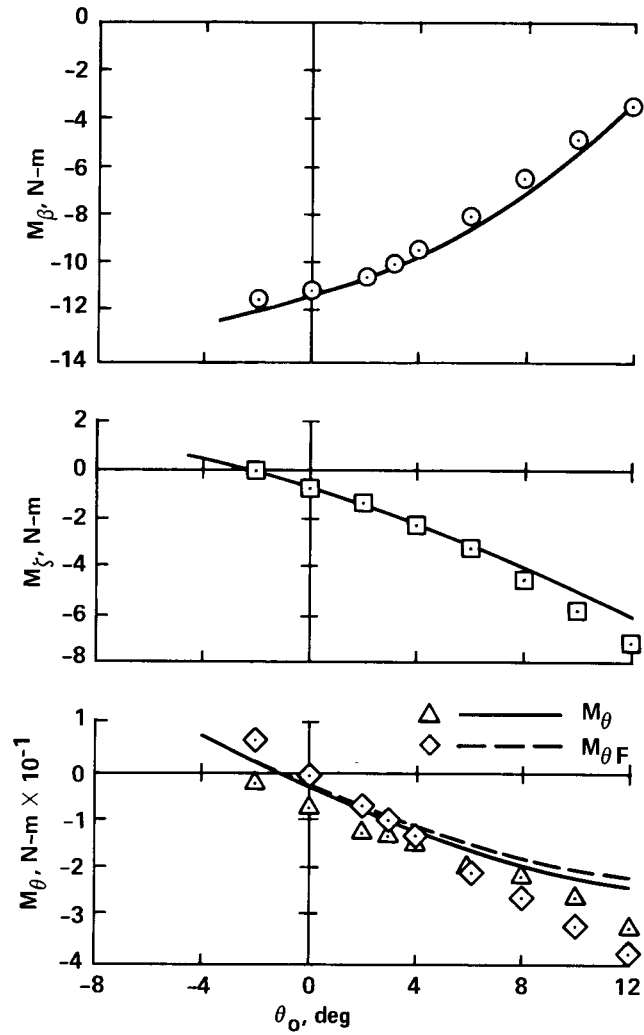
Figure 36.— Steady blade moment versus blade pitch angle, 5° precone, 0° droop, soft pitch flexure.
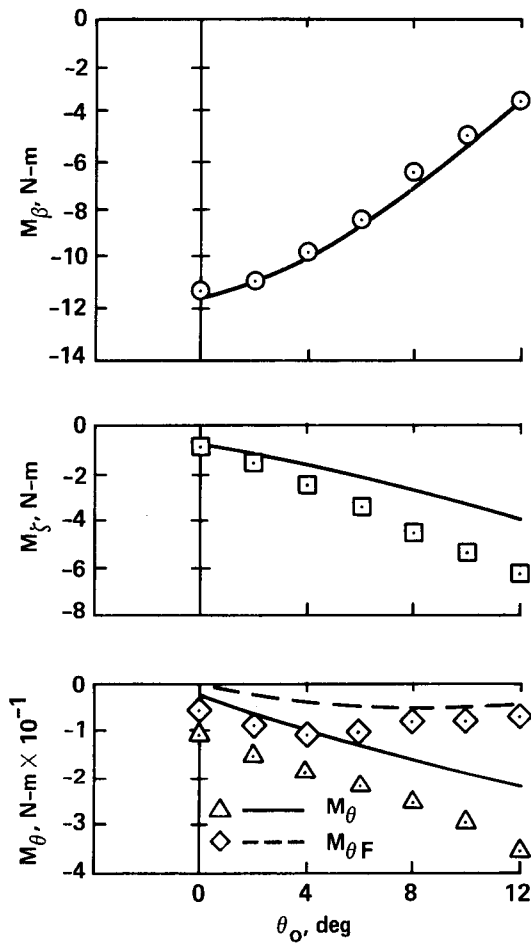
Figure 37.— Steady blade moment versus blade pitch angle, $0°$ precone, $-5°$ droop, soft pitch flexure.
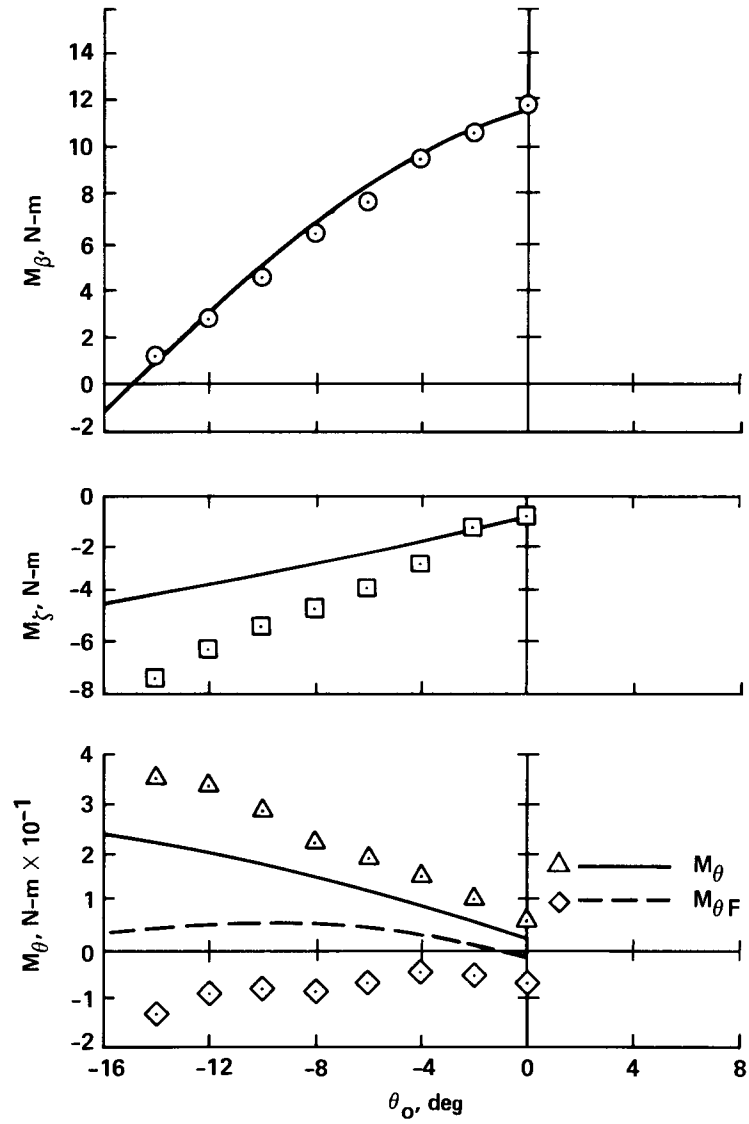
Figure 38.— Steady blade moment versus blade pitch angle, 0° precone, 5° droop, soft pitch flexure.
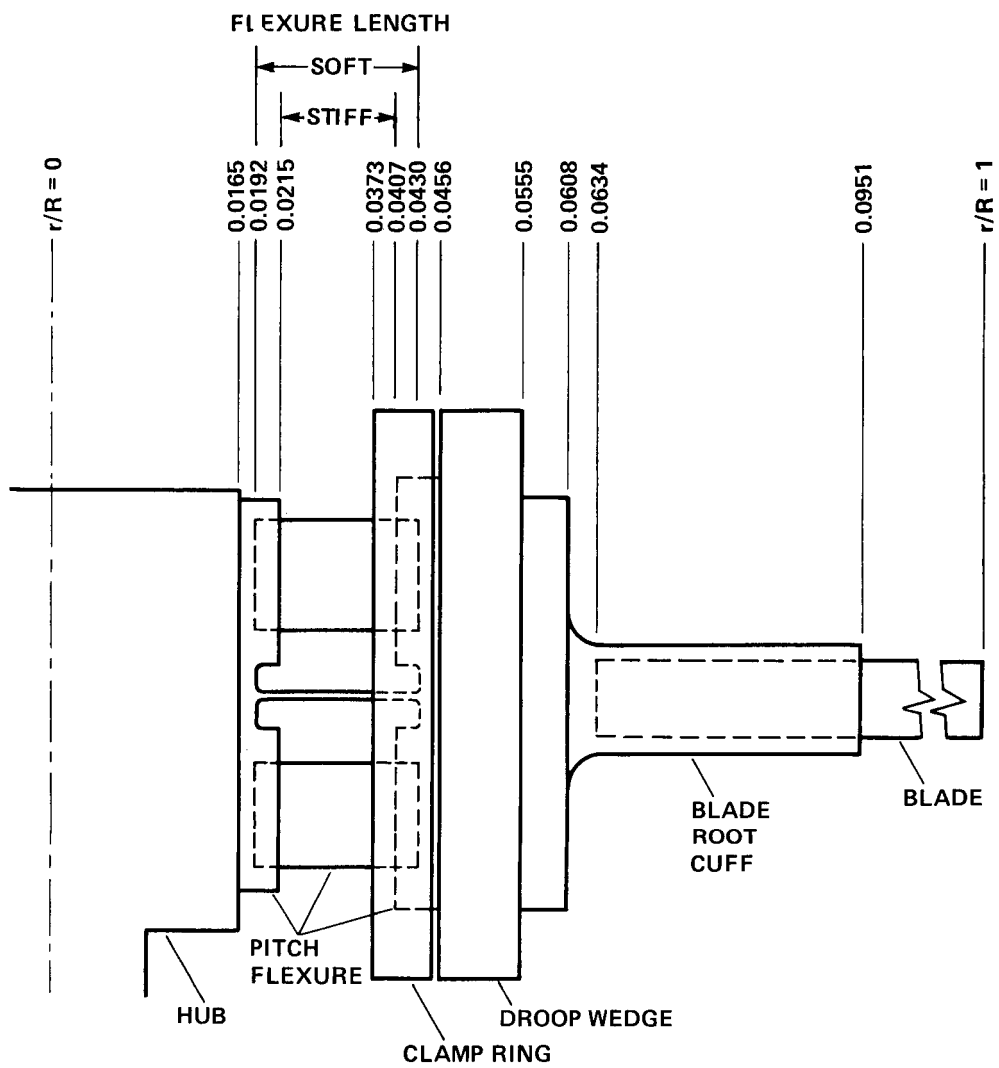
Figure 39.-- Radial location of model rotor hub and blade components.

Figure 40.— Blade chordwise center of gravity determination.
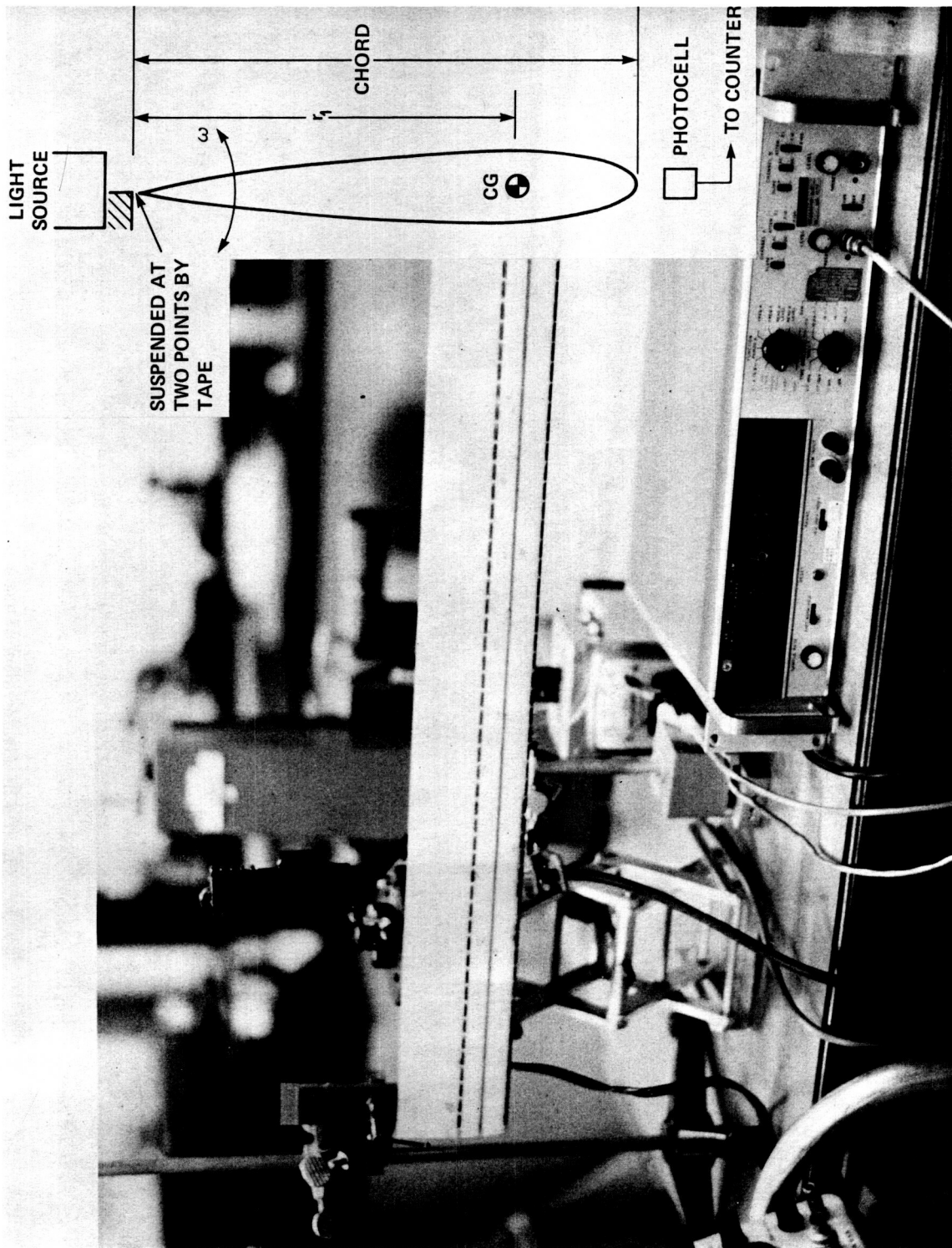
Figure 41.— Blade moment of inertia determination.
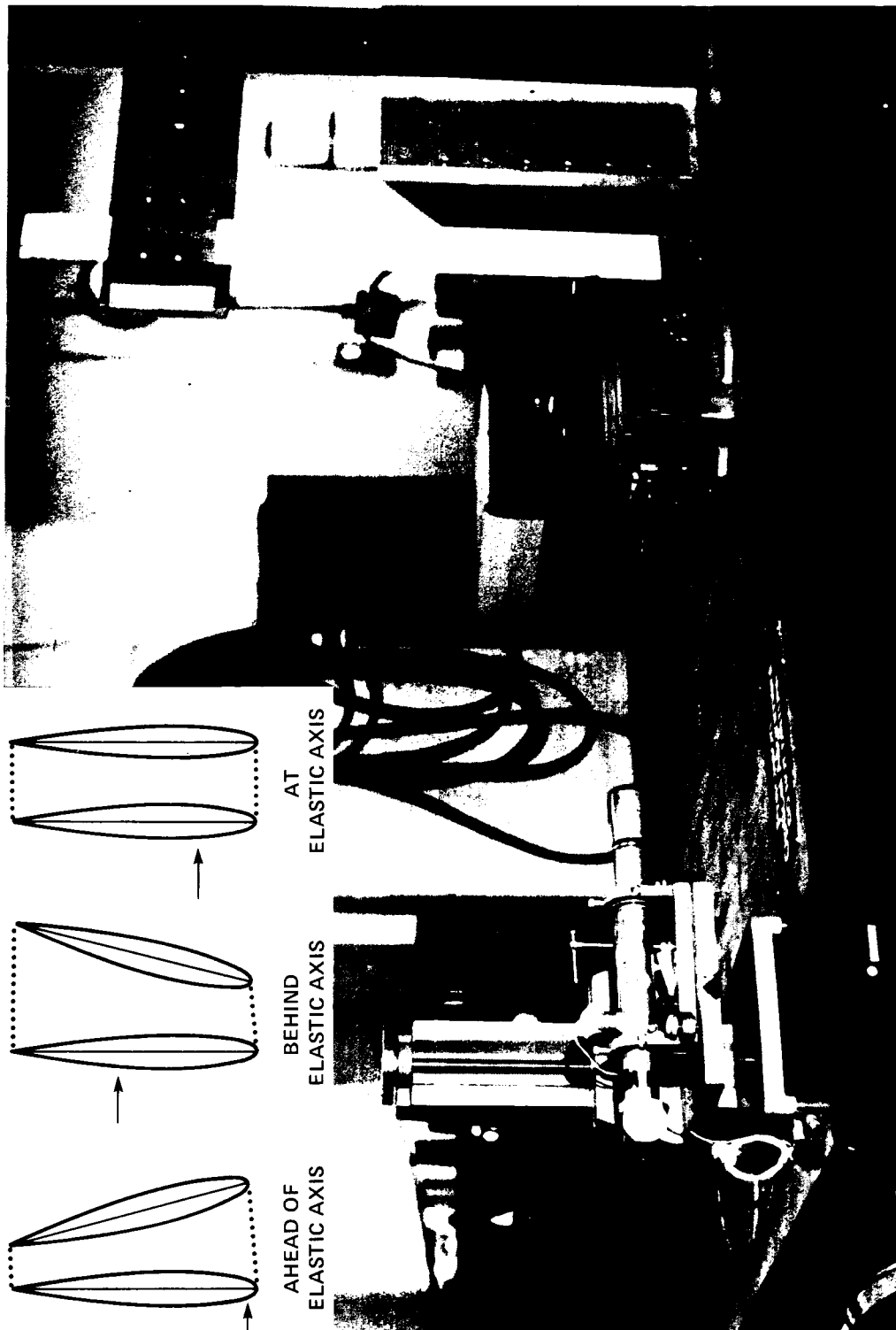
Figure 42.– Measurement of blade elastic axis location.

AT
ELASTIC AXIS

BEHIND
ELASTIC AXIS

AHEAD OF
ELASTIC AXIS
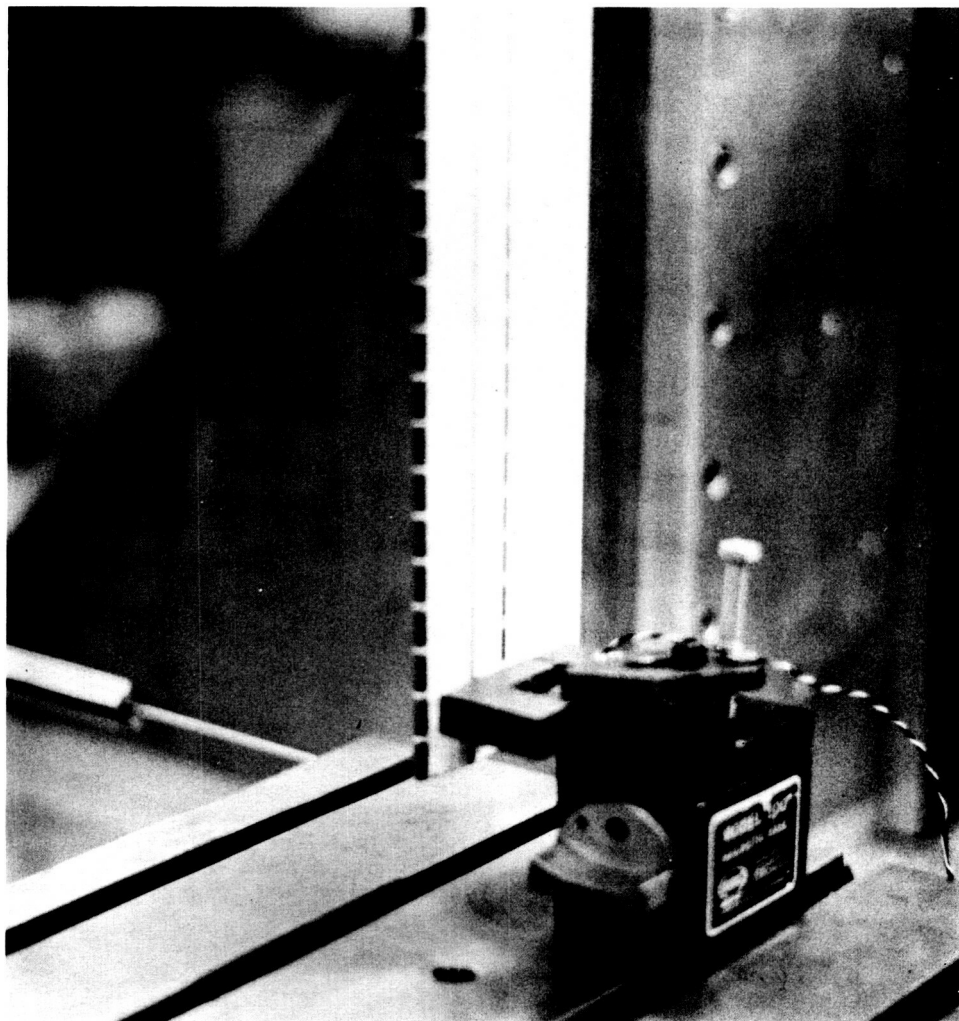
Figure 43.— Blade flapwise stiffness determination by force-deflection.

Figure 44.— Pitch flexure stiffness determination by moment-deflection.
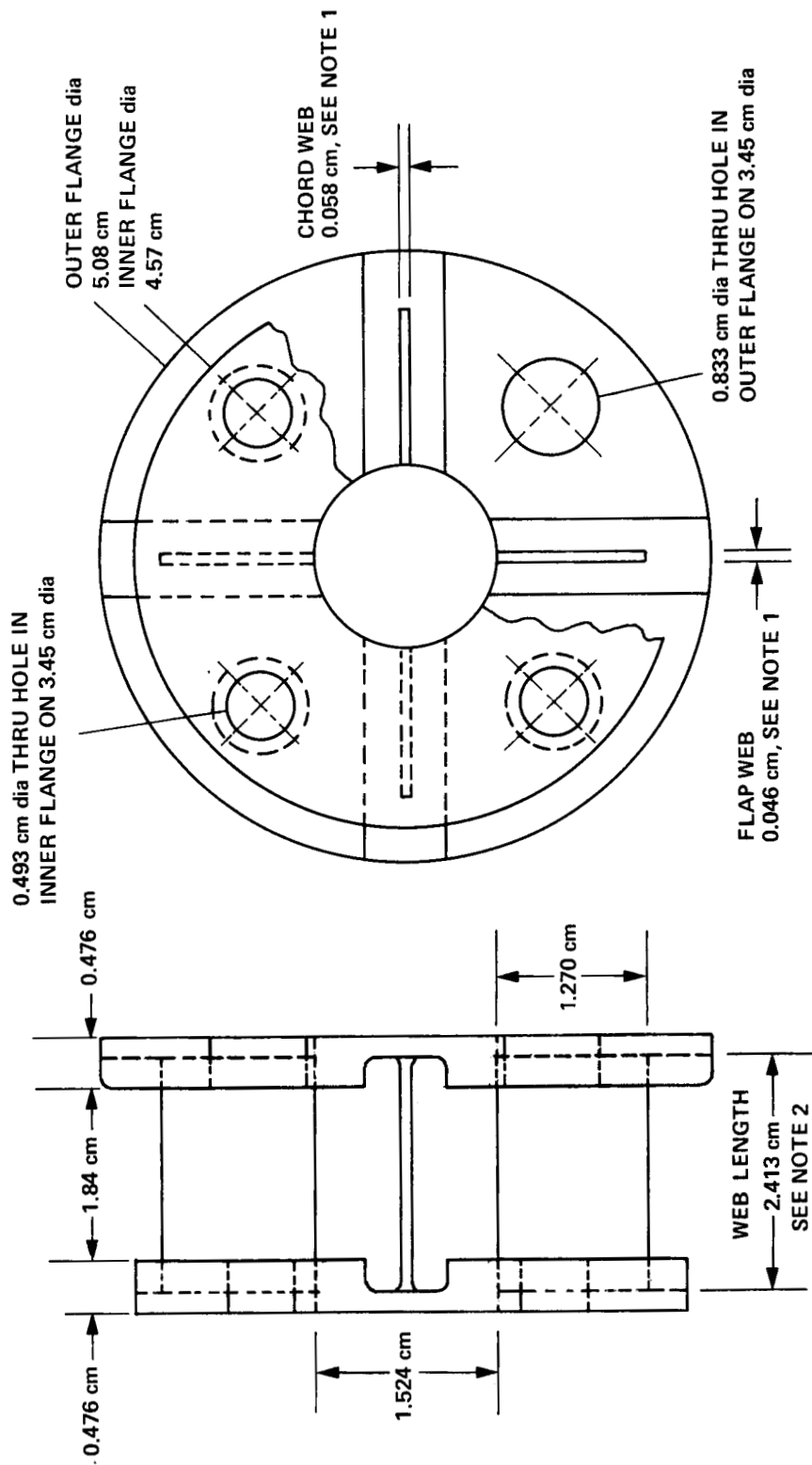
Figure 45.— Pitch flexure dimensions used for calculating bending and torsion stiffness.

77
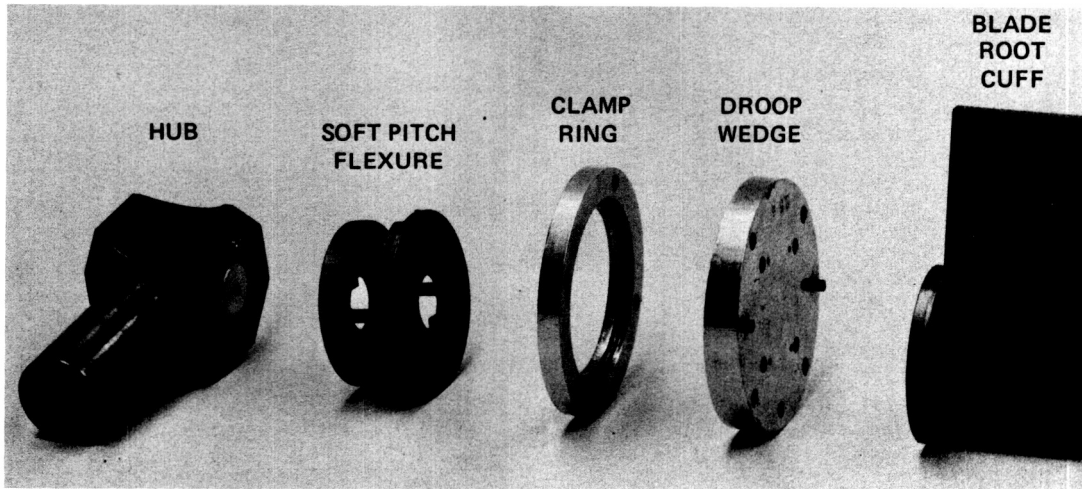
Figure 46.— Hub hardware polar moment of inertia determination.
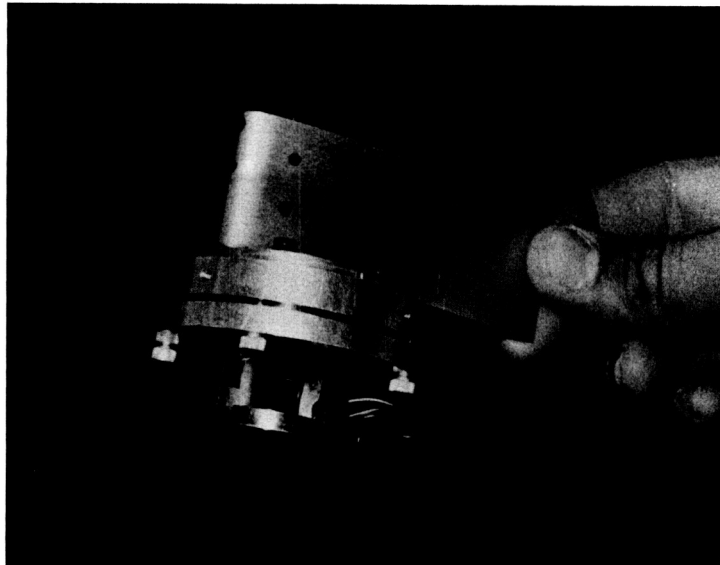


Figure 47.— Hub hardware polar moment of inertia determination using soft flexure.
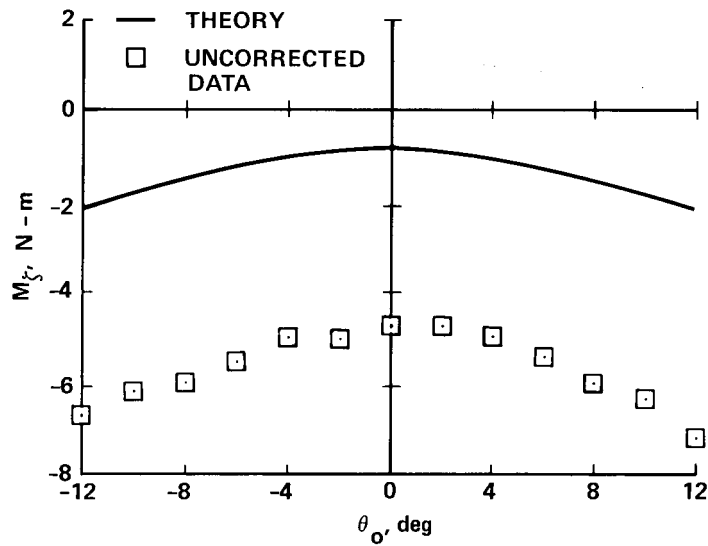
Figure 48.— Comparison of uncorrected experimental steady lead-lag moments with theory, no precone or droop, soft pitch flexure.
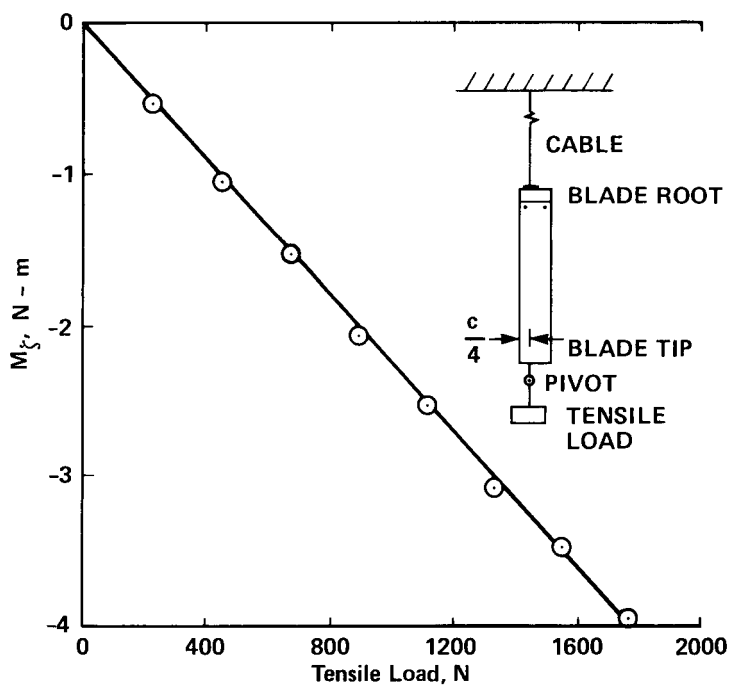


Figure 49.— Lead-lag bending moment versus tensile loading at the blade quarter chord location.
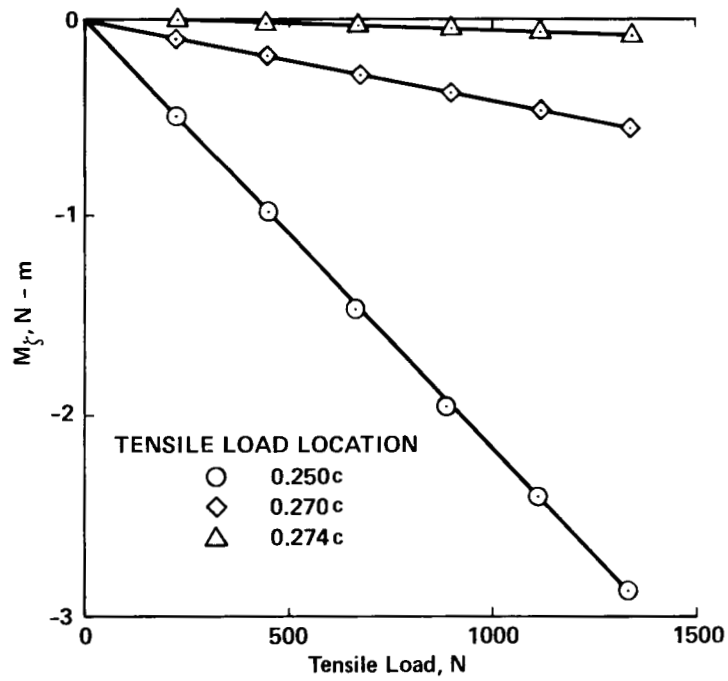
Figure 50.— Experimental determination of the blade tension axis location blade bending moment versus tensile loading.

| 1. Report No. NASA TP-2546 AVSCOM TR 85-A-9 | 2. Government Accession No. | 3. Recipient's Catalog No. |
|---|---|---|
| 4. Title and Subtitle AN EXPERIMENTAL INVESTIGATION OF THE FLAP-LAG-TORSION AEROELASTIC STABILITY OF A SMALL-SCALE HINGELESS HELICOPTER ROTOR IN HOVER | | 5. Report Date January 1986 |
| | | 6. Performing Organization Code |
| 7. Author(s) David L. Sharpe | | 8. Performing Organization Report No. 85142 |
| | | 10. Work Unit No. |
| 9. Performing Organization Name and Address Ames Research Center, Moffett Field, CA 94035 and Aeroflightdynamics Directorate, U.S. Army Aviation Research and Technology Activity | | 11. Contract or Grant No. |
| | | 13. Type of Report and Period Covered Technical Paper |
| 12. Sponsoring Agency Name and Address National Aeronautics and Space Administration, Washington, DC 20546 and U.S. Army Aviation Systems Command, St. Louis, MO 63120-1798 | | 14. Sponsoring Agency Code |

15. Supplementary Notes

Point of Contact: David L. Sharpe, Ames Research Center, MA 215-1, Moffett Field, CA 94035
(415) 694-5896 or FTS 464-5896

16. Abstract

A small scale, 1.92 m diam, torsionally soft, hingeless helicopter rotor was investigated in hover to determine isolated rotor stability characteristics. The two-bladed, untwisted rotor was tested on a rigid test stand at tip speeds up to 101 m/sec. The rotor mode of interest in this investigation was the lightly damped lead-lag mode. The dimensionless lead-lag frequency of the mode is approximately 1.5 at the highest tip speed. The hub was designed to allow variation in precone, blade droop, pitch control stiffness, and blade pitch angle. Measurements of modal frequency and damping were obtained for several combinations of these hub parameters at several values of rotor speed. Steady blade bending moments were also measured. The lead-lag damping measurements were found to agree well with theoretical predictions for low values of blade pitch angle. The test data confirmed the predicted effects of precone, droop, and pitch control stiffness parameters on lead-lag damping. The correlation between theory and experiment was found to be poor for the mid-to-high range of pitch angles where the theory substantially overpredicted the experimental lead-lag damping. The poor correlation in the mid-to-high blade pitch angle range is attributed to low Reynolds number nonlinear aerodynamics effects not included in the theory. The experimental results also revealed an asymmetry in lead-lag damping between positive and negative thrust conditions. Investigations of the rotor induced velocity field suggest that the asymmetry in lead-lag damping is not caused by the aerodynamic inflow but more likely from the influence of blade weight on the equilibrium blade deflection. Comparison of measured steady state blade bending and torsion loads with theoretical predictions showed good agreement after correcting the lead-lag bending moments for a small chordwise offset of the blade tension axis.

| 17. Key Words (Suggested by Author(s)) Helicopter model, Hingeless rotor, Aeroelastic stability, Structural coupling, Flap-lag-torsion, Rotor inflow, Rotating beam, Rotor stability, Rotor Dynamics | 18. Distribution Statement Unclassified – Unlimited Subject Category 02 |
|---|---|

| 19. Security Classif. (of this report) Unclassified | 20. Security Classif. (of this page) Unclassified | 21. No. of Pages 84 | 22. Price A05 |
|---|---|---|---|